NACA

RESEARCH MEMORANDUM

THE EFFECTS OF WING INCIDENCE ON THE AERODYNAMIC LOADING CHARACTERISTICS OF A SWEPTBACK WING-BODY COMBINATION AT TRANSONIC SPEEDS

By Harold L. Robinson

Langley Aeronautical Laboratory
Langley Field, Va.

NATIONAL ADVISORY COMMITTEE
FOR AERONAUTICS

WASHINGTON
October 12, 1954

NACA RM L54G23b

NATIONAL ADVISORY COMMITTEE FOR AERONAUTICS

RESEARCH MEMORANDUM

THE EFFECTS OF WING INCIDENCE ON THE AERODYNAMIC LOADING CHARACTERISTICS OF A SWEPTBACK WING-BODY COMBINATION AT TRANSONIC SPEEDS

By Harold L. Robinson

SUMMARY

The effects of 4° of wing incidence on the aerodynamic loading characteristics of a sweptback (angle of sweep, 45°), tapered (taper ratio, 0.6), and twisted $\left(4\frac{1}{2}^{\circ}\right.$ washout$\left.\right)$ wing-body combination with NACA 65A006 airfoil sections are presented herein. The data indicated that, at a given wing angle of attack, the flow field about the wing was changed by the body trailing vortex so that increasing wing incidence decreased the wing normal force and the root bending moment but did not appreciably change the wing pitching moment or the wing twisting moment. At a given total normal-force coefficient, however, increasing wing incidence slightly increased the wing normal force and the root bending moment, slightly decreased the wing pitching moment, and did not significantly affect the wing twisting moment. The pitching moment of the wing-body combination was decreased by increasing wing incidence when comparisons were made at either a given wing angle of attack or total normal-force coefficient. The pitching-moment decrease did not alter the longitudinal stability characteristics significantly. At subsonic speeds, the well-known pitch-up characteristics were associated with body forces as well as with the wing-tip stall phenomena.

INTRODUCTION

Increasing the wing incidence from that required for cruise conditions is often dictated to provide a reasonable landing-gear configuration. Recent data (ref. 1) indicated that an increase in wing incidence of a sweptback, tapered, twisted, and cambered wing-body combination had a detrimental effect on the lift-drag ratio. Other data (ref. 2) indicated that wing incidence had little effect on the lift-drag ratio. The wing of reference 2 had the same plan form as the wing of reference 1 but

the wing of reference 2 was not twisted and the airfoil was symmetrical. Also, the body of reference 1 was larger than the body of reference 2.

The effect of wing incidence on the aerodynamic loading characteristics of a 45° sweptback, tapered, twisted, and symmetrical-airfoil wing-body combination is discussed in the present report. The wing had the same plan form as the wing of references 1 and 2. The effects of wing twist for the wing-body combination of the present report may be found in reference 3. As stated in reference 3, the twist distribution of the wing is representative of that produced by aeroelastic bending. The magnitude of the twist, however, was not matched to any specific structure.

The results reported herein have been obtained from pressure measurements over the model surface. The angle-of-attack range, measured near the wing root, was 0° to 20°. The Mach number range varied from 0.60 to 1.13 and the corresponding Reynolds number range varied from 3.4×10^6 to 4.0×10^6 per foot of length.

SYMBOLS

A wing area including the portion covered by body, 1 sq ft

b wing span, 2 ft

c wing-section chord

$\bar{c}$ average wing-chord, A/b, 6 in.

c' mean aerodynamic chord, $\frac{2}{A}\int_0^{b/2} c^2 d(y)$, 6.125 in.

d distance from quarter-chord line to wing center of pressure

M stream Mach number

P pressure coefficient,
$$\frac{\text{Local static pressure - Stream static pressure}}{\text{Dynamic pressure}}$$

C_B root bending-moment coefficient,
$$\frac{1}{A/2\left(b/2 - R_{max}\right)}\int_{R_{max}}^{b/2}\int_0^c \left(P_L - P_U\right)\left(y - R_{max}\right) dx\, dy$$

$C_{M_{c'/4}}$ total pitching-moment coefficient, $C_{M_{FW}} + C_{M_{W_{c'/4}}}$

$C_{M_{FW}}$ body pitching-moment coefficient,

$$-\frac{1}{Ac'}\int_0^{2\pi}\int_0^{L} RP\left(x_{c'/4} - x\right)\cos\theta\, dx\, d\theta$$

$C_{M_{W_{c'/4}}}$ wing pitching-moment coefficient,

$$\frac{2}{Ac'}\int_{R_{max}}^{b/2}\left[\int_0^{c}\left(P_L - P_U\right)\left(x_{c/4} - x\right)d(x) + \int_0^{c}\left(P_L - P_U\right)\left(x_{c'/4} - x_{c/4}\right)d(x)\right]dy$$

$c_{m_{c/4}}$ section pitching moment, $\frac{1}{c^2}\int_0^{c}\left(P_L - P_U\right)\left(x_{c/4} - x\right)dx$

C_N total normal-force coefficient, $C_{N_{FW}} + C_{N_W}$

$C_{N_{FW}}$ body normal-force coefficient, $-\frac{1}{A}\int_0^{2\pi}\int_0^{L} RP\cos\theta\, dx\, d\theta$

C_{N_W} wing normal-force coefficient, $\frac{2}{A}\int_{R_{max}}^{b/2}\int_0^{c}\left(P_L - P_U\right)dx\, dy$

c_{n_W} section normal-force coefficient, $\frac{1}{c}\int_0^{c}\left(P_L - P_U\right)dx$

$C_{T_{c/4}}$ wing twisting-moment coefficient,

$$\frac{2}{Ac'}\int_{R_{max}}^{b/2}\int_0^{c}\left(P_L - P_U\right)\left(x_{c/4} - x\right)\cos\Lambda\, dx\, dy$$

i wing incidence angle, measured at 18-percent-semispan station

L body length

[redacted]

R	body radius at any station
x	distance measured from nose of body or wing leading edge parallel to vertical plane of symmetry
y	distance measured from vertical plane of symmetry
α	wing angle of attack measured near wing-body juncture (18 percent semispan station)
θ	meridian station, origin at top of body
Λ	sweepback angle of quarter-chord line
λ	taper ratio, $\frac{\text{Tip chord}}{\text{Root chord}}$

Subscripts:

U	wing upper surface
L	wing lower surface
c/4	section quarter chord
c'/4	mean aerodynamic quarter chord

APPARATUS AND MEASUREMENTS

Tunnel

All the data discussed herein were obtained from tests conducted in the Langley 8-foot transonic wind tunnel. The tunnel has a dodecagonal slotted test section and is capable of continuously variable operation through the speed range up to a Mach number of 1.14. At subsonic Mach numbers, deviations in Mach number did not exceed 0.004, and at supersonic Mach numbers, the maximum Mach number deviations did not exceed 0.006. A more complete description of the tunnel is given in reference 4.

Tunnel-wall-interference corrections were not applied because choking and blockage effects are negligible, especially for the small ratio of model size to tunnel size of the present tests. The model was mounted in the tunnel as shown in the photograph (fig. 1), and was offset from the tunnel center line in conformity with the practice in the Langley 8-foot transonic tunnel.

[redacted]

Model

A drawing of the model is presented in figure 2. The model is the same as the twisted wing model of reference 3. The body is the same as that referred to as the cylindrical body in reference 5 wherein the loads for the body alone have been presented. The wing tips were washed out as shown by the curve in the upper right-hand corner of figure 2. The incidence angle of each wing section shown in this curve is for the arbitrarily designated 4° incidence configuration. The section incidence angles for the 0° incidence configuration were 4° less than those shown on the curve. The arbitrarily designated wing incidence angle is the angle between the 18-percent-semispan-station chord and the body horizontal plane of symmetry. The sweepback angle has been measured with respect to the section quarter-chord line. The body-meridian stations and wing-span stations along which the orifices were located have been shown in figure 2.

Measurements

The angle of attack was measured by an electrical strain-gage pendulum device mounted internally near the base of the support sting. Sting and model deflections occurring ahead of this point, because of forces and moments acting on the model, were determined from static tests. These corrections were applied to the angles of attack; the maximum deflections occurring during the investigation were approximately 0.5°.

The wing angles of attack reported herein are referred to a wing chord near the root, as shown in figure 2. This particular chord (18-percent-semispan station) was chosen because, for the 0° incidence configuration (ref. 3) this chord was alined with the body center line. The accuracy of the angle-of-attack measurements is believed to be within ±0.1° for this measuring system.

Pressure.- The pressures existing on the surfaces of the model were measured by connecting the orifices to a multitubed manometer. In order to determine the forces on the model, these pressures were integrated graphically. The average accuracy of the pressure coefficients presented herein is estimated to be within ±0.005.

PRESENTATION OF RESULTS

Pressure Distribution

The pressure distributions obtained for both configurations are compared in figures 3 and 4 for the body and the wing, respectively. Data

[redacted]

for the 0° incidence configuration (ref. 3) are shown by the faired lines while data for the 4° incidence configuration are represented by the symbols. As previously mentioned, the wing angles of attack were measured with respect to a chord line near the wing root. Obviously, the body angle of attack at a given wing angle of attack was 4° lower for the 4° incidence configuration than for the 0° incidence configuration.

Normal-Force and Pitching-Moment Coefficients

Body.- The normal-force and pitching-moment coefficients for the body in the presence of the wing are presented as a function of Mach number at a constant angle of attack α in figures 5 and 6, respectively. Data were not available at some of the Mach numbers at the angles selected; accordingly, the fairing of these curves, as well as that of other curves presented as functions of Mach number at a constant angle of attack, was accomplished with the aid of suitable cross plots. Such points are indicated by the absence of symbols.

Wing and wing-body combination.- The normal-force (fig. 7) and the pitching-moment characteristics (fig. 8) of the wing and the wing-body combination are presented as composite plots. The wing data at the top of figures 7 and 8 are section data. The data in the lower right-hand corner of the figures represent the integrations of the pressures over the wing surface and the ordinate of the curves in the lower left-hand corner is the sum of the forces (fig. 7) and moments (fig. 8) on the wing and the body. The fairing of the 0° incidence data in the lower parts of figure 8 do not follow that of reference 3 in the region above $C_{N_W} = 0.5$ in some cases.

The origin locations for each spanwise station for the data presented at the top of figures 7 and 8 are proportional to the spanwise distance. Therefore, the plots (top of figs. 7 and 8) provide the spanwise loading characteristics as well as the section characteristics. The average body section normal-load coefficient $C_{N_{FW}} \frac{b}{D_{max}}$ has also been presented in figure 7.

The variations of the wing normal-force coefficient and the wing pitching-moment coefficient around the mean aerodynamic quarter chord with Mach number are presented in figures 9 and 10, respectively.

Wing Root Bending Moment

The wing-root bending-moment coefficients for the two incidence configurations are compared in figure 11, where variation of the wing root bending moment with Mach number and with wing normal-force coefficient is shown.

[redacted]

The pressures over one wing panel were graphically integrated so as to obtain the moment around the root chord, and the coefficients were based on half the total wing area, including the portion buried by the body, and the exposed semispan. This type of coefficient was chosen merely on the basis of consistency with previously published NACA papers (refs. 3 and 6, for example).

Twisting-Moment Coefficient

The twisting-moment coefficients are compared in figure 12. The twisting moment is defined as the sum over a wing panel of the section moments around the local quarter-chord line of the sweptback wing. The section moments are not taken in a plane parallel to the body center line as pitching moments are usually defined. The coefficients are based on half the total wing area and the mean aerodynamic chord. This coefficient is a measure of the aerodynamic loads causing wing torsion. Rather than re-integrate the wing pressures to obtain this coefficient, it was found convenient to compute this coefficient from the relation: $C_{T_{c/4}} = -\frac{d}{c'} C_{N_w}$.

DISCUSSION

Body

Pressure distribution.- At a given wing angle of attack the pressure coefficients over the body in the wing region were about the same even though the body for the 4° incidence configuration was at an angle of attack 4° lower than that of the body of the 0° incidence configuration (fig. 3). Consequently, the induced pressures over the body in the wing region were larger for the 4° incidence configuration than for the 0° incidence configuration when compared at a given body angle of attack.

Comparison of the pressure data at a given body angle of attack (comparing 0° incidence data at $\alpha \approx 0°$, 4°, and 8° with 4° incidence data at $\alpha \approx 4°$, 8°, and 12°, respectively) indicated that the pressures over the forward portions of the body were not affected by wing incidence to any significant extent. The body pressures in a region starting immediately ahead of the wing, however, were influenced by wing incidence. The region affected by wing incidence was not appreciably affected by Mach number (fig. 3). It has been observed previously (ref. 7), however, that the body pressures ahead of the wing were influenced by the presence of the wing, and that the leading edge of this region moved back as the Mach number was increased.

[redacted]

Normal force.- As expected, the body normal-force coefficient at a given wing angle of attack (fig. 5) or at a given wing normal-force coefficient (fig. 7) was slightly smaller for the 4° incidence configuration than for the 0° incidence configuration. This difference in normal force was caused by the pressure differences over the forward portions of the body associated with the different body angle of attack. The effect of wing incidence on the body normal-force characteristics was not affected significantly by Mach number (fig. 5).

Pitching moment.- The body pitching moment was more negative for the 4° incidence configuration than for the 0° incidence configuration when compared at a given wing angle of attack or wing normal-force coefficient (figs. 6 and 8). Wing incidence, however, had a minor effect on the body pitching moments when compared at a given body angle of attack. The effect of Mach number on the effects of wing incidence on the body pitching moments was insignificant (fig. 6).

Wing

Pressure distribution.- The pressure data of figure 4 indicate that, at $\alpha \approx 0°$, 4°, and 8°, when flow separation was not encountered, the effect on the pressures was such that the effective angle of attack was less for the 4° incidence configuration than for the 0° incidence configuration. At a given wing angle of attack, the body of the 4° incidence configuration operates at a lower angle of attack than the body of the 0° incidence configuration. Consequently, the upwash due to the body trailing vortices was reduced for the 4° incidence configuration. At angles of attack near 12°, the upwash for the 4° incidence configuration also was less than the upwash for the 0° incidence configuration. However, where the flow over the wing has separated, the configuration operating at the lower effective angles of attack (4° incidence configuration) may exhibit the greater induced pressures because the flow separation was not as severe for the 4° incidence configuration as for the 0° incidence configuration. The differences just discussed were diminished as the Mach number was increased. Only insignificant differences between the two configurations were noted at supersonic Mach numbers. At angles of attack near 20°, well beyond the stall angle (stall angle is defined herein as the angle where the lift curve becomes nonlinear), wing incidence had little effect on the induced pressures.

Normal force.- At a given angle of attack below stall, the section normal load was generally slightly lower for the 4° incidence configuration than for the 0° incidence configuration (fig. 7). As discussed in the preceding section, this load decrease is caused by the lower body normal force which resulted in less upwash for the 4° incidence configuration. Consequently, the 4° wing incidence increase resulted in a lower wing normal-force coefficient at a given angle of attack.

[redacted]

Except for a small decrease in load near the wing root for the 4° incidence configuration, however, the span-load distribution is not changed significantly by wing incidence at a given wing normal-force coefficient below stall.

At lifting conditions near stall ($\alpha \approx 12°$), the section normal-load was sometimes larger for the 4° incidence configuration than for the 0° incidence configuration. As discussed previously (wing-pressure distribution), this phenomenon was associated with the separated flow near stall angle of attack. Furthermore, the differences of section normal force just discussed were diminished as the Mach number was increased and were insignificant at supersonic speeds. This decrease of section normal load at some span stations was balanced by an increase at other span stations so that increasing the wing incidence had only a minor effect on the wing normal force near $\alpha \approx 12°$. The data of figure 9 indicated that, generally, the effect of wing incidence on the wing normal force was not significantly affected by Mach number.

Pitching moment.- At normal-force values below stalling conditions, there was little change in the section pitching moment because of wing incidence (fig. 8). Near stalling angles, the section pitching-moment differences due to wing incidence were similar to the section normal-load phenomena. The differences due to incidence, however, did not become insignificant at supersonic speeds but were diminished.

Generally, at a given wing normal-force coefficient, the wing pitching moments around the quarter chord of the mean aerodynamic chord were only slightly more negative for the 4° incidence configuration than for the 0° incidence configuration. This phenomenon was due mainly to the lower section normal-force coefficient at a given wing normal-force coefficient for the inboard station of the 4° incidence configuration. Little if any of the wing pitching-moment effects due to incidence were associated with section pitching-moment changes around the section quarter chord.

The pitching-moment coefficient for the wing-body combination was approximately 0.03 more negative for the 4° incidence configuration because of the more negative pitching moments of the body for the 4° incidence configuration.

The static longitudinal stability was not affected to any important extent by wing incidence. Furthermore, comparisons of the wing-body pitching moment with the wing pitching moment (fig. 8) indicated that the well-known pitch-up tendency was associated to an important degree with the body loads.

The effects of wing incidence on the pitching moments did not vary significantly with Mach number (figs. 8 and 10).

[redacted]

Root bending moment.- The data presented in figure 11 indicated that, although the root bending moments for the 4° incidence configuration were slightly lower than those for the 0° incidence configuration at a given angle of attack, incidence had little effect on the root bending moments at a given wing normal-force coefficient. Consequently, the spanwise location of the center of pressure was not significantly affected by wing incidence. The root bending moments, however, were slightly higher for the 4° incidence configuration at a given wing-body normal-force coefficient. Furthermore, the effects of wing incidence on the root bending-moment coefficients were insignificantly affected by Mach number.

Torsional loading characteristics.- The aerodynamic effects of wing incidence on the torsional loading characteristics were negligible (fig. 12). This phenomenon was expected since the section pitching moments were not affected to any important extent by wing incidence.

CONCLUSIONS

Analysis of the effects of wing incidence (incidence angle measured near the wing-body juncture of a $4\frac{1}{2}^{\circ}$ washout wing) on the aerodynamic loading characteristics of a sweptback wing-body combination indicated:

1. At a given wing angle of attack below stall, the wing normal force was reduced by increasing wing incidence. At a given normal force for the wing-body combination, however, increasing wing incidence 4° slightly increased the wing normal force.

2. At a given wing normal-force coefficient, increasing wing incidence slightly reduced the wing pitching-moment coefficient.

3. The pitching moment for the wing-body combination was reduced significantly when the incidence angle was increased. The slope of the pitching-moment curve, however, was not significantly affected by wing incidence.

4. The root bending moment was reduced slightly by increasing wing incidence when comparison was made at a given wing angle of attack, was not significantly affected when comparison was made at a given wing normal force, and was increased slightly when comparisons were made at a given wing-body normal force.

5. Wing incidence had an insignificant effect on the torsional loading characteristics of the wing.

[redacted]

6. Mach number had an insignificant effect on the effects of wing incidence on the aerodynamic loading characteristics through a Mach number range from 0.6 to 1.13.

7. At subsonic speeds, the well-known pitch-up characteristics were associated with the body forces as well as with the wing-tip stall phenomena.

Langley Aeronautical Laboratory,
National Advisory Committee for Aeronautics,
Langley Field, Va., July 9, 1954.

REFERENCES

1. Cooper, J. Lawrence: A Transonic Wind-Tunnel Investigation of the Effects of Twist and Camber With and Without Incidence, Twist, and Body Indentation of the Aerodynamic Characteristics of a 45° Sweptback Wing-Body Configuration. NACA RM L54B15, 1954.

2. Morgan, Frances G., Jr.: Transonic Wind-Tunnel Investigation of the Effects of Wing Incidence Angle on the Characteristics of Two Wing-Body Combinations. NACA RM L52K06a, 1953.

3. Williams, Claude V.: An Investigation of the Effects of a Geometric Twist on the Aerodynamic Loading Characteristics of a 45° Sweptback Wing-Body Configuration at Transonic Speeds. NACA RM L54H18, 1954.

4. Ritchie, Virgil S., and Pearson, Albin O.: Calibration of the Slotted Test Section of the Langley 8-Foot Transonic Tunnel and Preliminary Experimental Investigation of Boundary-Reflected Disturbances. NACA RM L51K14, 1952.

5. Robinson, Harold L.: Pressures and Associated Aerodynamic and Load Characteristics for Two Bodies of Revolution at Transonic Speeds. NACA RM L53L28a, 1954.

6. Loving, Donald L.: The Effect of a Change in Body Shape on the Loading of a 45° Sweptback Wing-Body Combination at Transonic Speeds. NACA RM L54B09, 1954.

7. Loving, Donald L., and Estabrooks, Bruce B.: Transonic-Wing Investigation in the Langley 8-Foot High-Speed Tunnel at High Subsonic Mach Numbers and at a Mach Number of 1.2. Analysis of Pressure Distribution of Wing-Fuselage Configuration Having a Wing of 45° Sweepback, Aspect Ratio 4, Taper Ratio 0.6, and NACA 65A006 Airfoil Section. NACA RM L51F07, 1951.

[redacted]

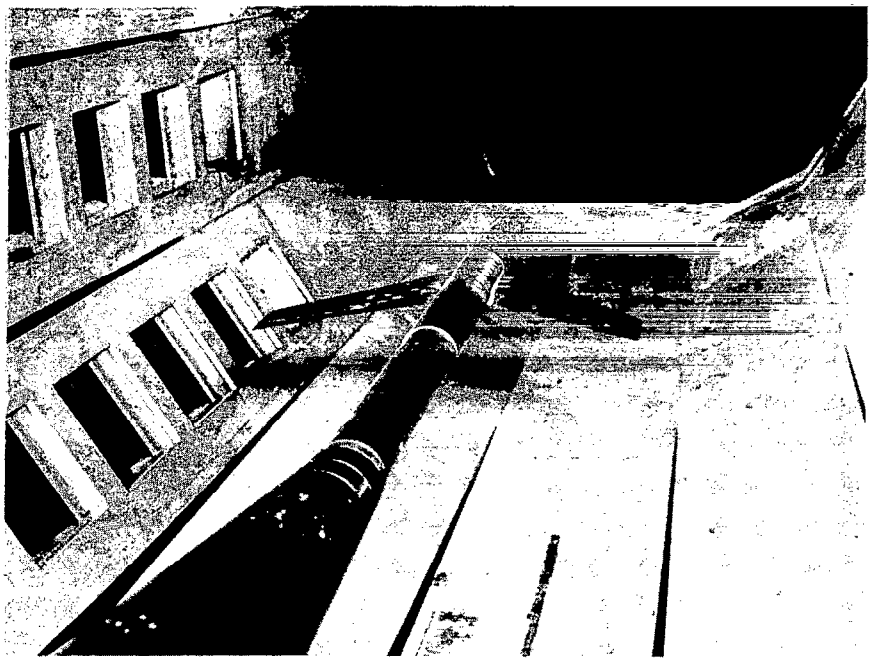

L-79101

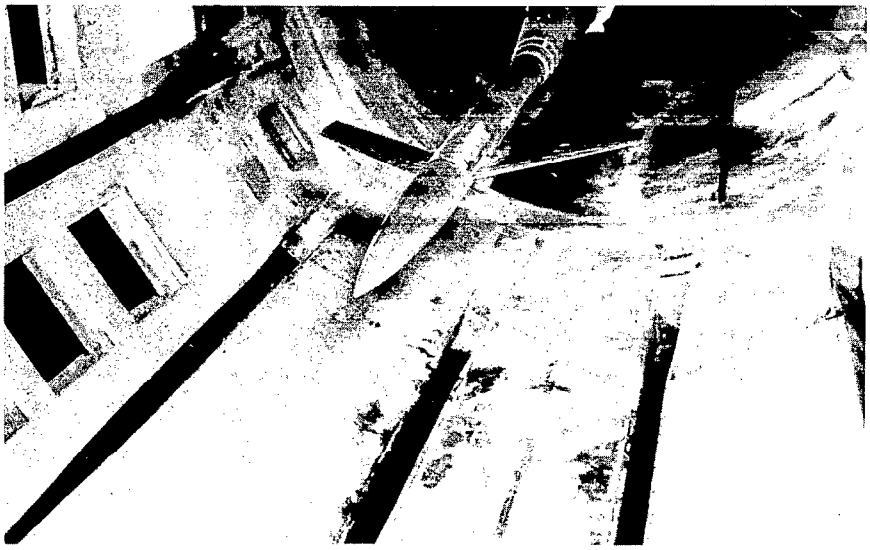

L-79100

Figure 1.- Photographs of model in Langley 8-foot transonic tunnel.

[redacted]

Nose ordinates

Distance from nose (in.)	Body radius (in.)
0	0
0.200	0.092
.300	.119
.500	.171
1.000	.289
2.000	.482
3.000	.645
4.000	.788
6.000	1.037
8.000	1.236
10.000	1.386
12.000	1.496
14.000	1.573
16.000	1.625
18.000	1.657
20.000	1.667

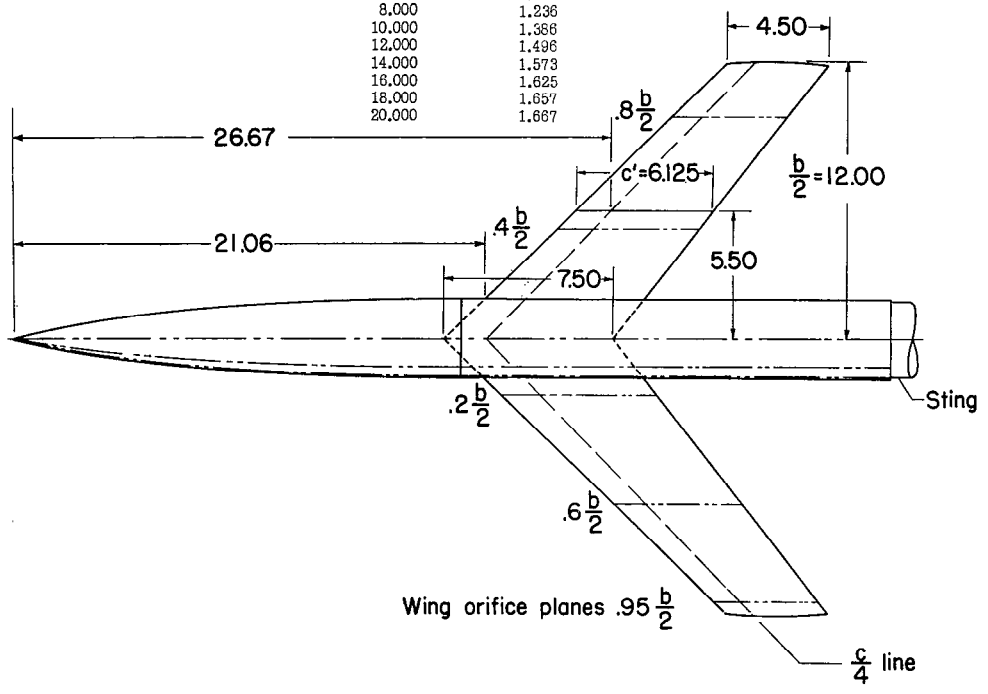

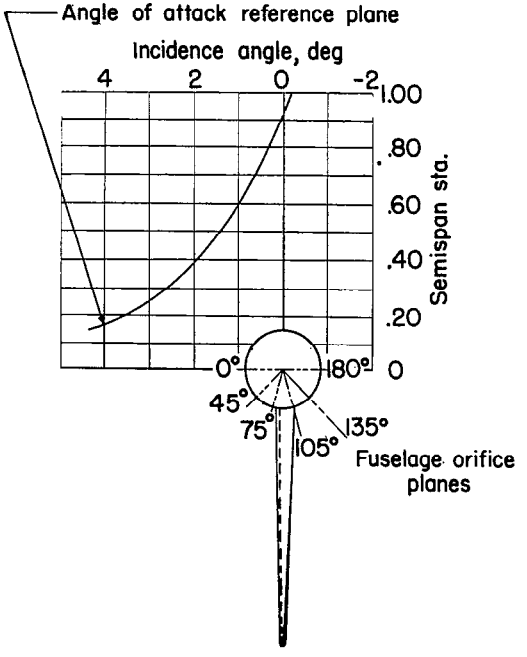

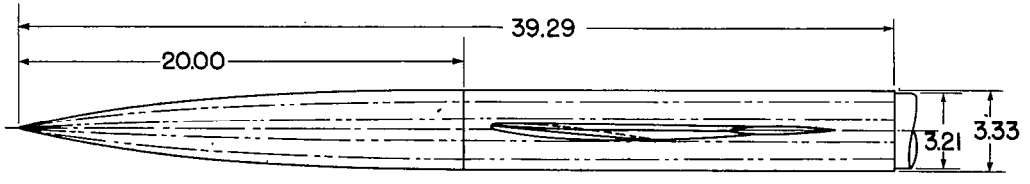

Wing details

Airfoil section	NACA 65A006
Aspect ratio	4
Taper ratio	.6
Wing area	144 sq in.
Sweepback angle	45°

Figure 2.- Model details; 4° incidence configuration.

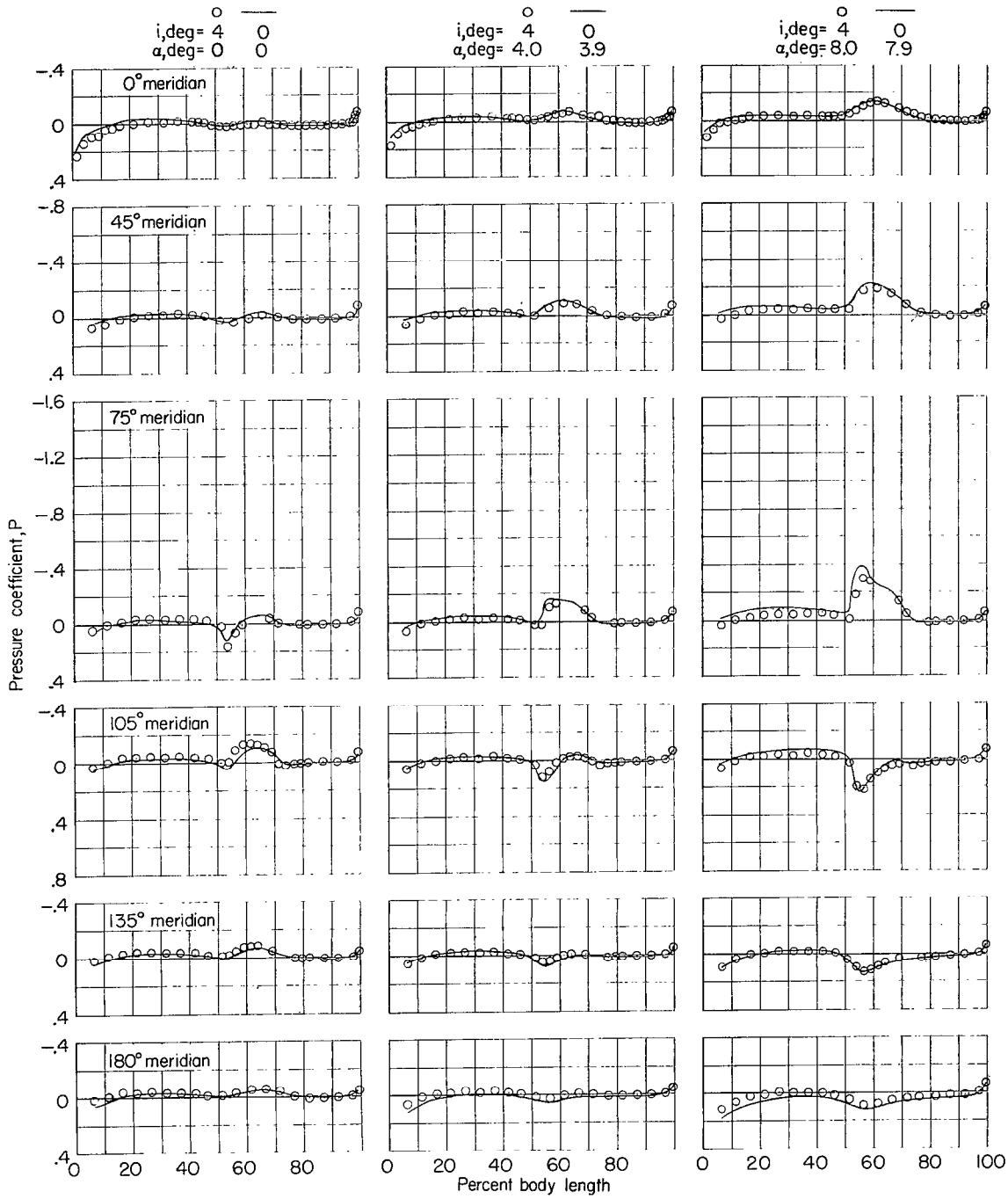

(a) M = 0.60.

Figure 3.- Comparison of pressure coefficient for the body.

[redacted]

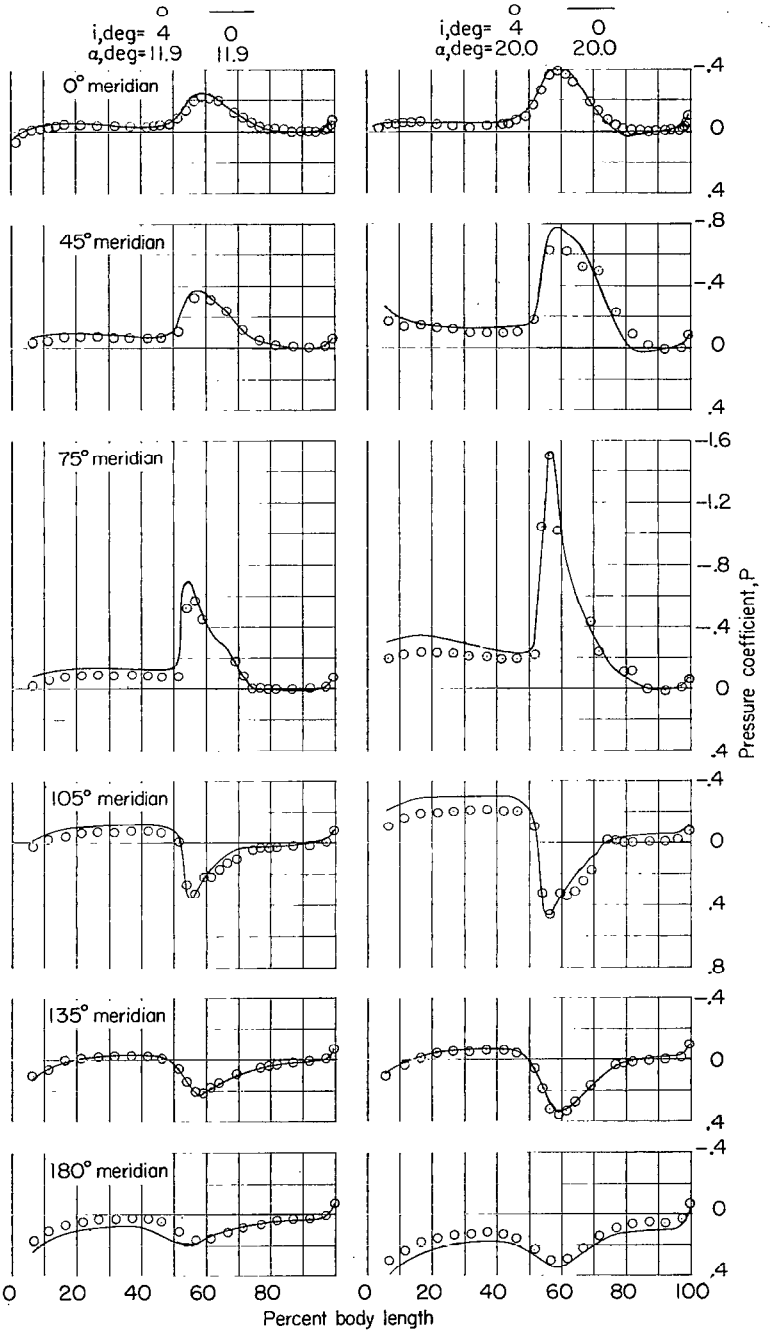

(a) Concluded.

Figure 3.- Continued.

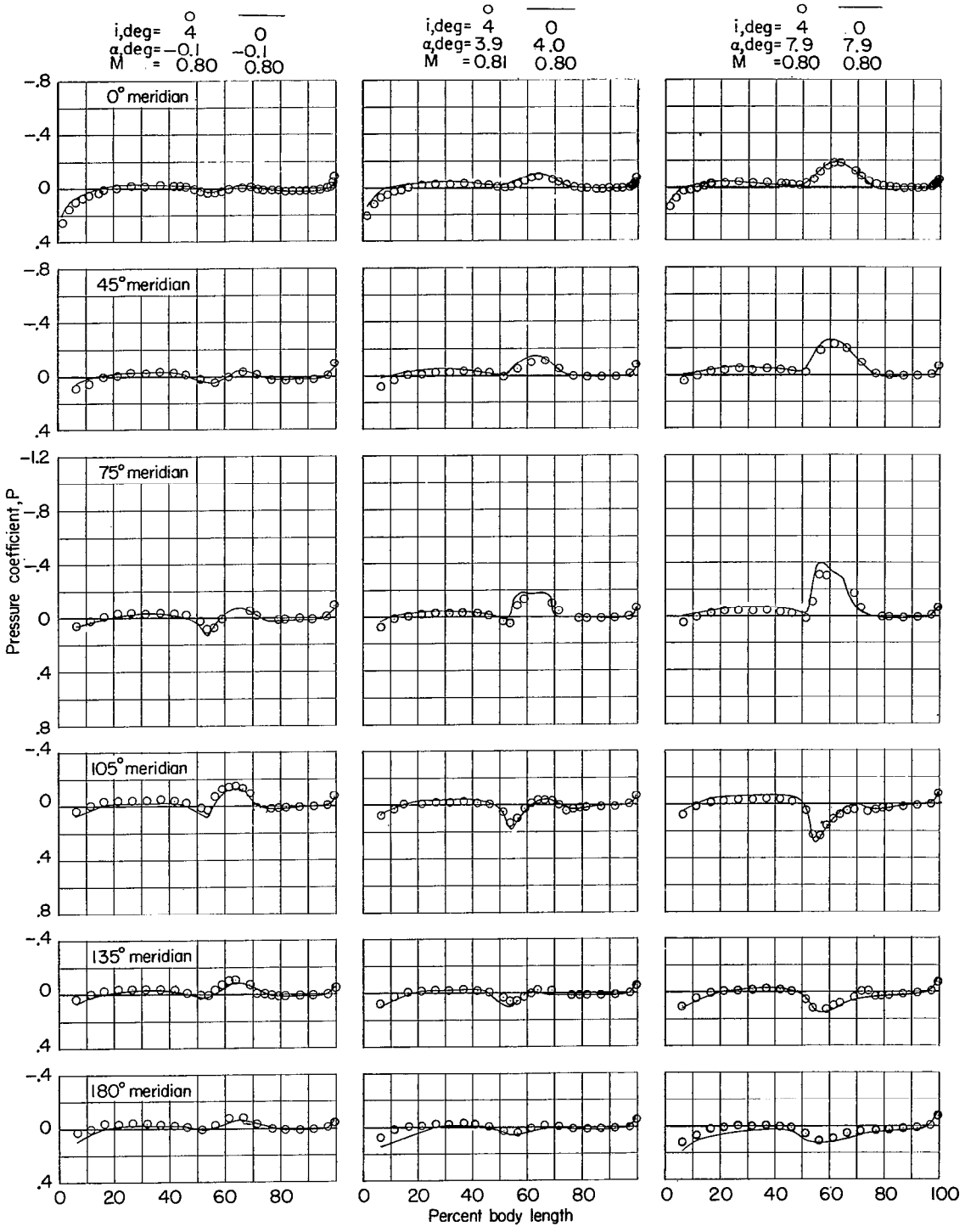

(b) $M \approx 0.80$.

Figure 3.- Continued.

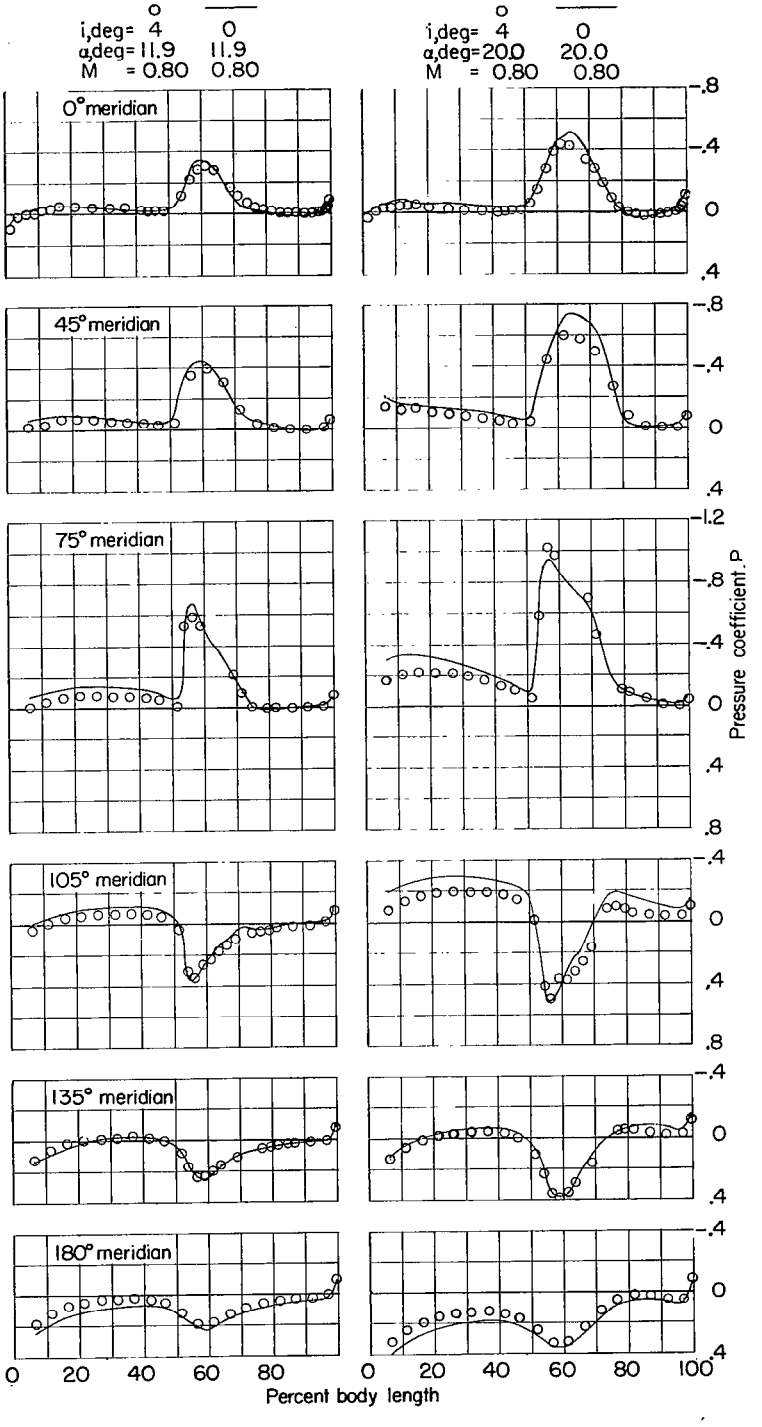

(b) Concluded.

Figure 3.- Continued.

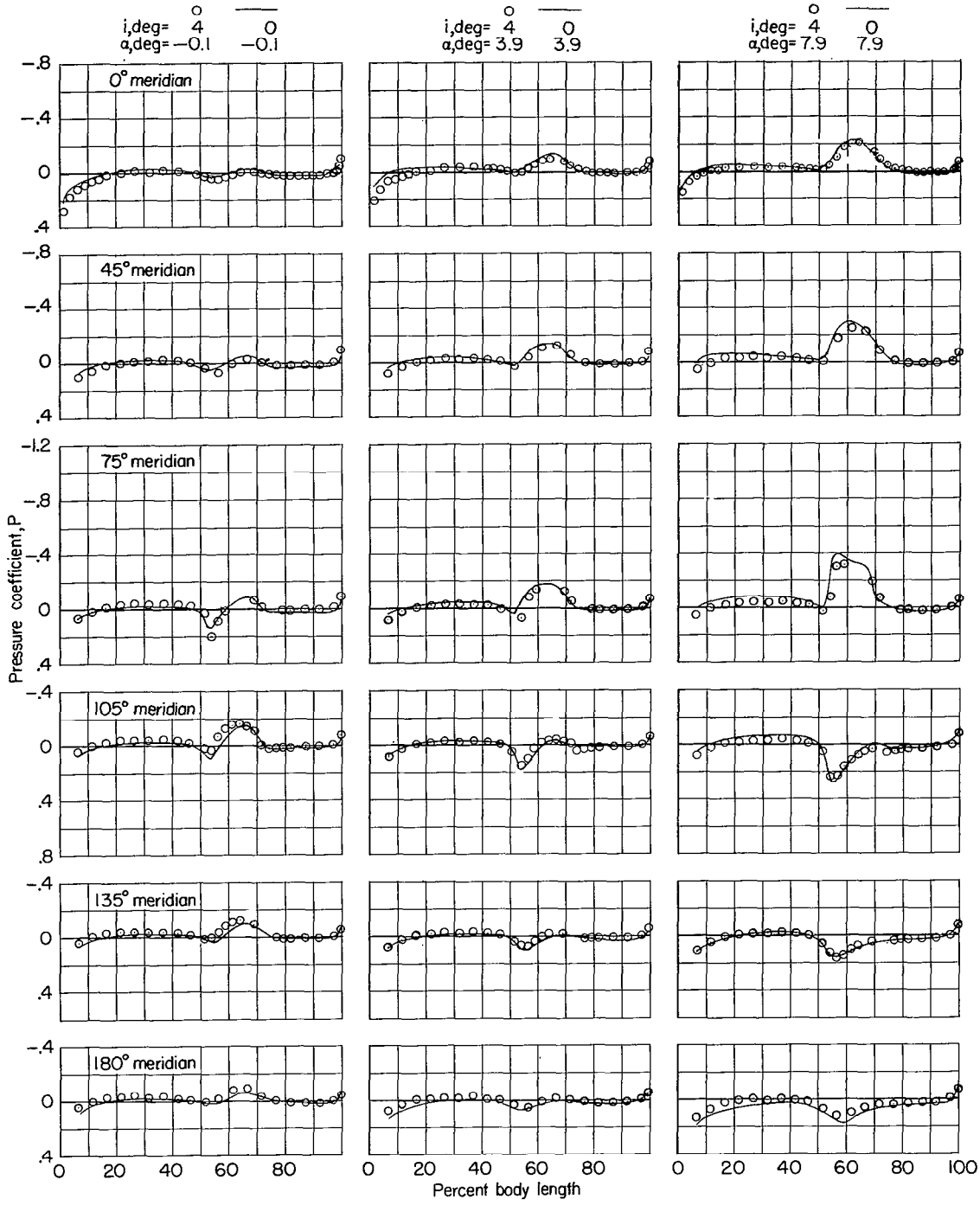

(c) M = 0.85.

Figure 3.- Continued.

[redacted]

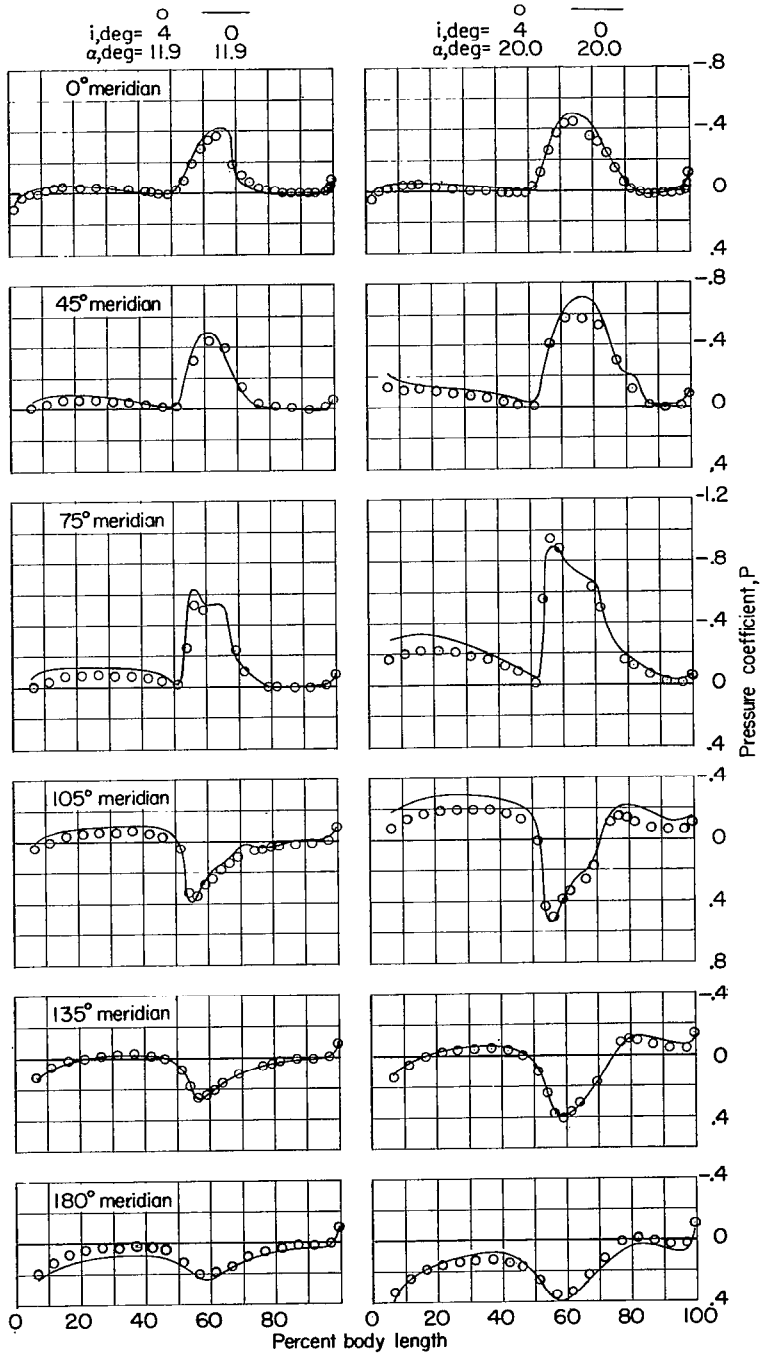

(c) Concluded.

Figure 3.- Continued.

[redacted]

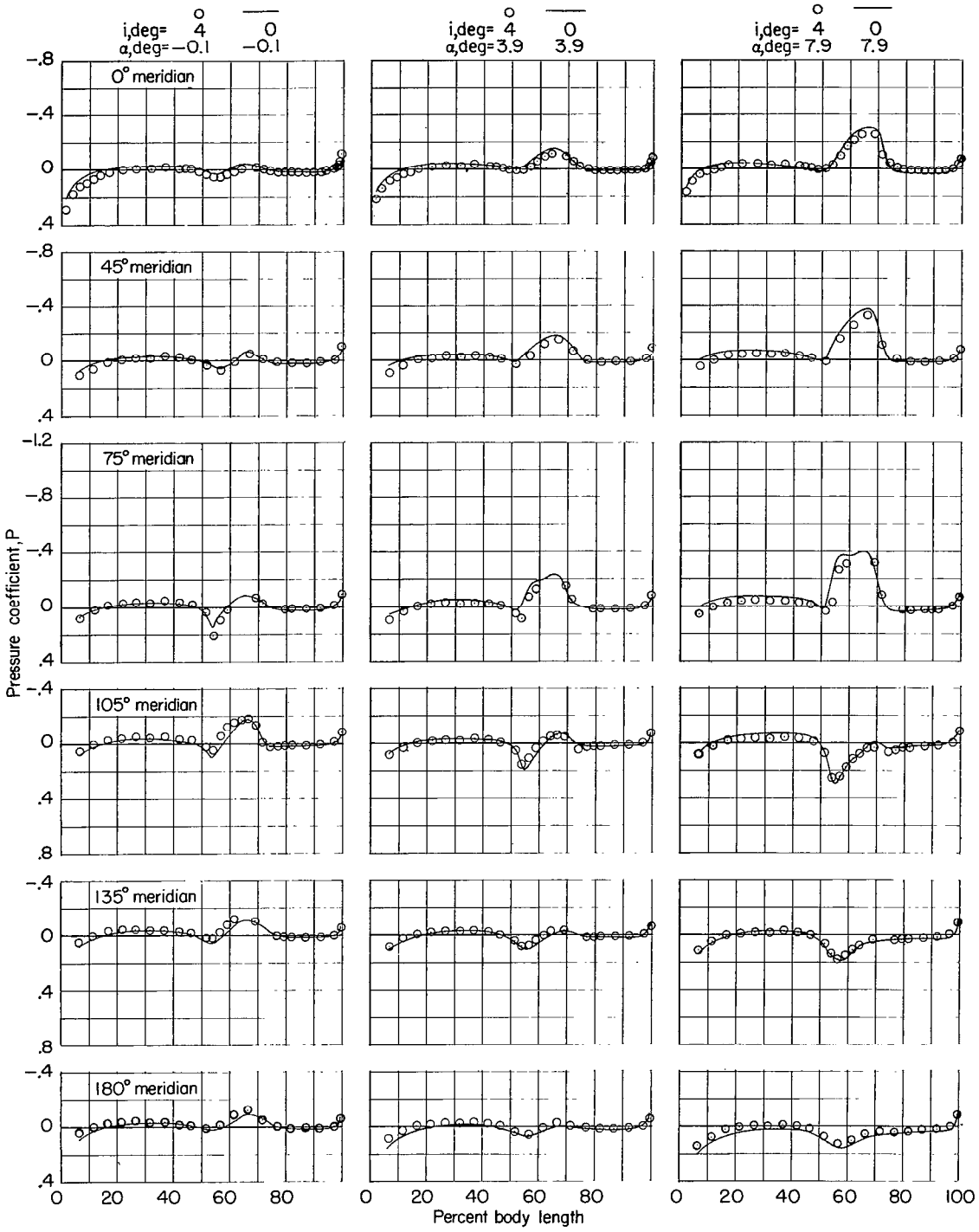

(d) M = 0.90.

Figure 3.- Continued.

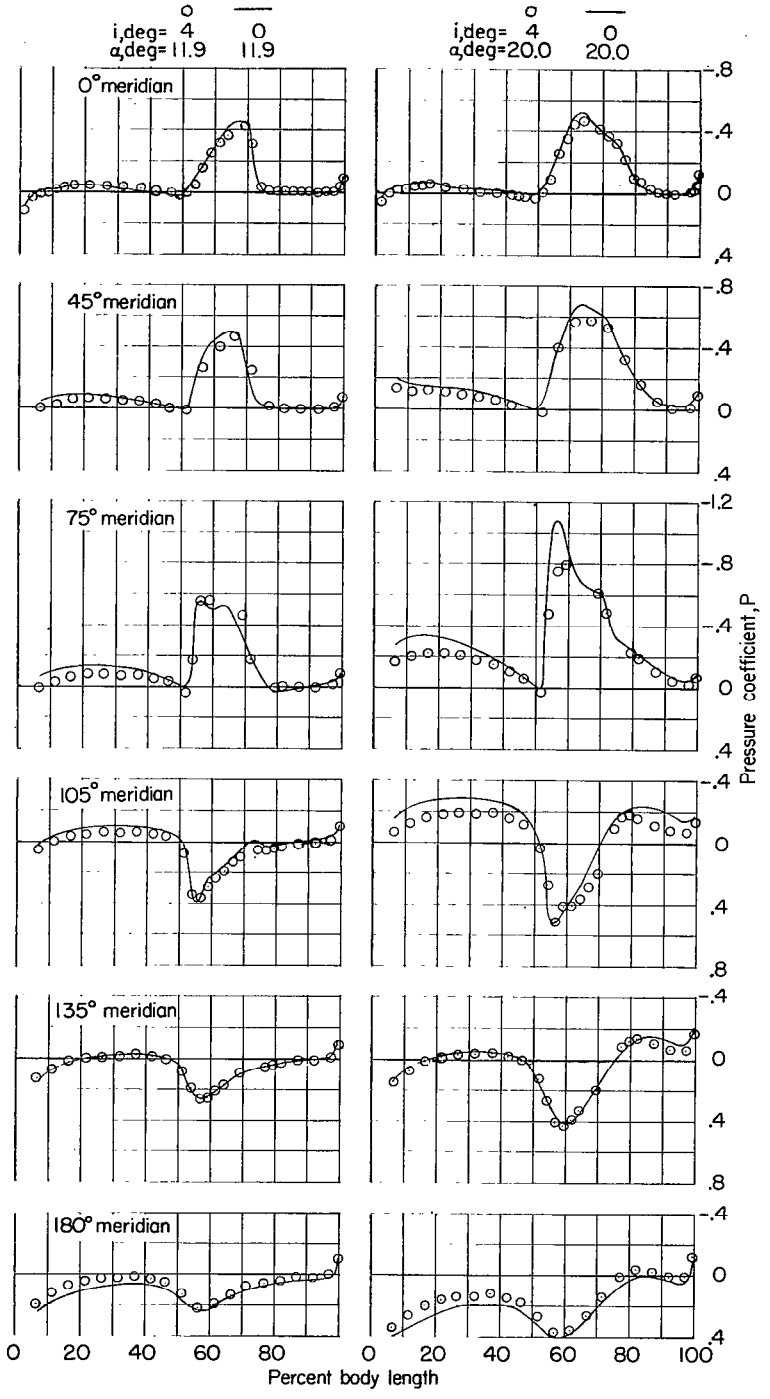

(d) Concluded.

Figure 3.- Continued.

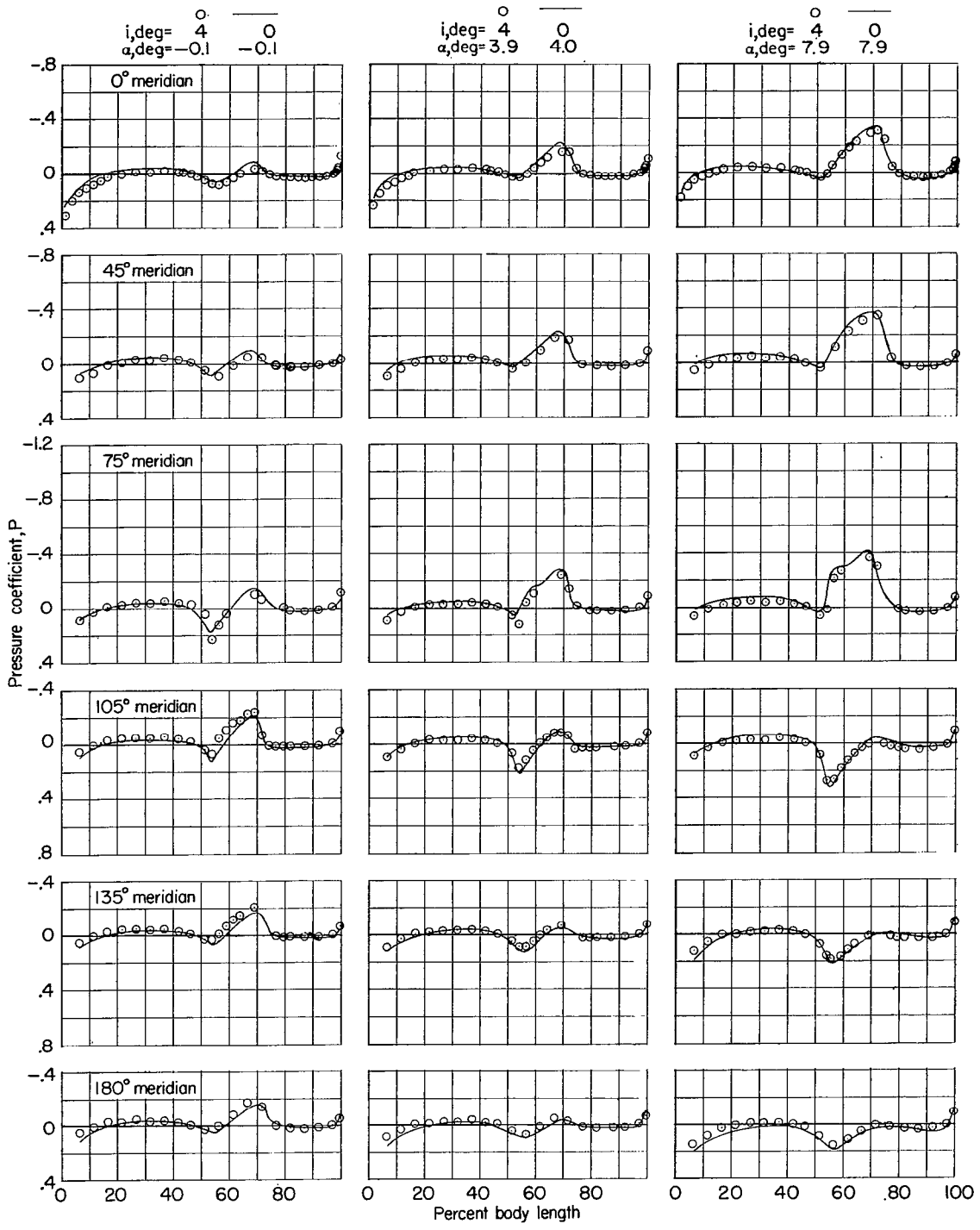

(e) M = 0.95.

Figure 3.- Continued.

[redacted]

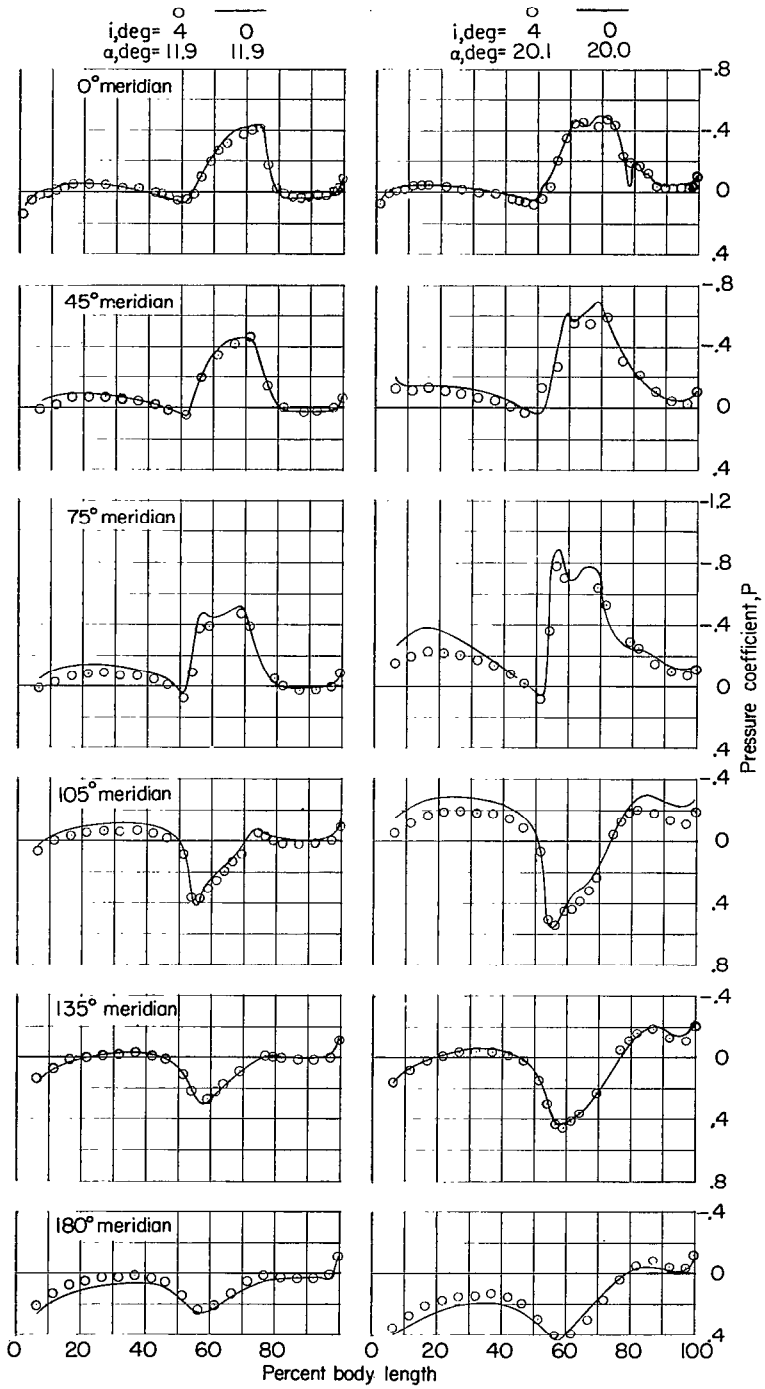

(e) Concluded.

Figure 3.- Continued.

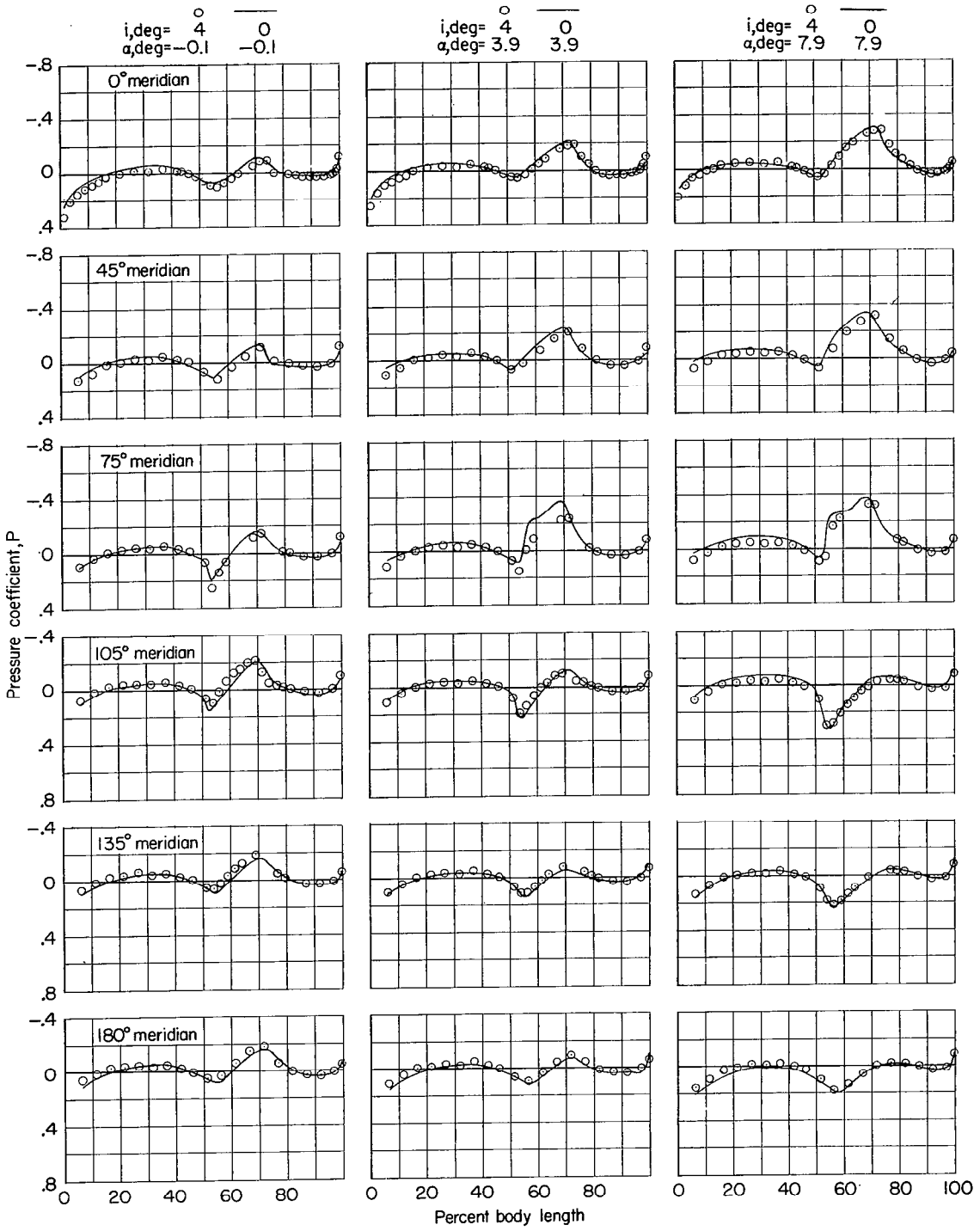

(f) M = 0.98.

Figure 3.- Continued.

[redacted]

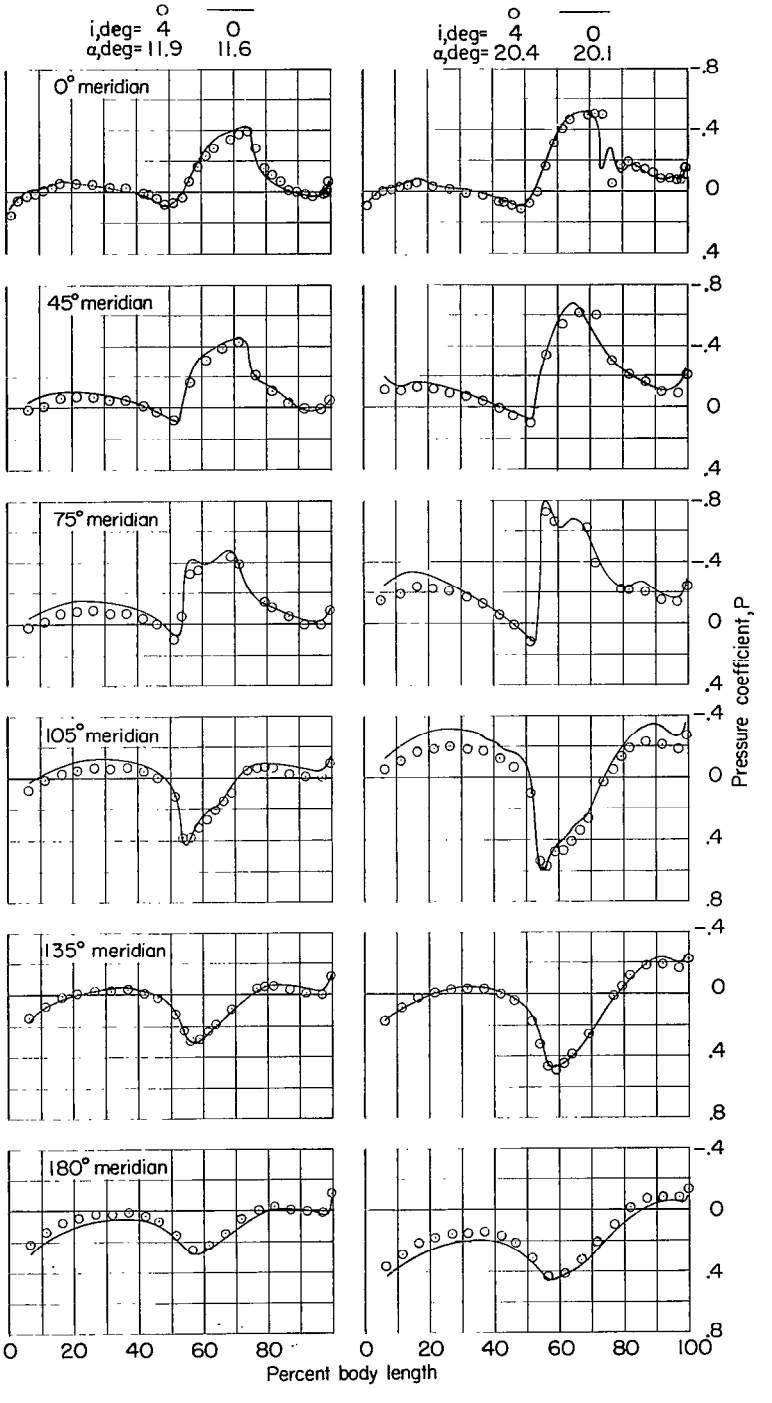

(f) Concluded.

Figure 3.- Continued.

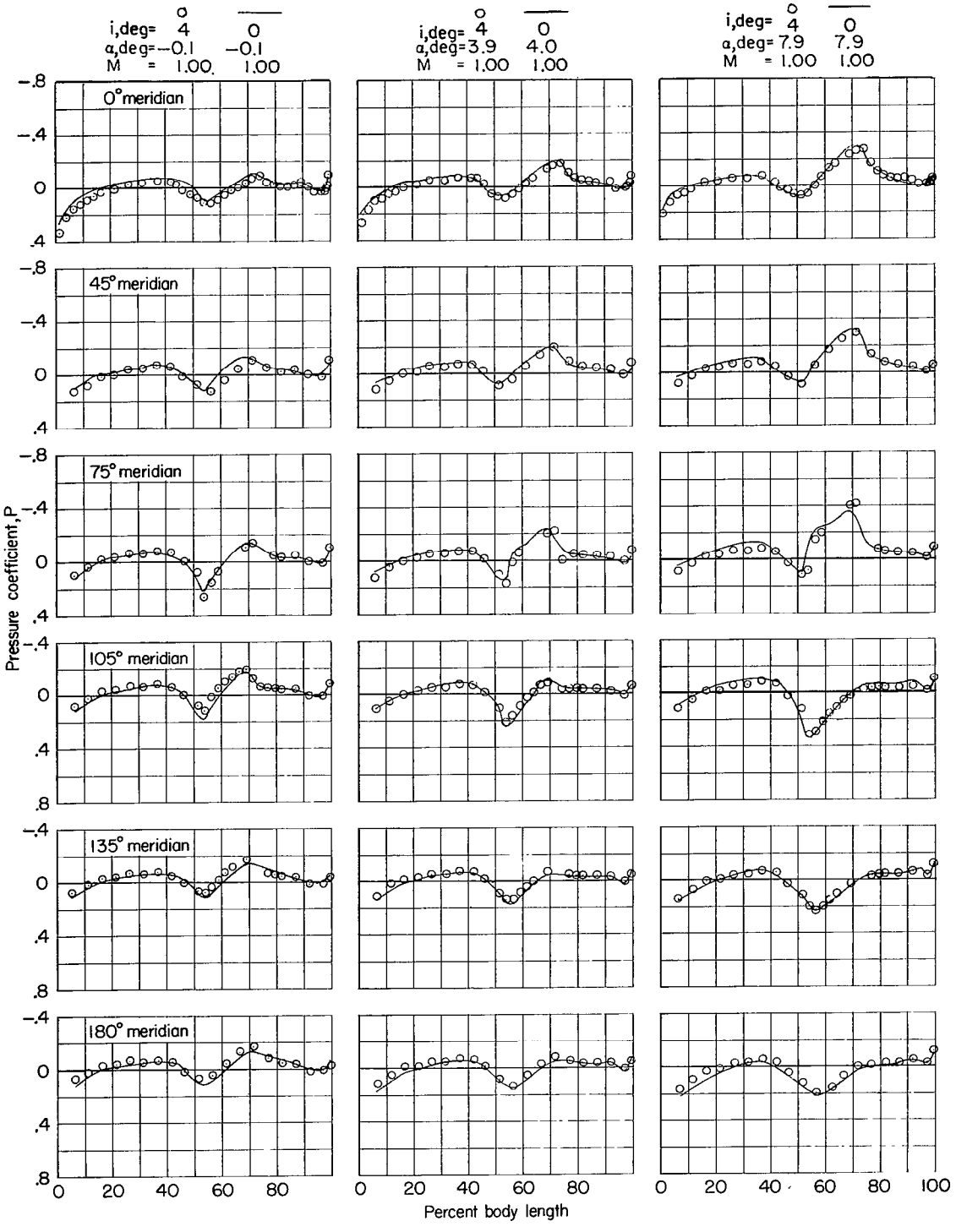

(g) M ≈ 1.00.

Figure 3.- Continued.

[redacted]

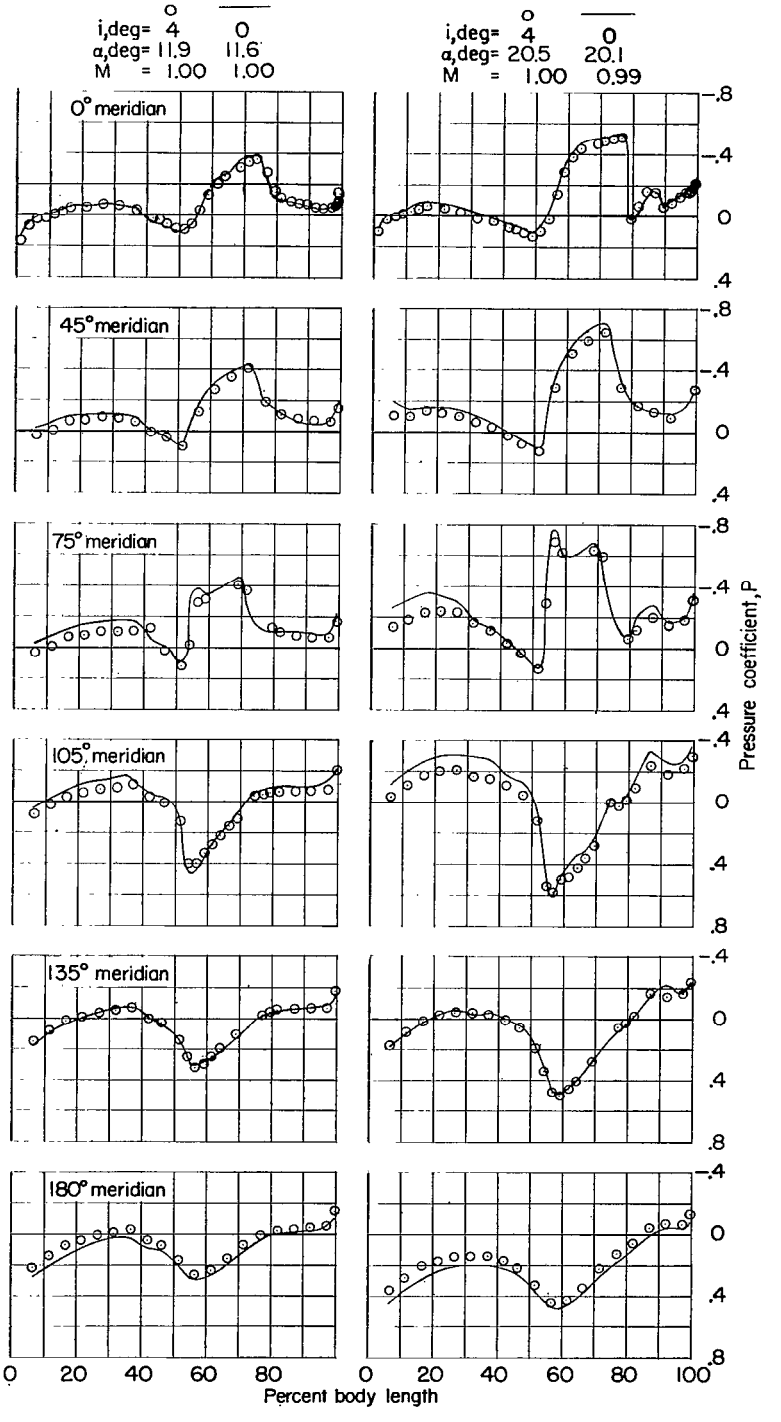

(g) Concluded.

Figure 3.- Continued.

[redacted]

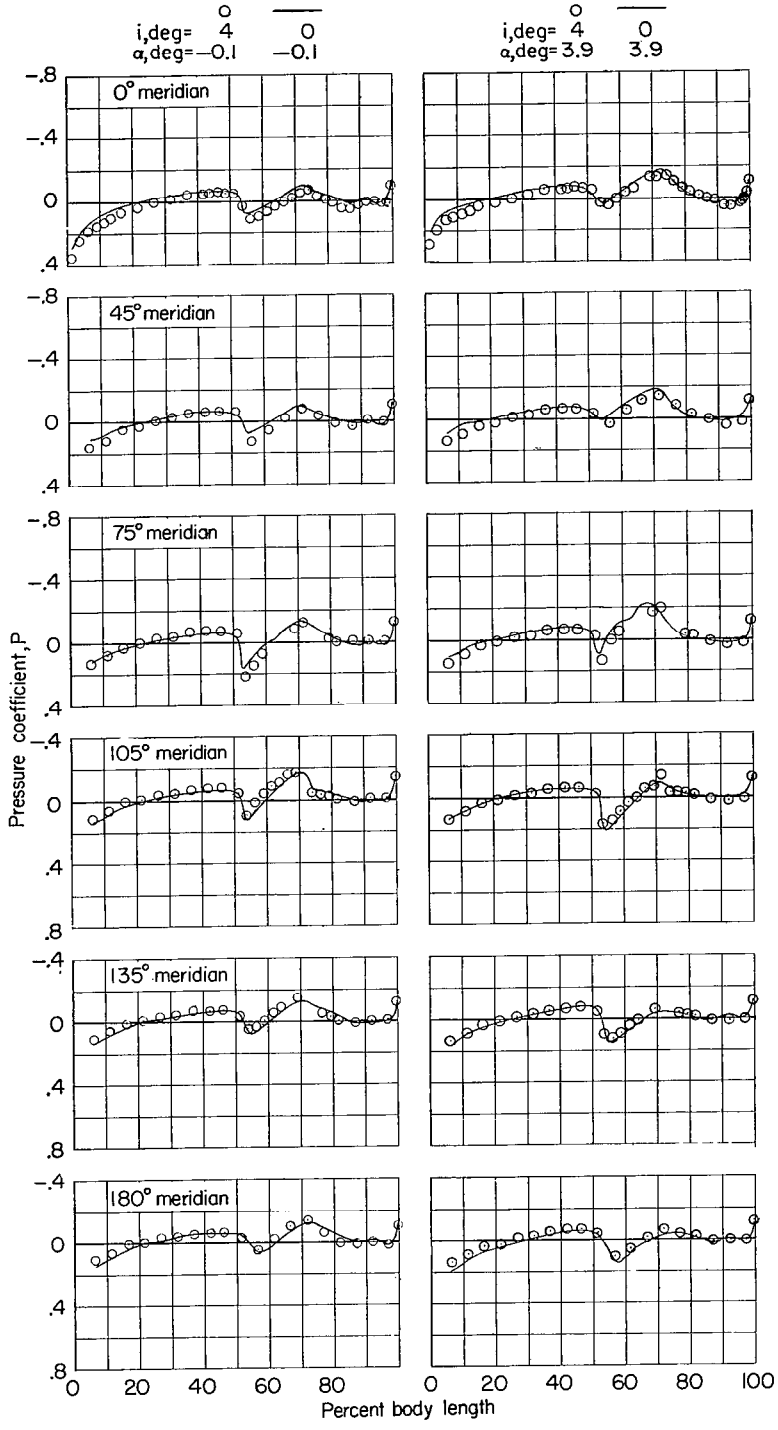

(h) M = 1.03.

Figure 3.- Continued.

[redacted]

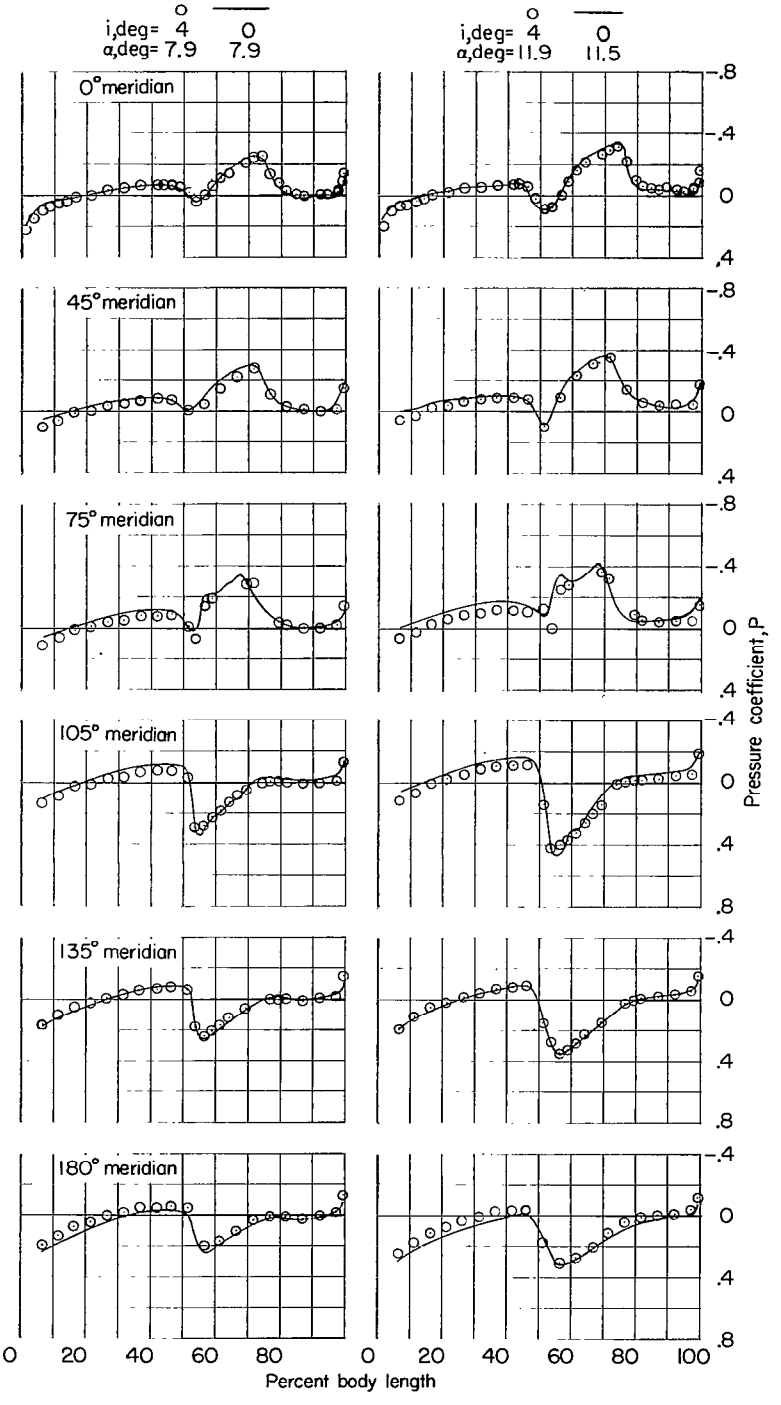

(h) Concluded.

Figure 3.- Continued.

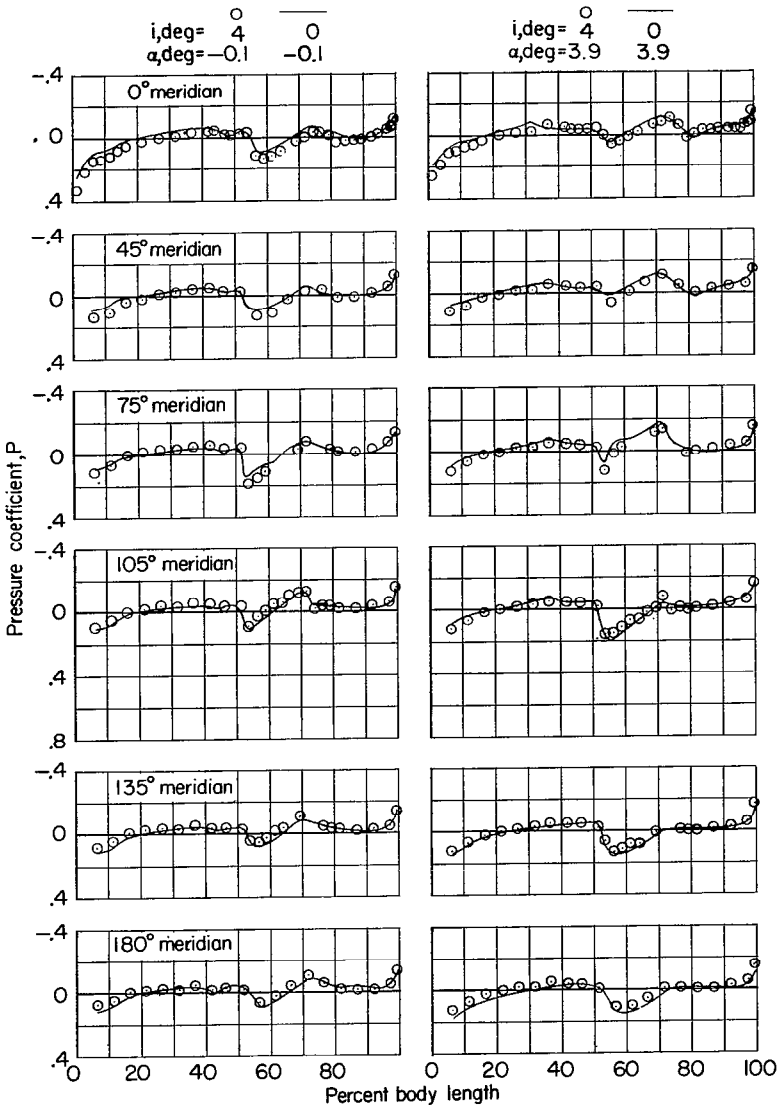

(i) M = 1.08.

Figure 3.- Continued.

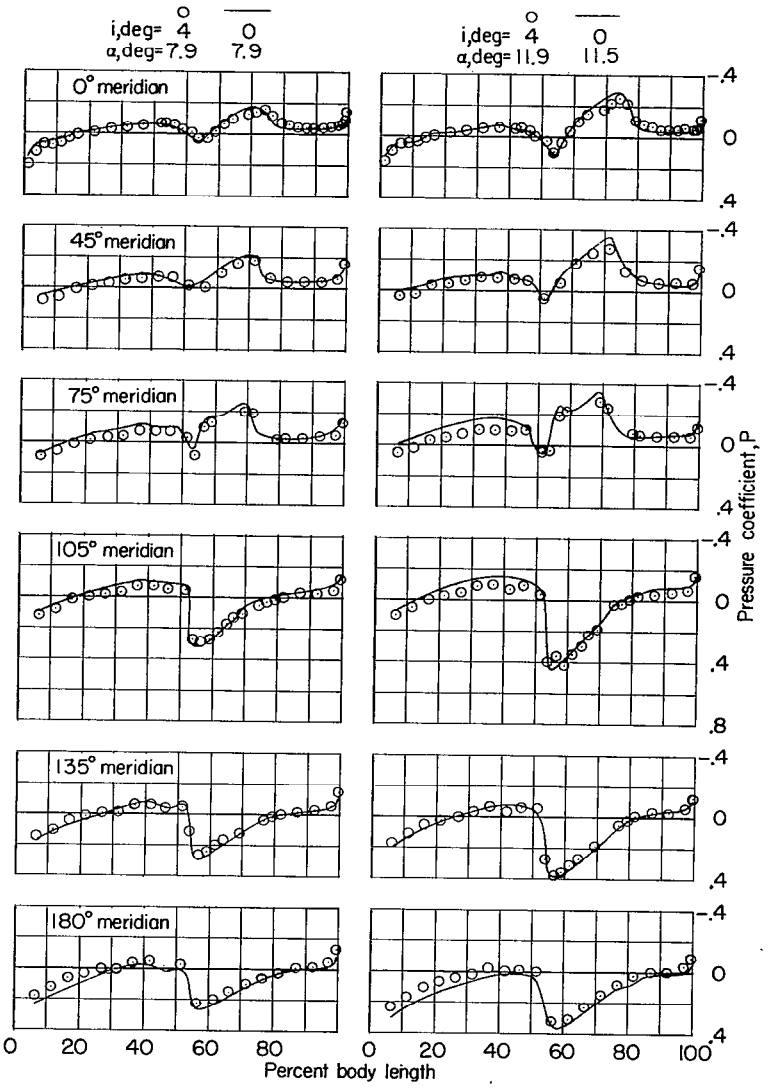

(i) Concluded.

Figure 3.- Continued.

[redacted]

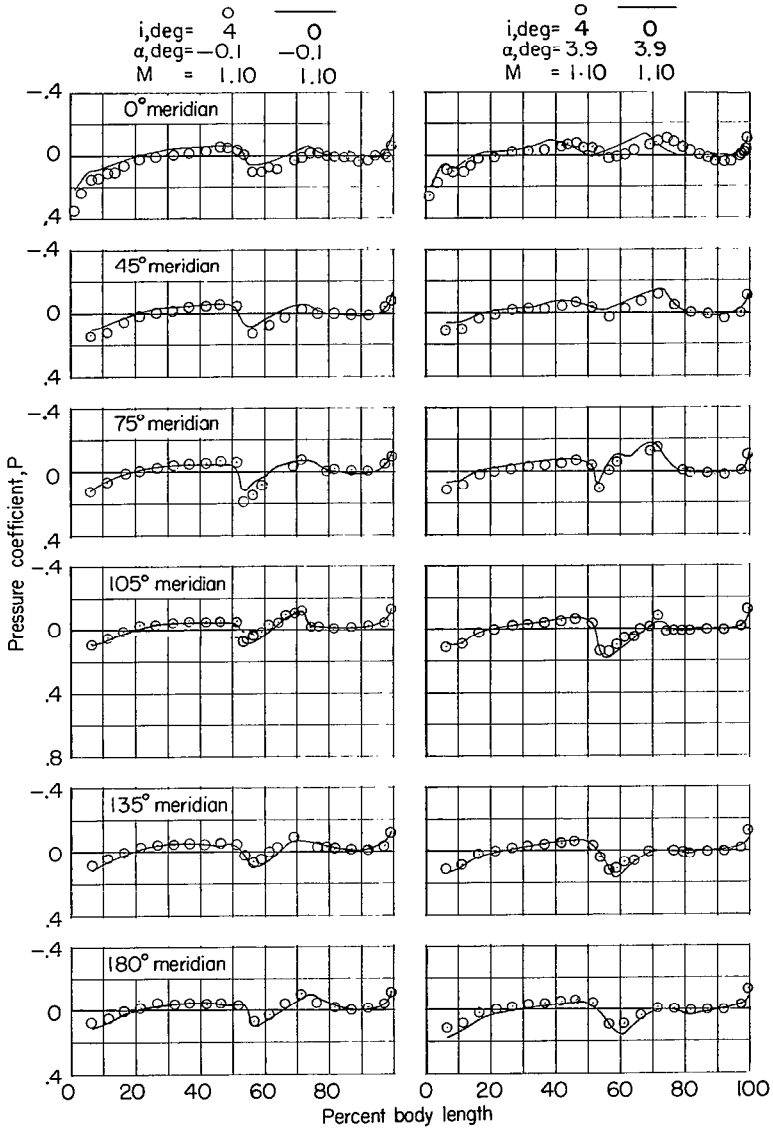

(j) $M \approx 1.10$.

Figure 3.- Continued.

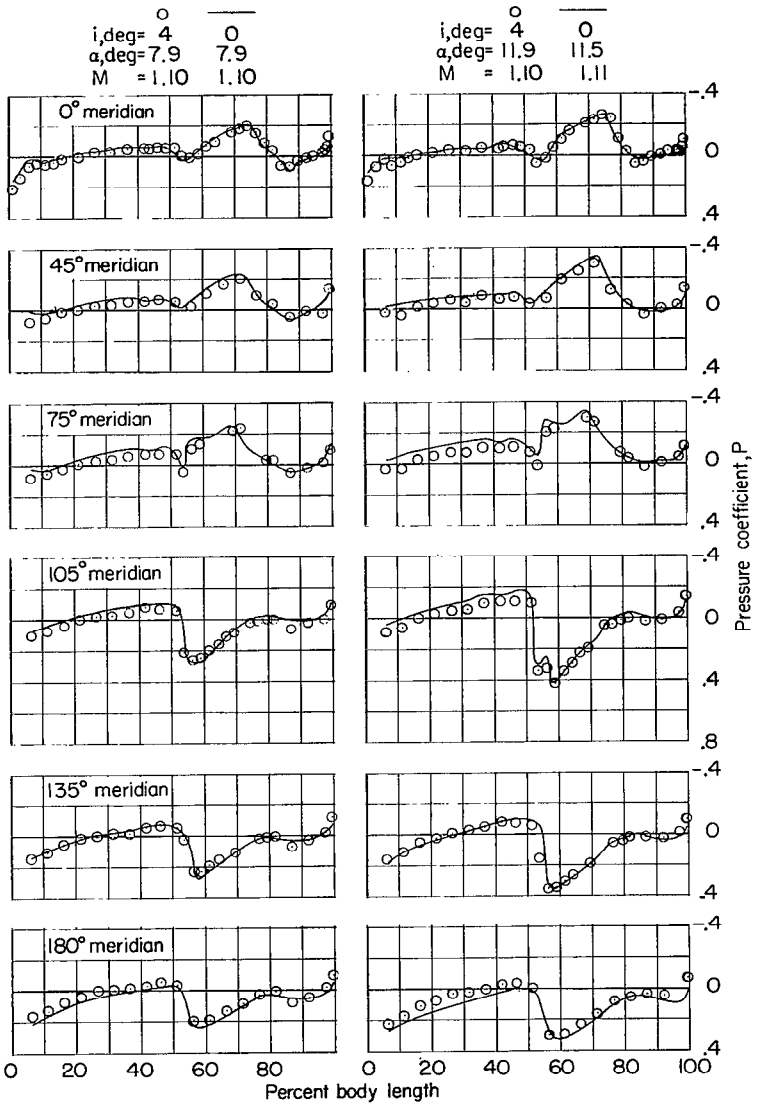

(j) Concluded.

Figure 3.- Continued.

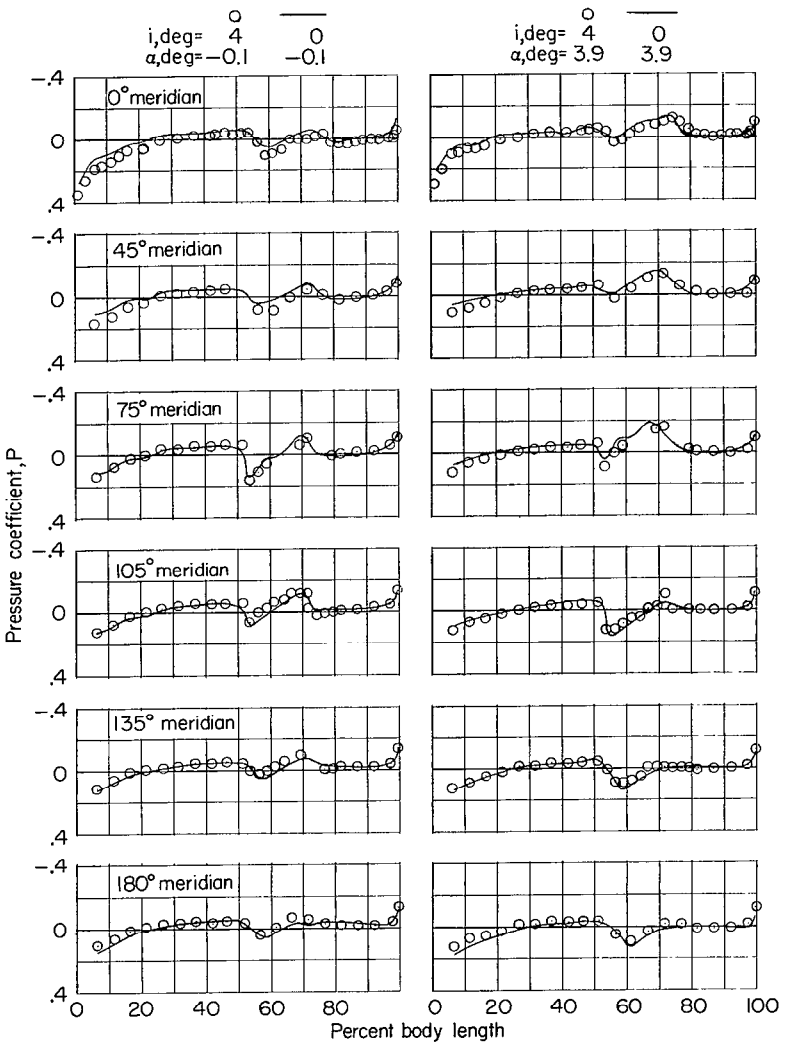

(k) M = 1.13.

Figure 3.- Continued.

[redacted]

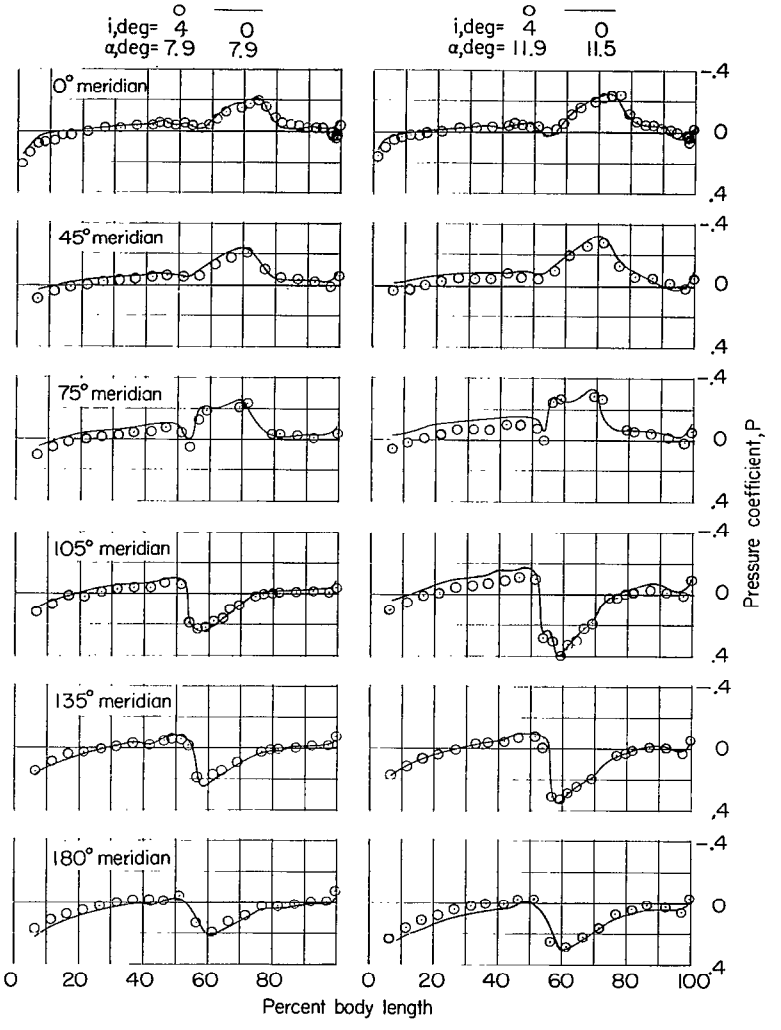

(k) Concluded.

Figure 3.- Concluded.

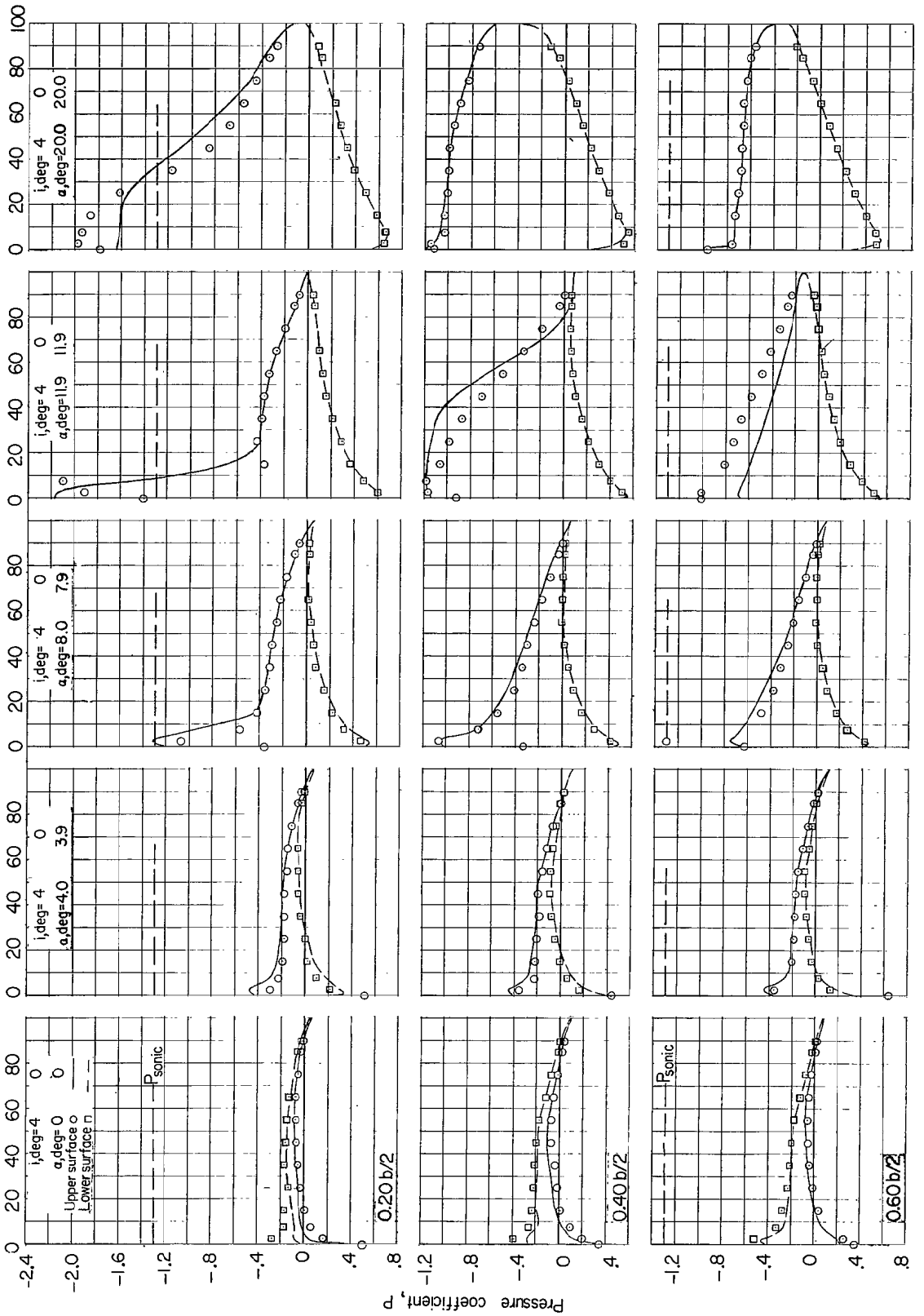
i,deg= 4 0
α,deg= 0 b
Upper surface o —
Lower surface □ – –
P_{sonic}
0.20b/2
0.40b/2
0.60b/2
i,deg= 4 0
α,deg=4.0 3.9
i,deg= 4 0
α,deg=8.0 7.9
i,deg= 4 0
α,deg=11.9 11.9
i,deg= 4 0
α,deg=20.0 20.0
Pressure coefficient, P

[redacted]

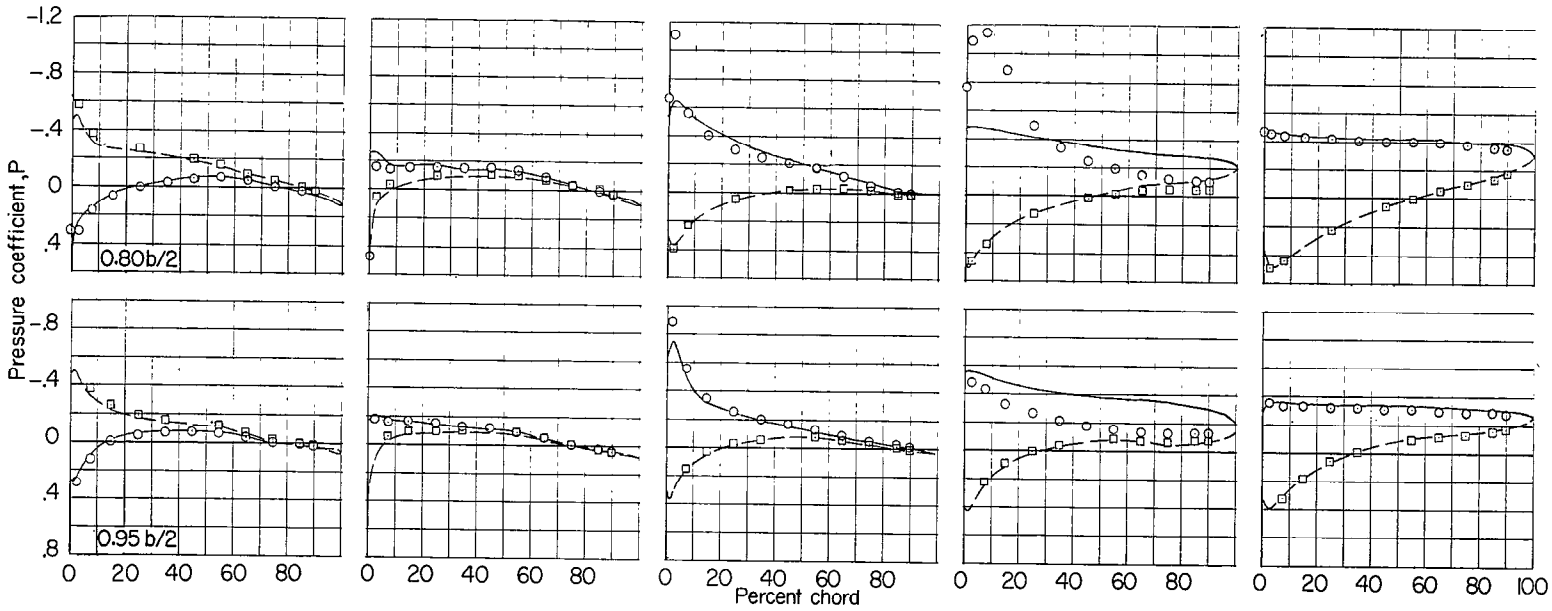

(a) M = 0.60.

Figure 4.- Comparison of pressure coefficients for the wing.

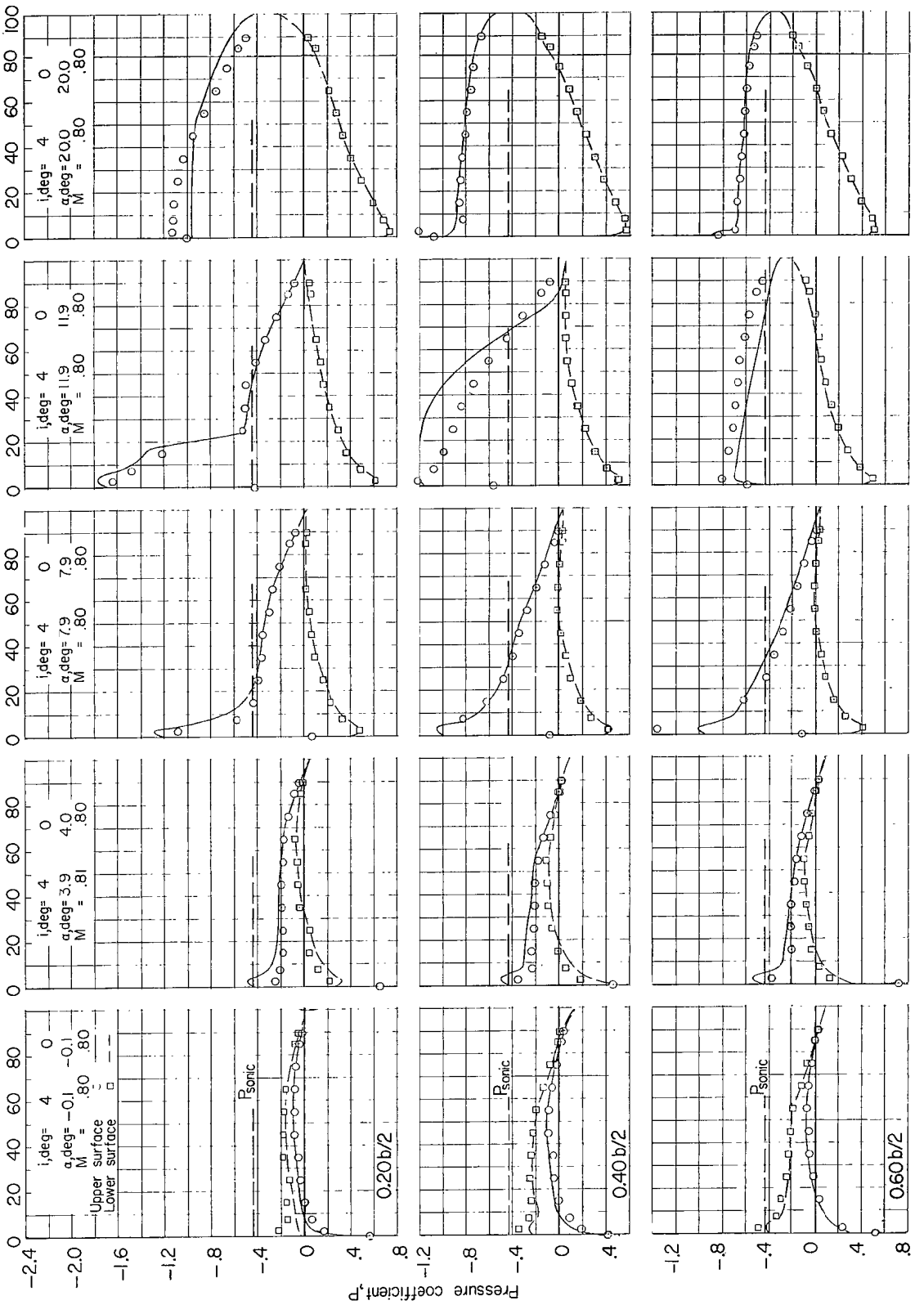
i,deg= 4 0
α,deg=-0.1 -0.1
M = .80 .80
Upper surface
Lower surface
Psonic
0.20b/2
i,deg= 4 0
α,deg=3.9 4.0
M = .81 .80
i,deg= 4 0
α,deg= 7.9 7.9
M = .80 .80
i,deg= 4 0
α,deg=11.9 11.9
M = .80 .80
i,deg= 4 0
α,deg=20.0 20.0
M = .80 .80
0.40b/2
0.60b/2
Pressure coefficient, P

[redacted]

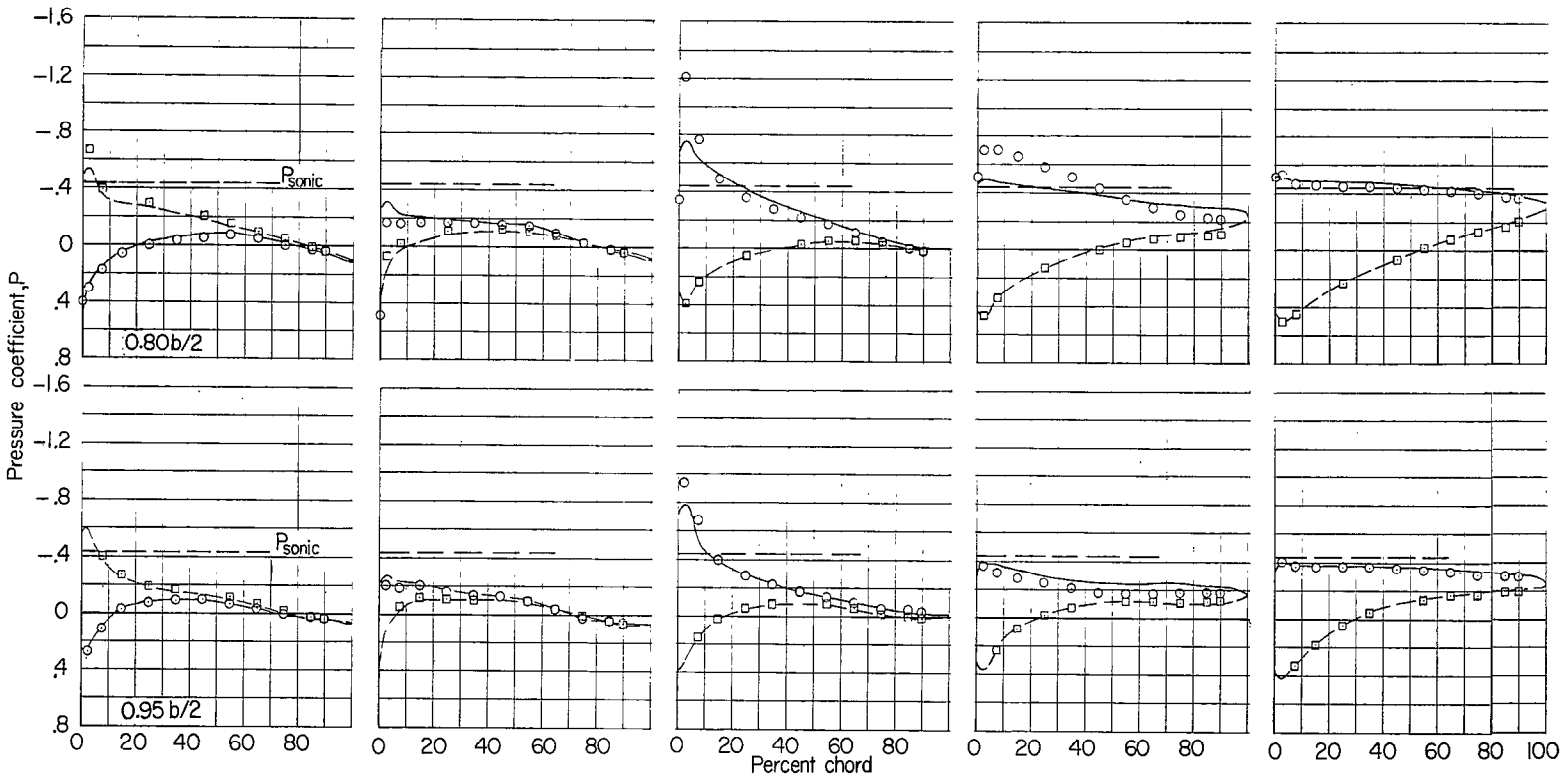

(b) $M \approx 0.80$.

Figure 4.- Continued.

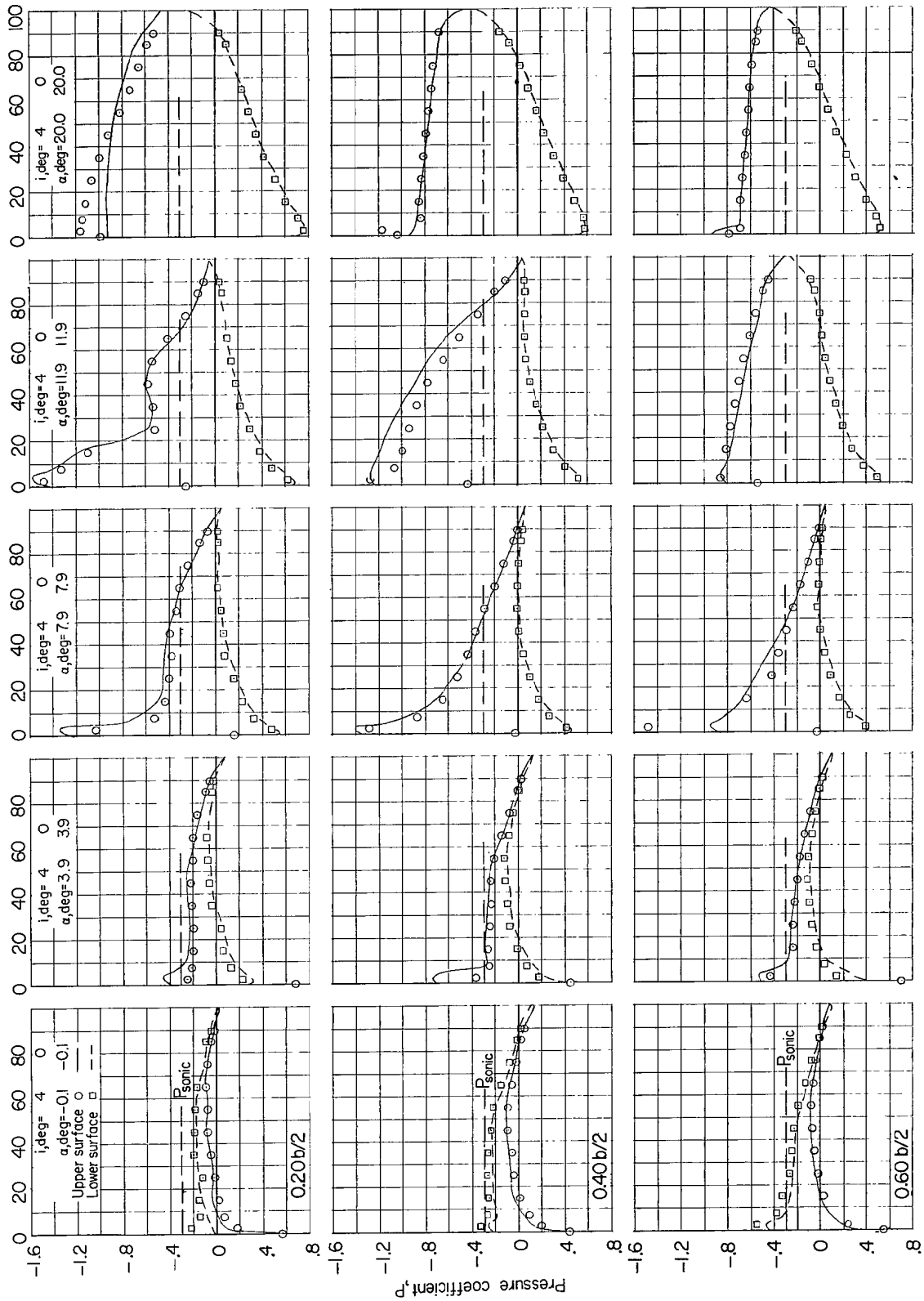
i,deg= 4 0
α,deg=−0.1 −0.1
Upper surface ○ ——
Lower surface □ – –
Psonic
0.20b/2
i,deg= 4 0
α,deg=3.9 3.9
i,deg= 4 0
α,deg=7.9 7.9
i,deg=4 0
α,deg=11.9 11.9
i,deg= 4 0
α,deg=20.0 20.0
0.40 b/2
0.60 b/2
Pressure coefficient, P
−1.6
−1.2
−.8
−.4
0
.4
.8
0
20
40
60
80
100

[redacted]

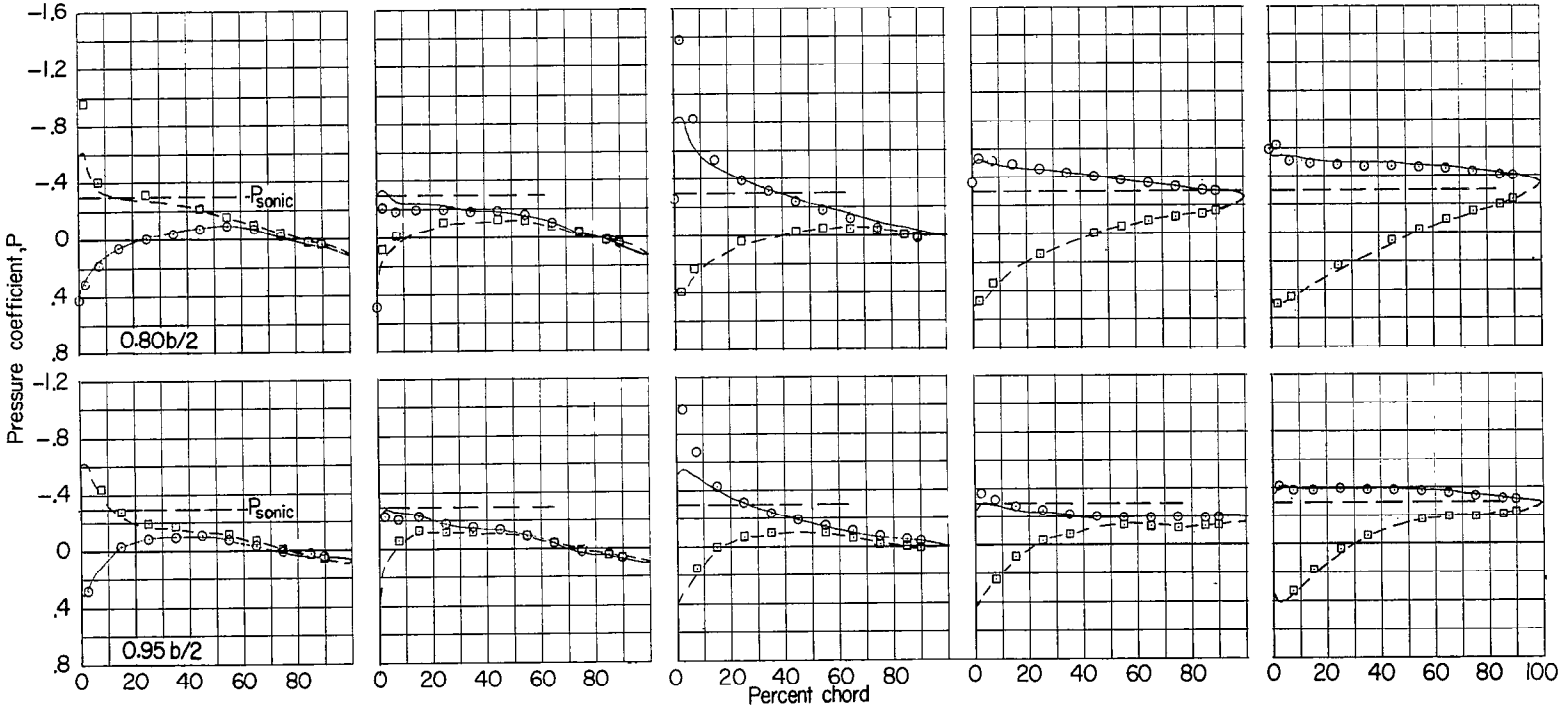

(c) M = 0.85.

Figure 4.- Continued.

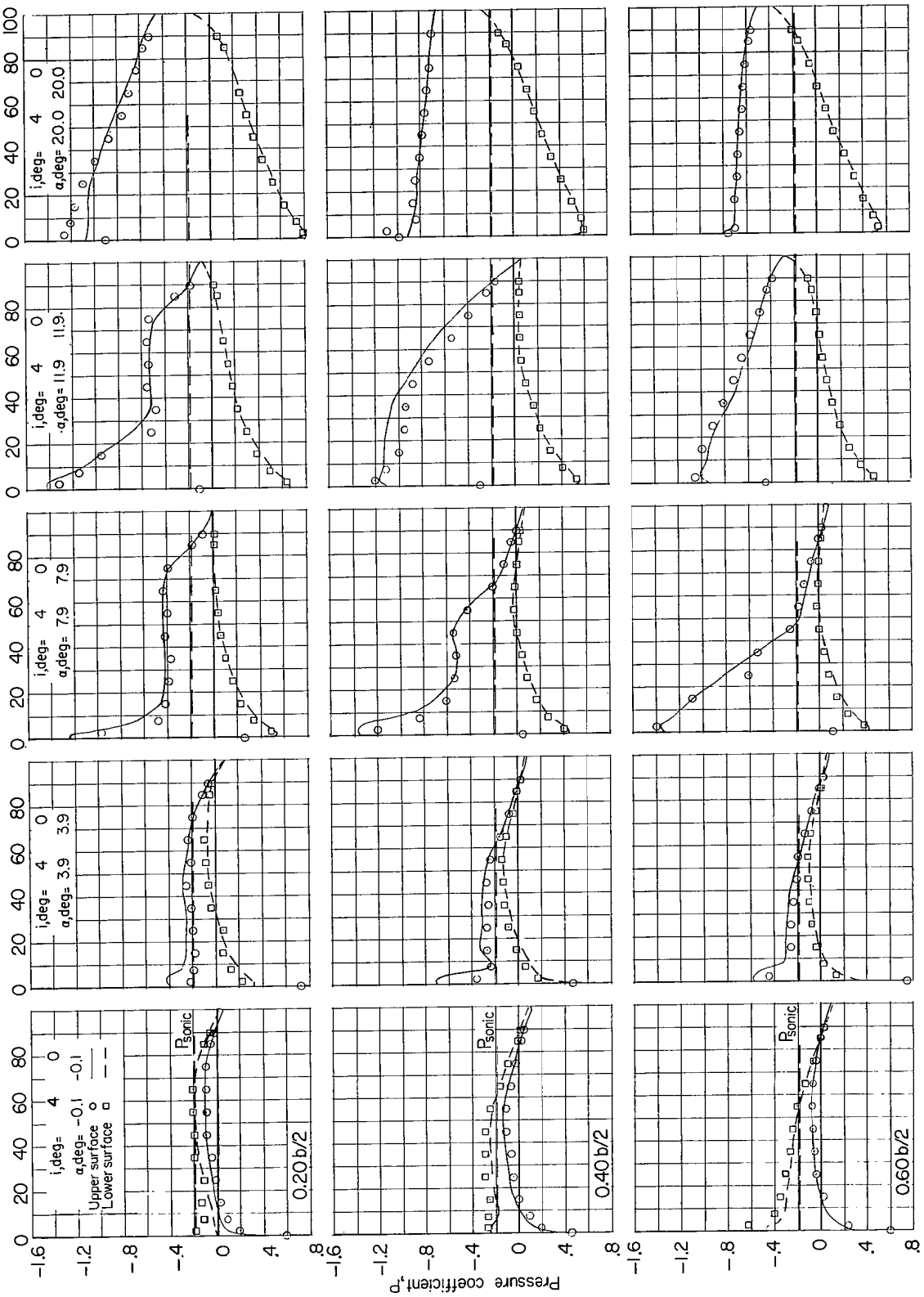
i,deg= 4 0
α,deg= -0.1 -0.1
Upper surface
Lower surface
i,deg= 4 0
α,deg= 3.9 3.9
i,deg= 4 0
α,deg= 7.9 7.9
i,deg= 4 0
α,deg= 11.9 11.9
i,deg= 4 0
α,deg= 20.0 20.0
Psonic
0.20b/2
0.40b/2
0.60b/2
Pressure coefficient, cp

[redacted]

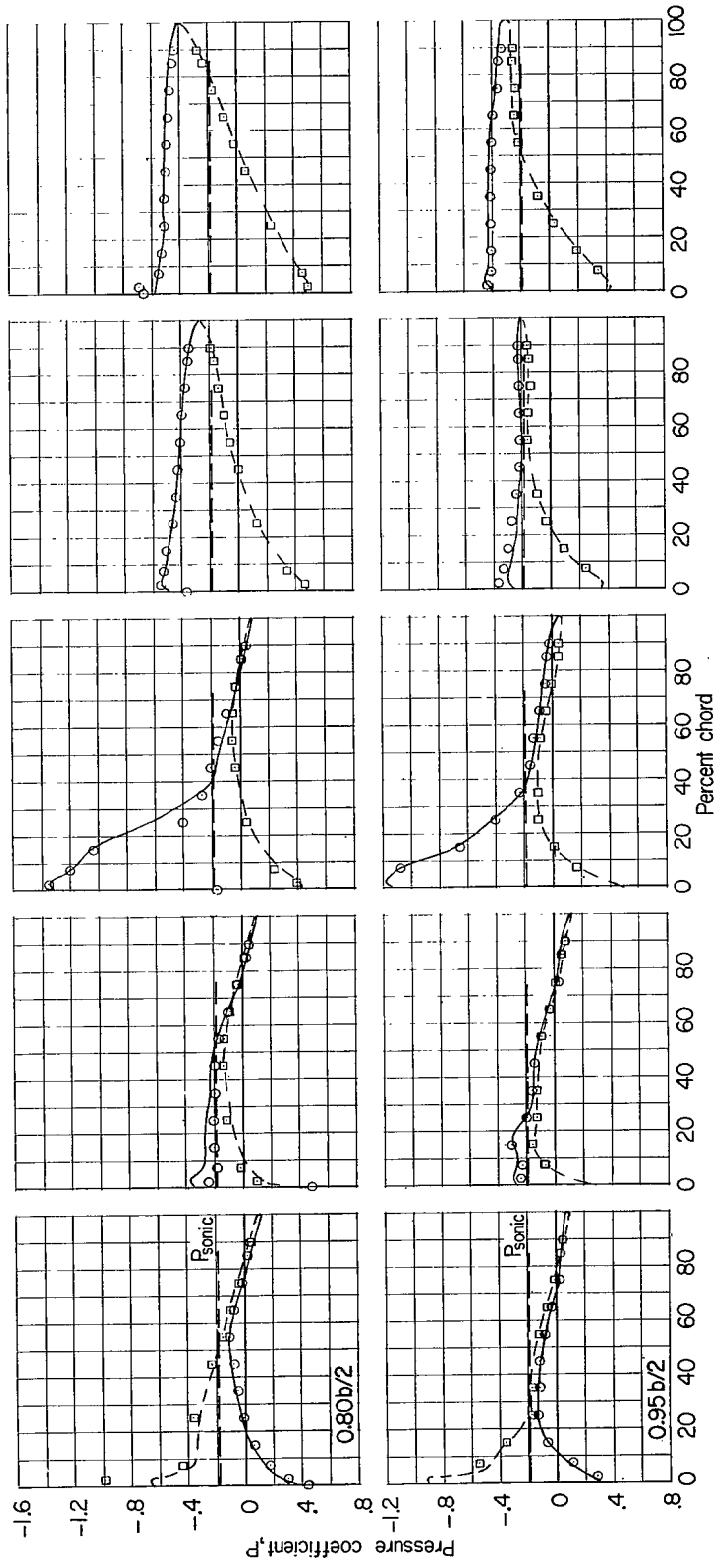

(d) M = 0.90.

Figure 4.- Continued.

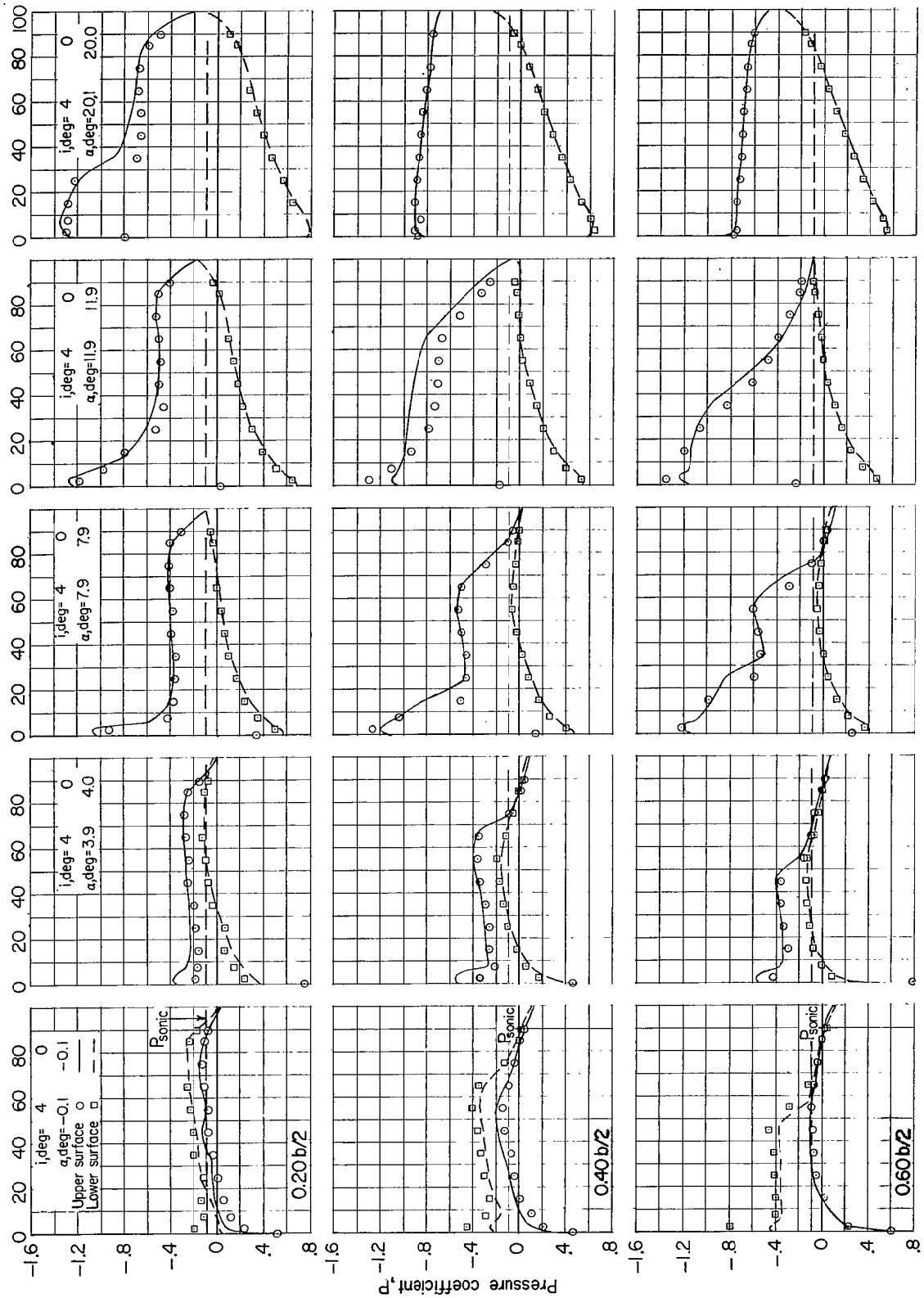
i,deg= 4 0
α,deg=−0.1 −0.1
Upper surface ○
Lower surface □
P_{sonic}
0.20b/2
i,deg= 4 0
α,deg=3.9 4.0
i,deg= 4 0
α,deg=7.9 7.9
i,deg= 4 0
α,deg=11.9 11.9
i,deg= 4 0
α,deg=20.1 20.0
0.40b/2
0.60b/2
Pressure coefficient, P

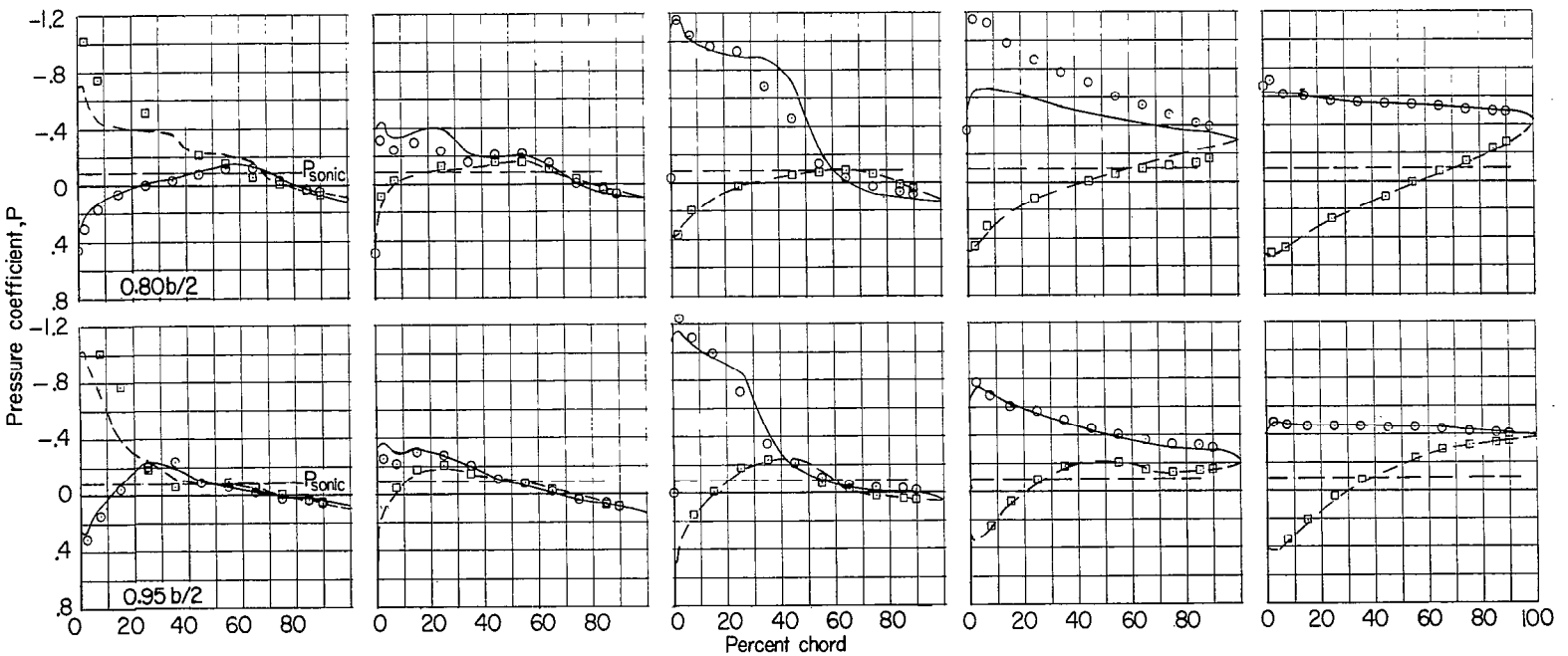

(e) M = 0.95.

Figure 4.- Continued.

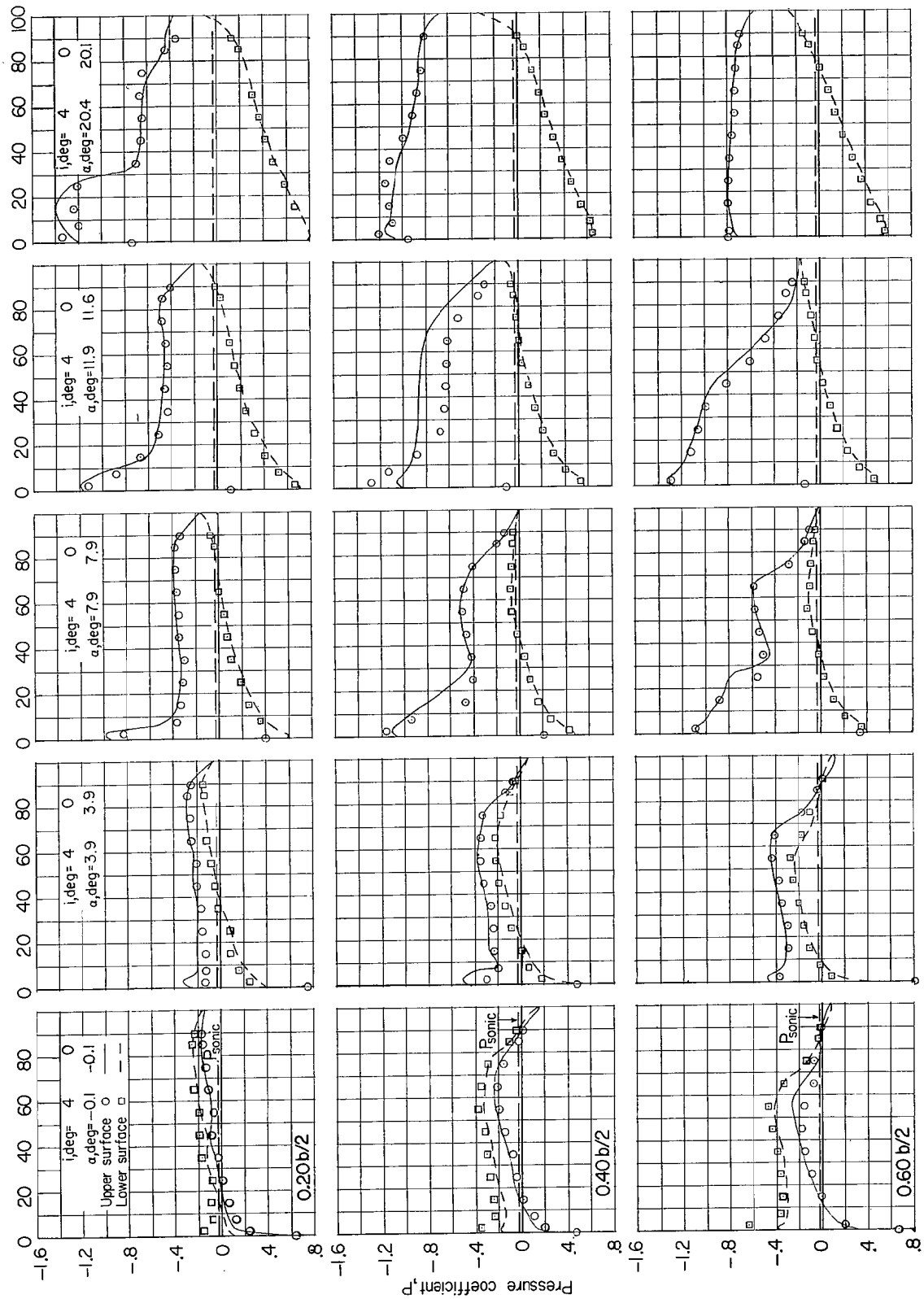
i,deg= 4 0
α,deg=-0.1 -0.1
Upper surface ○ ——
Lower surface □ — —
Psonic
0.20b/2
i,deg= 4 0
α,deg=3.9 3.9
i,deg= 4 0
α,deg=7.9 7.9
i,deg= 4 0
α,deg=11.9 11.6
i,deg= 4 0
α,deg=20.4 20.1
0.40b/2
0.60 b/2
Pressure coefficient, P
-1.6
-1.2
-.8
-.4
0
.4
.8
0
20
40
60
80
100

[redacted]

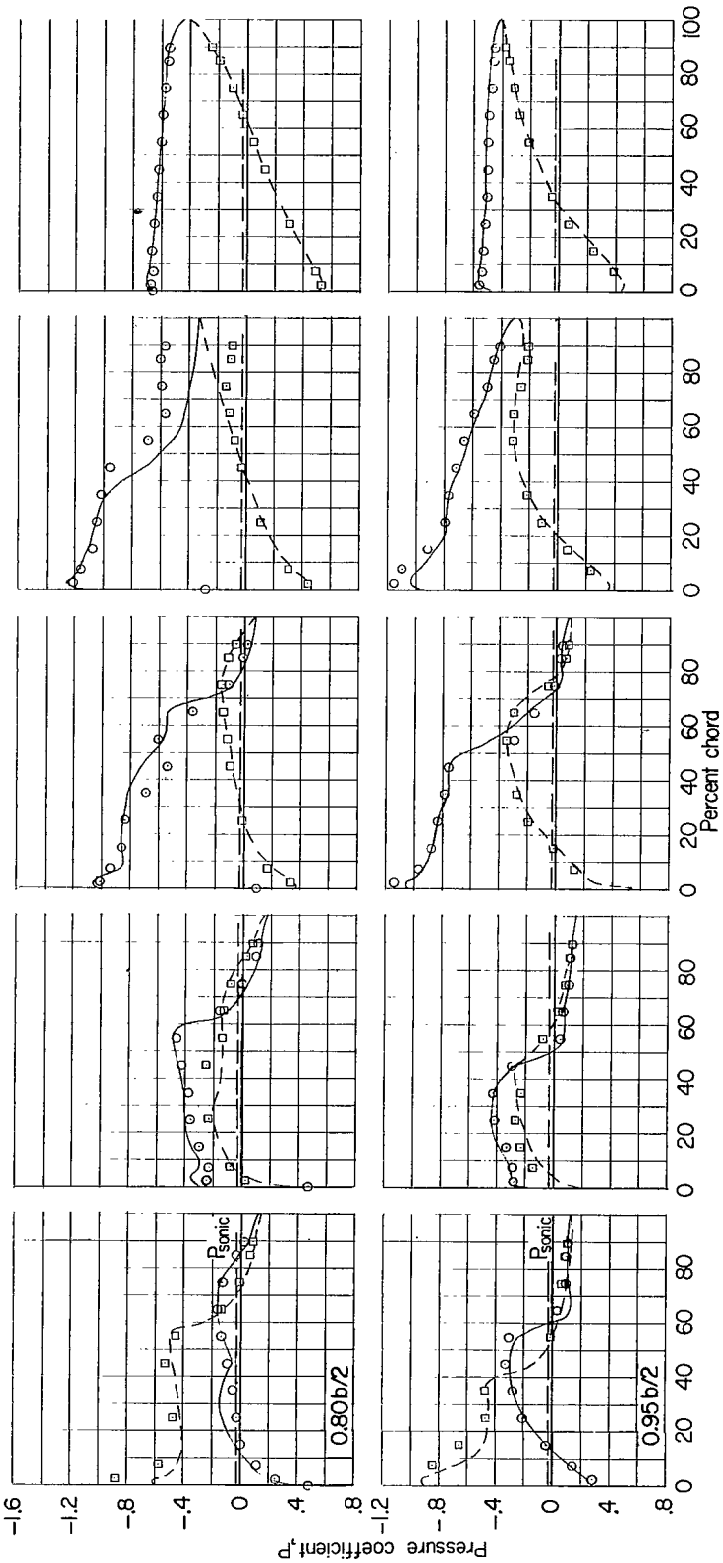

(f) M = 0.98.

Figure 4.- Continued.

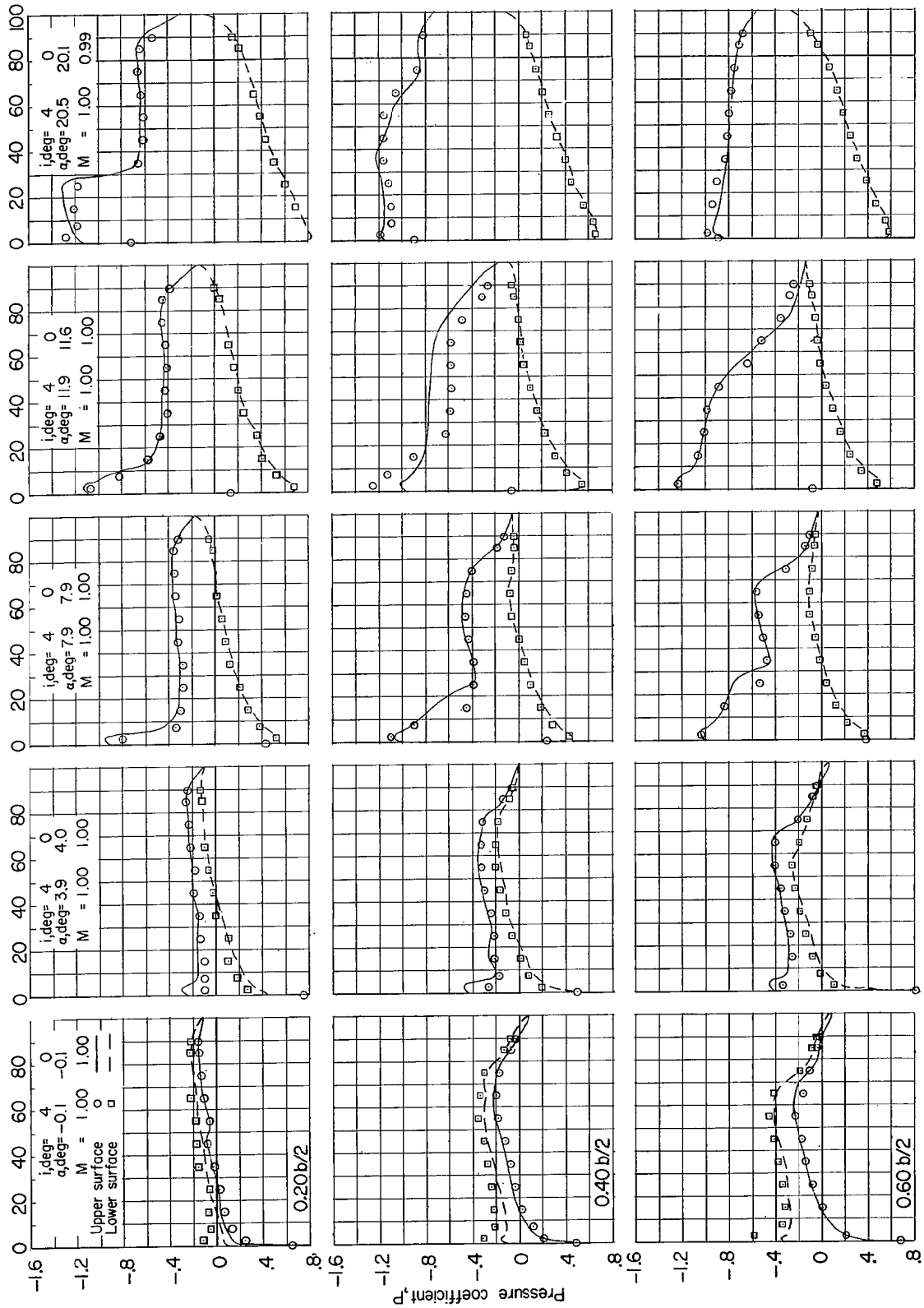
i,deg= 4 0
α,deg=-0.1 -0.1
M = 1.00 1.00
Upper surface o
Lower surface □
0.20b/2
i,deg= 4 0
α,deg= 3.9 4.0
M = 1.00 1.00
i,deg= 4 0
α,deg= 7.9 7.9
M = 1.00 1.00
i,deg= 4 0
α,deg= 11.9 11.6
M = 1.00 1.00
i,deg= 4 0
α,deg= 20.5 20.1
M = 1.00 0.99
0.40 b/2
0.60 b/2
Pressure coefficient, P
-1.6
-1.2
-.8
-.4
0
.4
.8
0
20
40
60
80
100

[redacted]

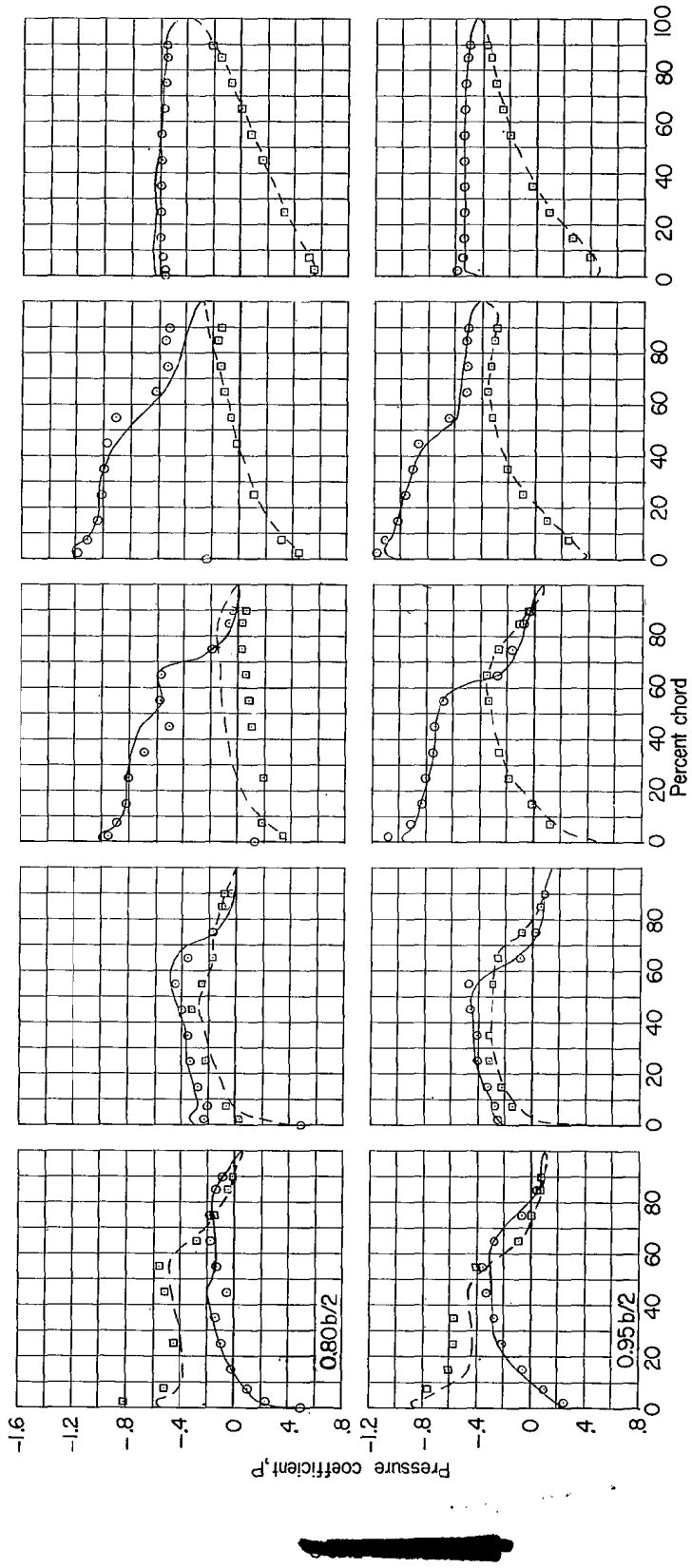

(g) $M \approx 1.00$.

Figure 4.- Continued.

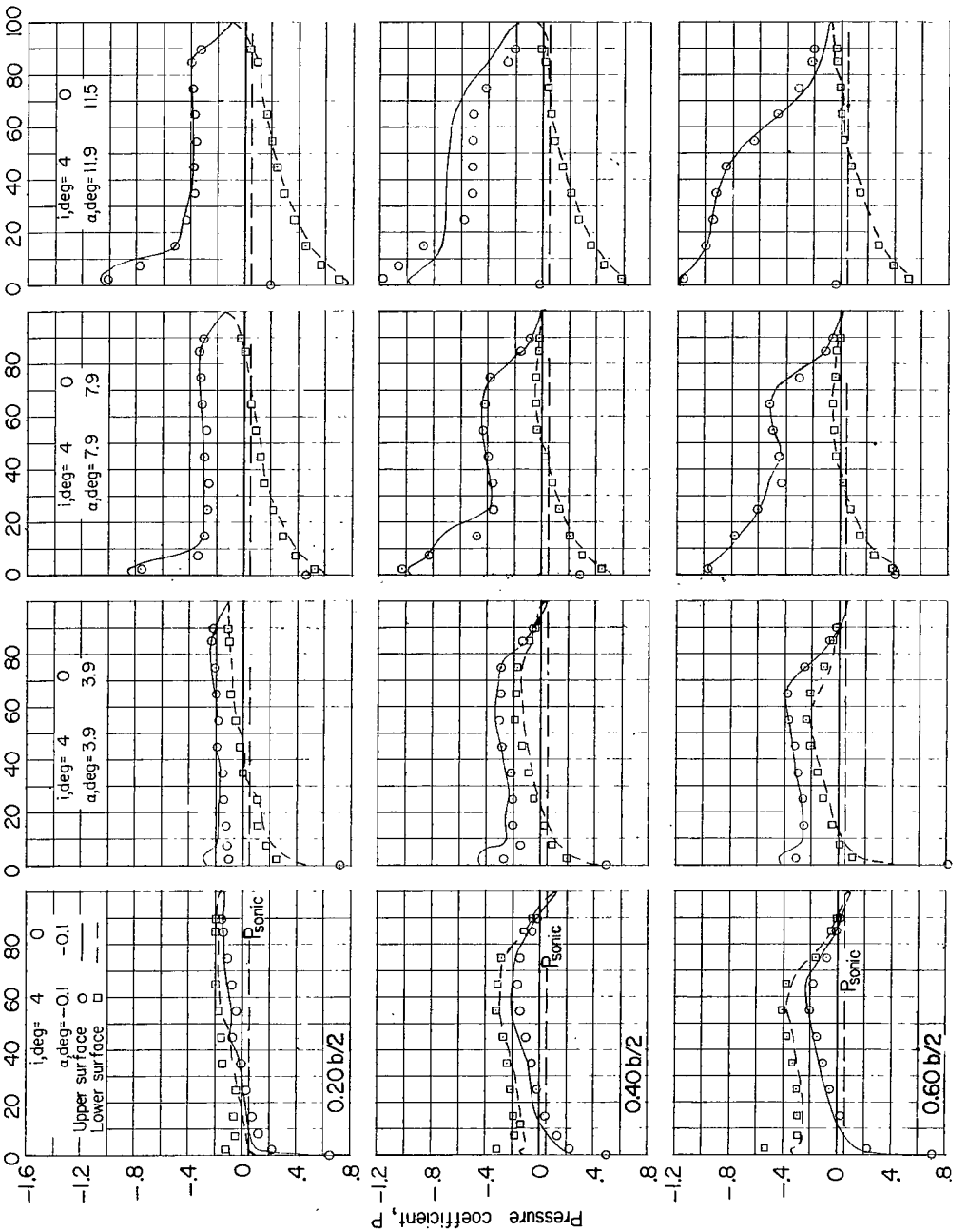
Pressure coefficient, P
0.20 b/2
0.40 b/2
0.60 b/2
Psonic
i,deg= 4 0 −0.1
α,deg=−0.1
Upper surface o
Lower surface □
i,deg= 4 0
α,deg= 3.9
i,deg= 4 0
α,deg= 7.9
i,deg= 4 0
α,deg= 11.9

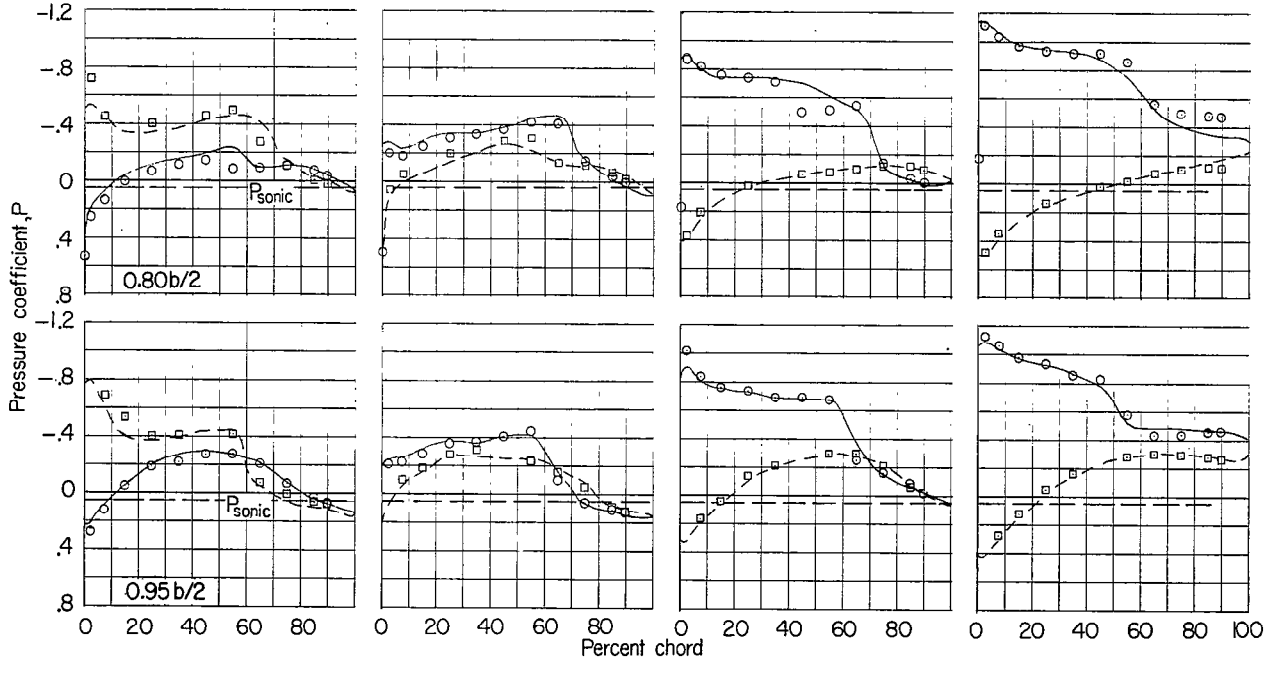

(h) M = 1.03.

Figure 4.- Continued.

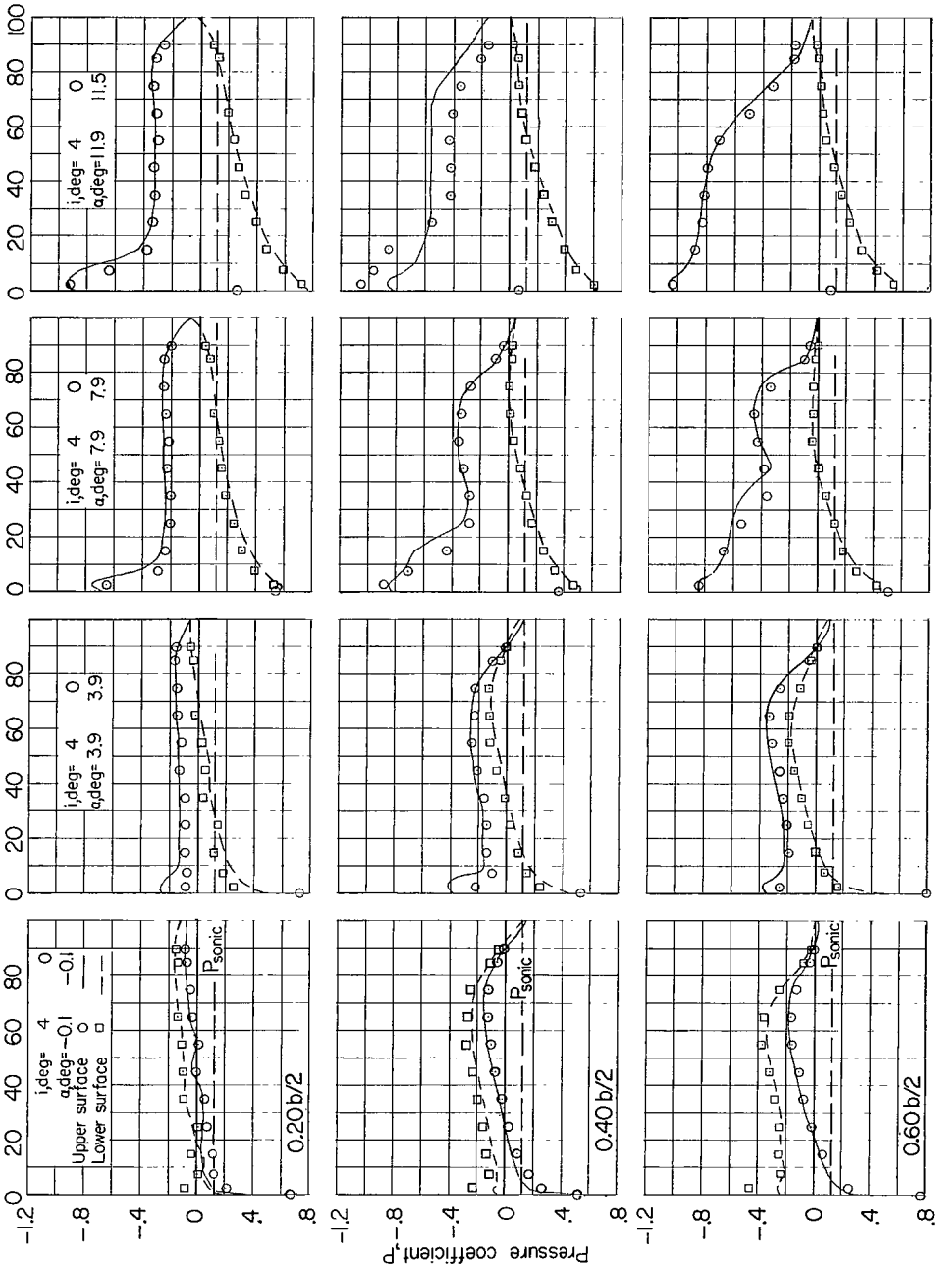
i,deg= 4 0 −0.1
α,deg=−0.1
Upper surface
Lower surface
P sonic
0.20b/2
0.40b/2
0.60b/2
i,deg= 4 0
α,deg= 3.9 3.9
i,deg= 4 0
α,deg= 7.9 7.9
i,deg= 4 0
α,deg=11.9 11.5
Pressure coefficient, P

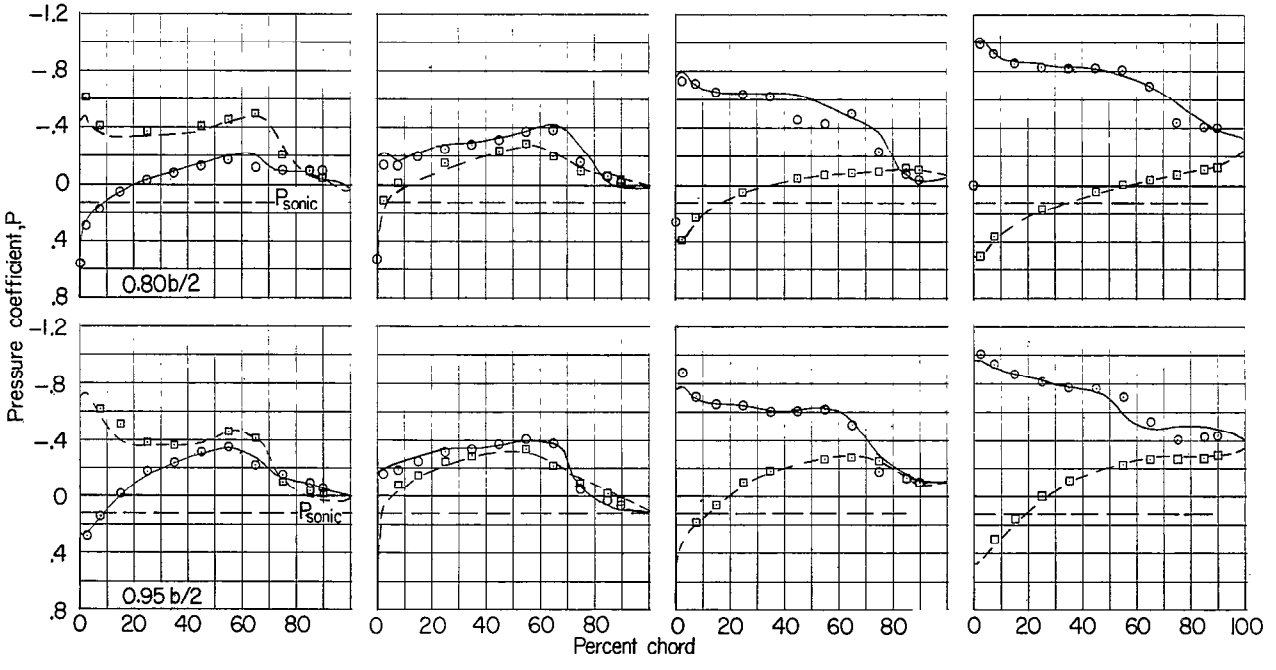

(i) M = 1.08.

Figure 4.- Continued.

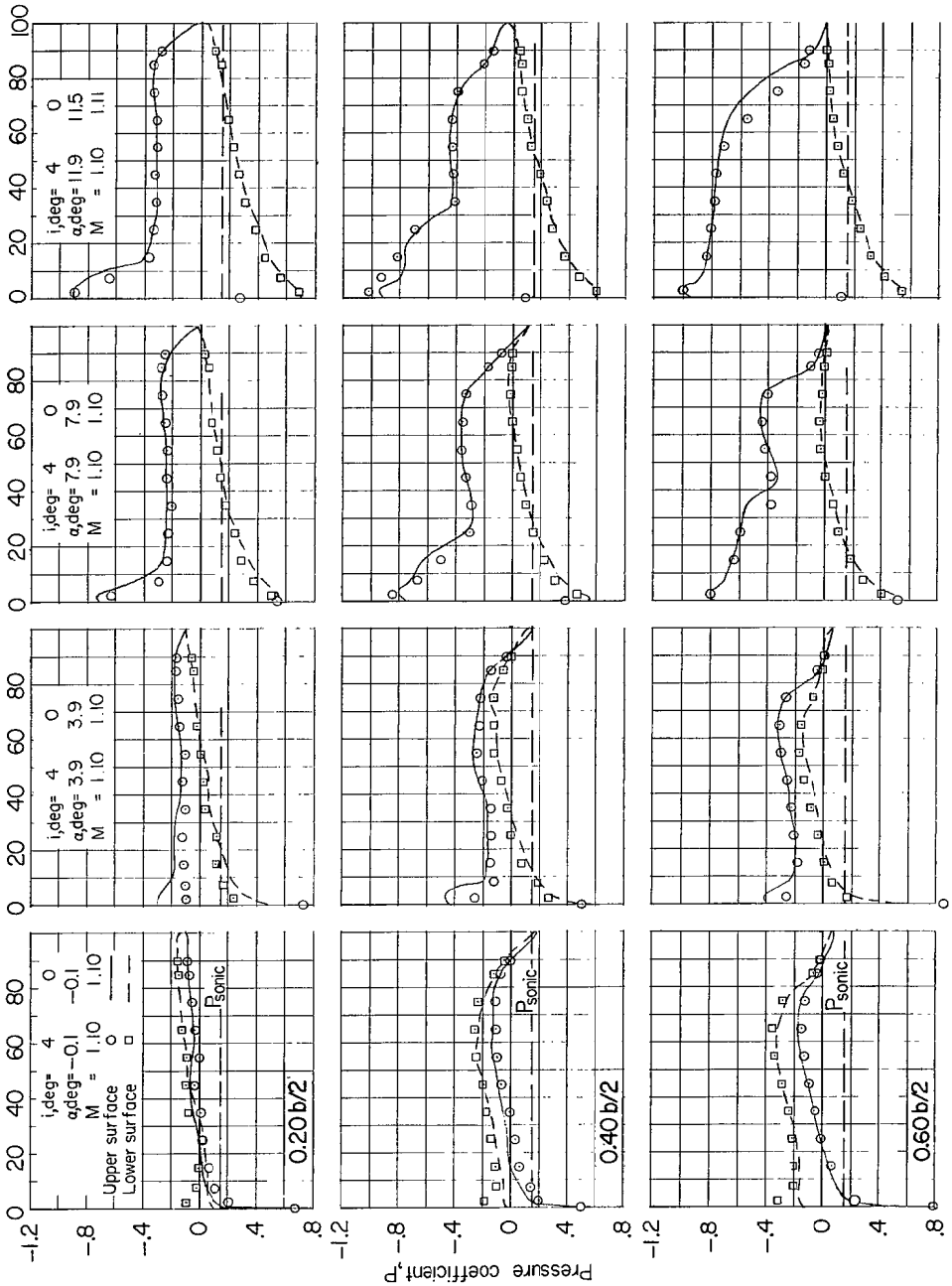
i,deg= 4 0
α,deg=-0.1 -0.1
M = 1.10 1.10
Upper surface ○ ——
Lower surface □ — —
i,deg= 4 0
α,deg= 3.9 3.9
M = 1.10 1.10
i,deg= 4 0
α,deg= 7.9 7.9
M = 1.10 1.10
i,deg= 4 0
α,deg= 11.9 11.5
M = 1.10 1.11
Psonic
0.20b/2
0.40b/2
0.60b/2
Pressure coefficient, P
-1.2
-.8
-.4
0
.4
.8
0
20
40
60
80
100

[redacted]

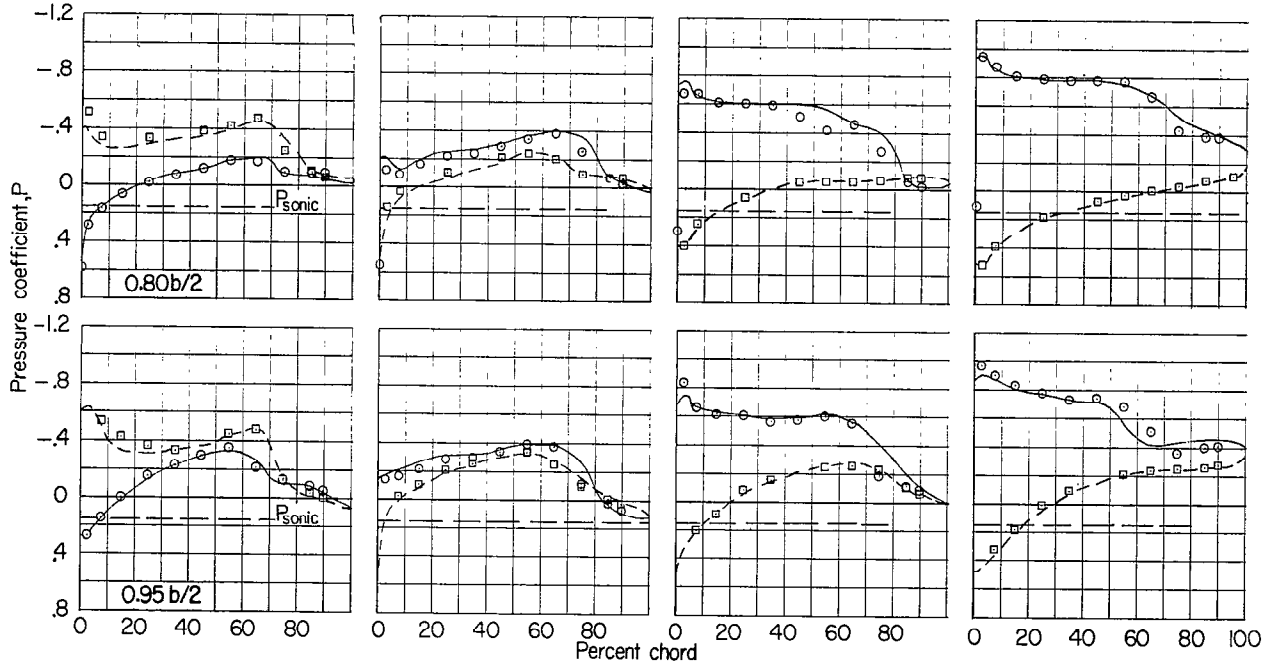

(j) $M \approx 1.10$.

Figure 4.- Continued.

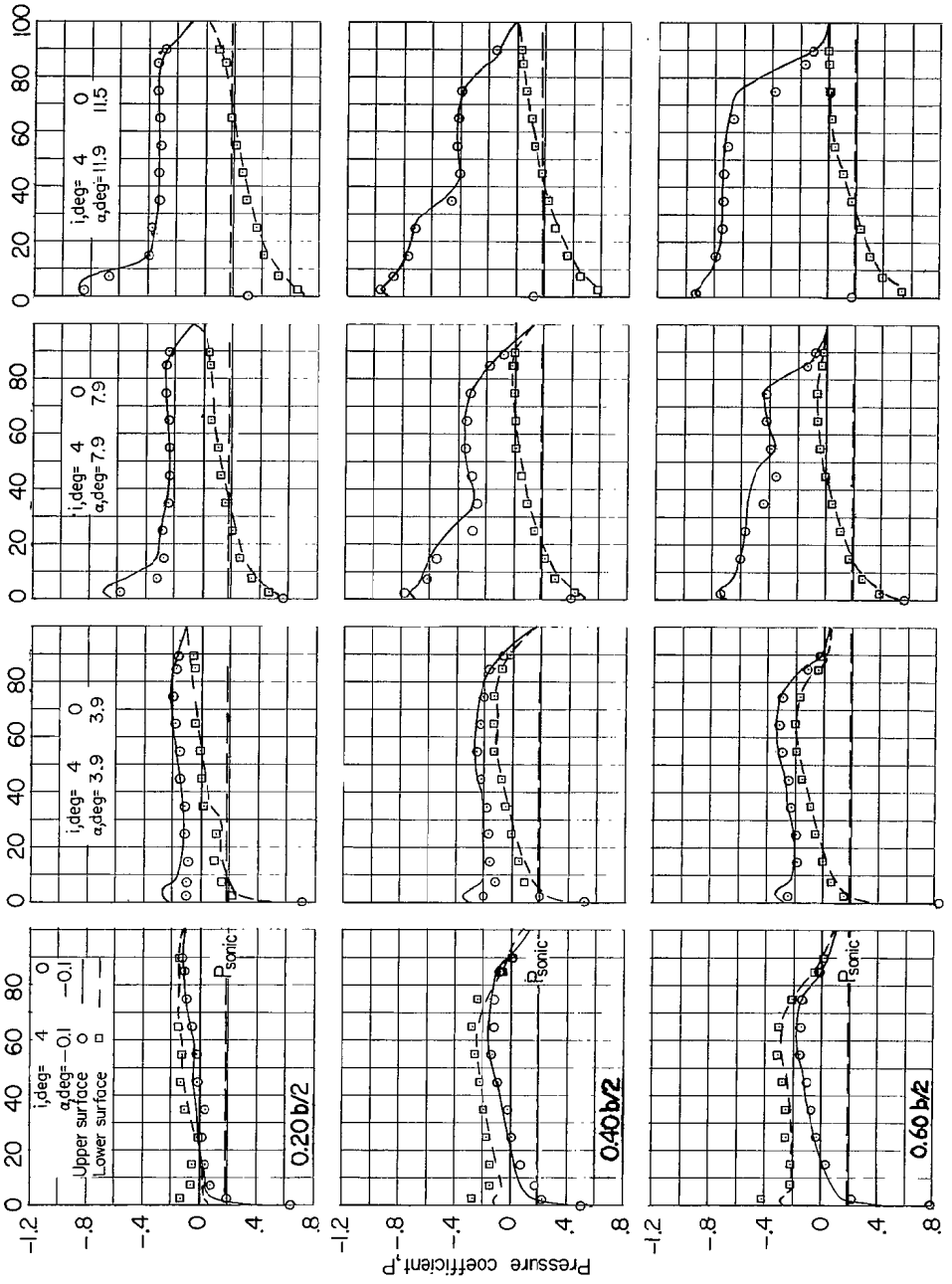
i,deg= 4 0
α,deg=11.9 11.5
i,deg= 4 0
α,deg=7.9 7.9
i,deg= 4 0
α,deg= 3.9 3.9
i,deg= 4 0
α,deg=-0.1 -0.1
Upper surface ○ —
Lower surface □ — —
Psonic
0.20 b/2
0.40 b/2
0.60 b/2
Pressure coefficient, P
-1.2
-.8
-.4
0
.4
.8
0
20
40
60
80
100

[redacted]

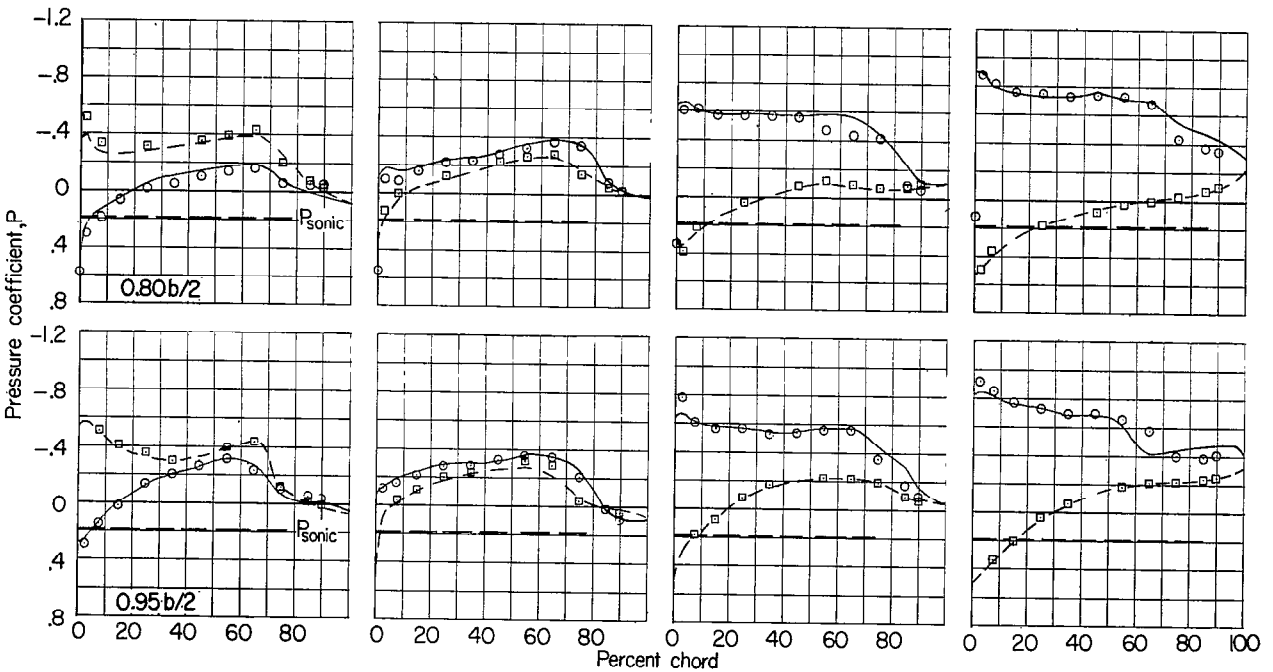

(k) M = 1.13.

Figure 4.- Concluded.

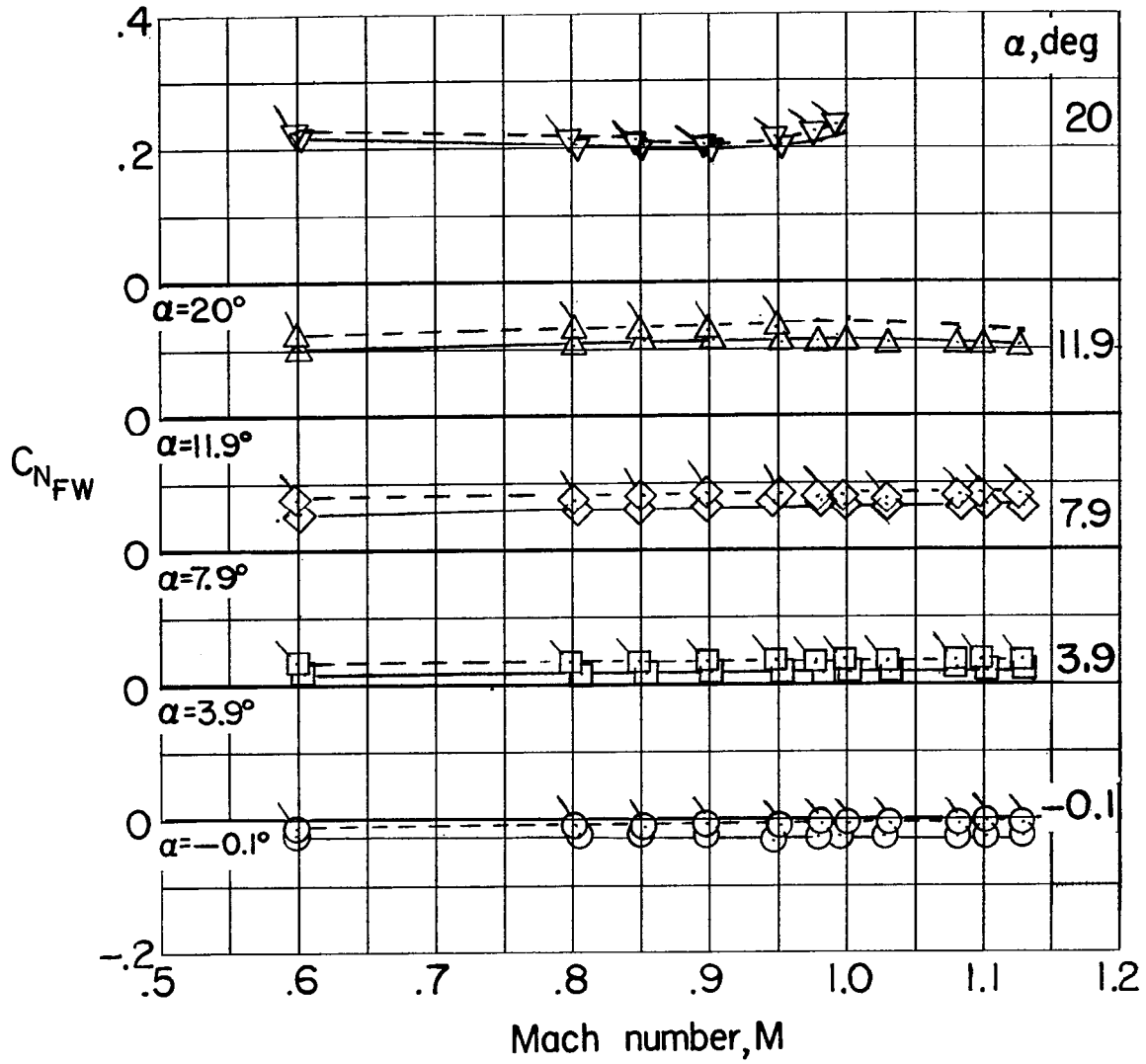

Figure 5.- Body normal-force coefficient in presence of wing. (Flagged symbols represent 0° incidence; unflagged symbols represent 4° incidence.)

[redacted]

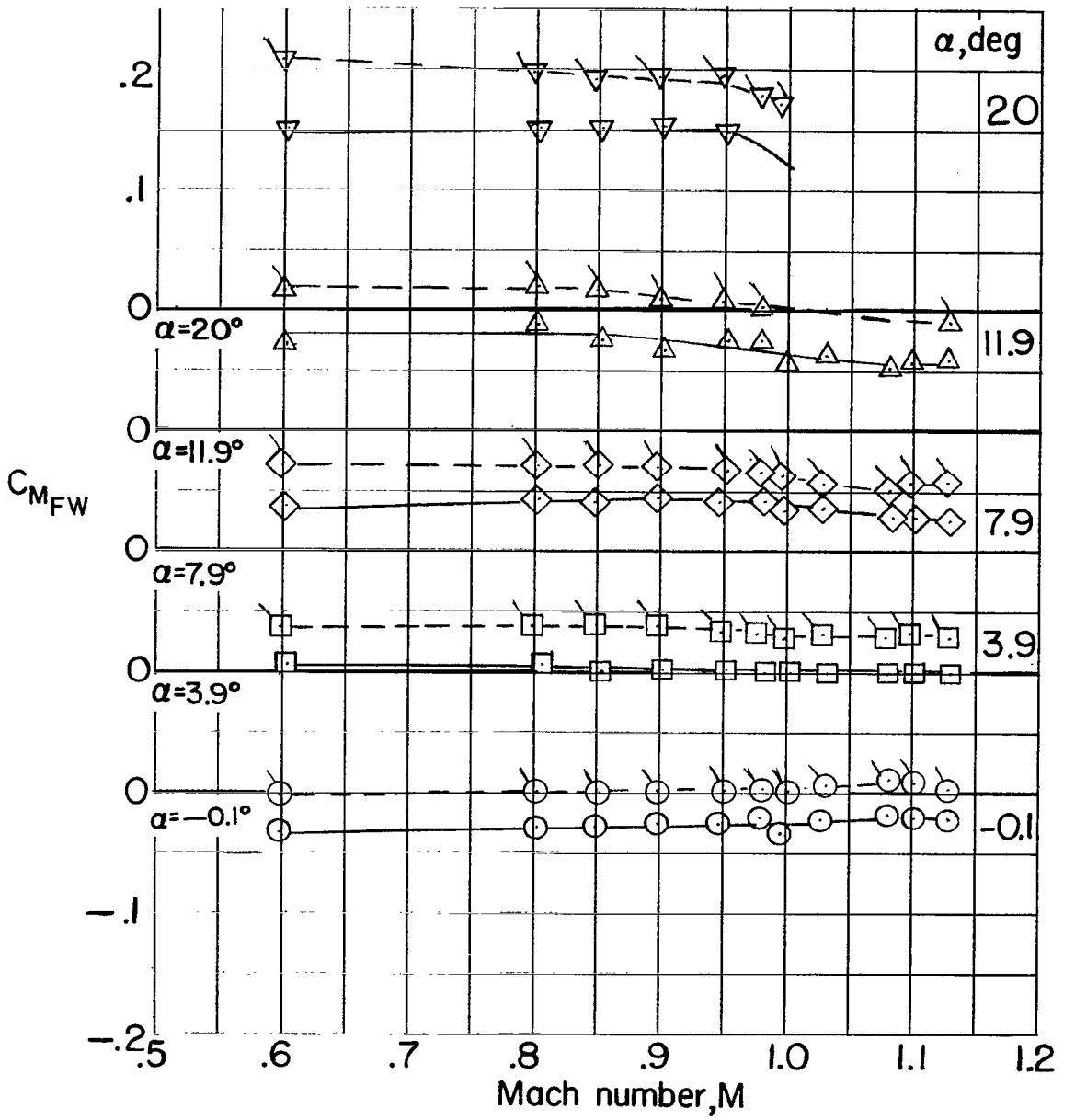

Figure 6.- Body pitching-moment coefficient in presence of the wing. (Flagged symbols represent 0° incidence; unflagged symbols represent 4° incidence.)

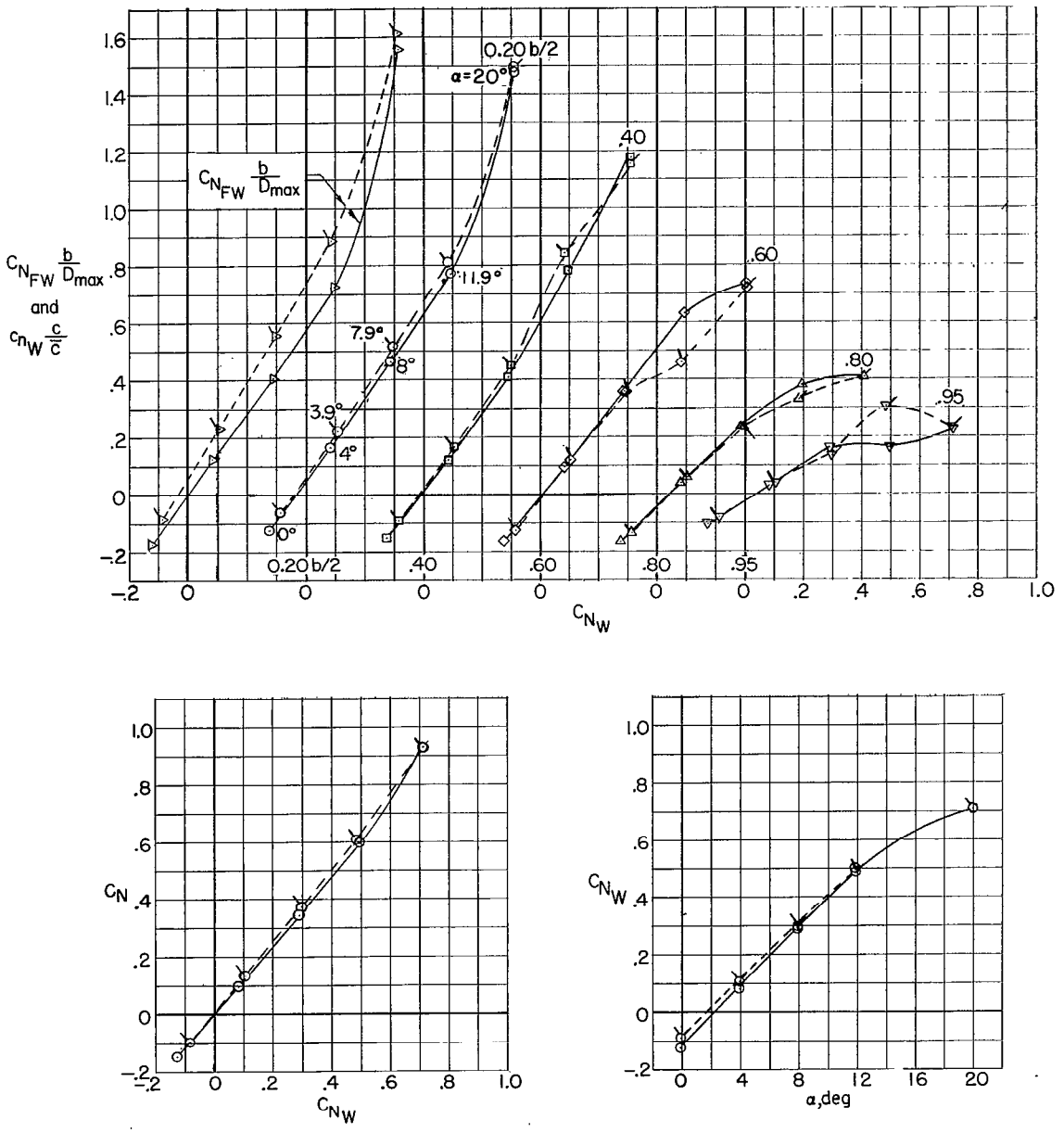

(a) M = 0.60.

Figure 7.- Wing and wing-body normal-force characteristics. (Flagged symbols represent 0° incidence; unflagged symbols represent 4° incidence.)

[redacted]

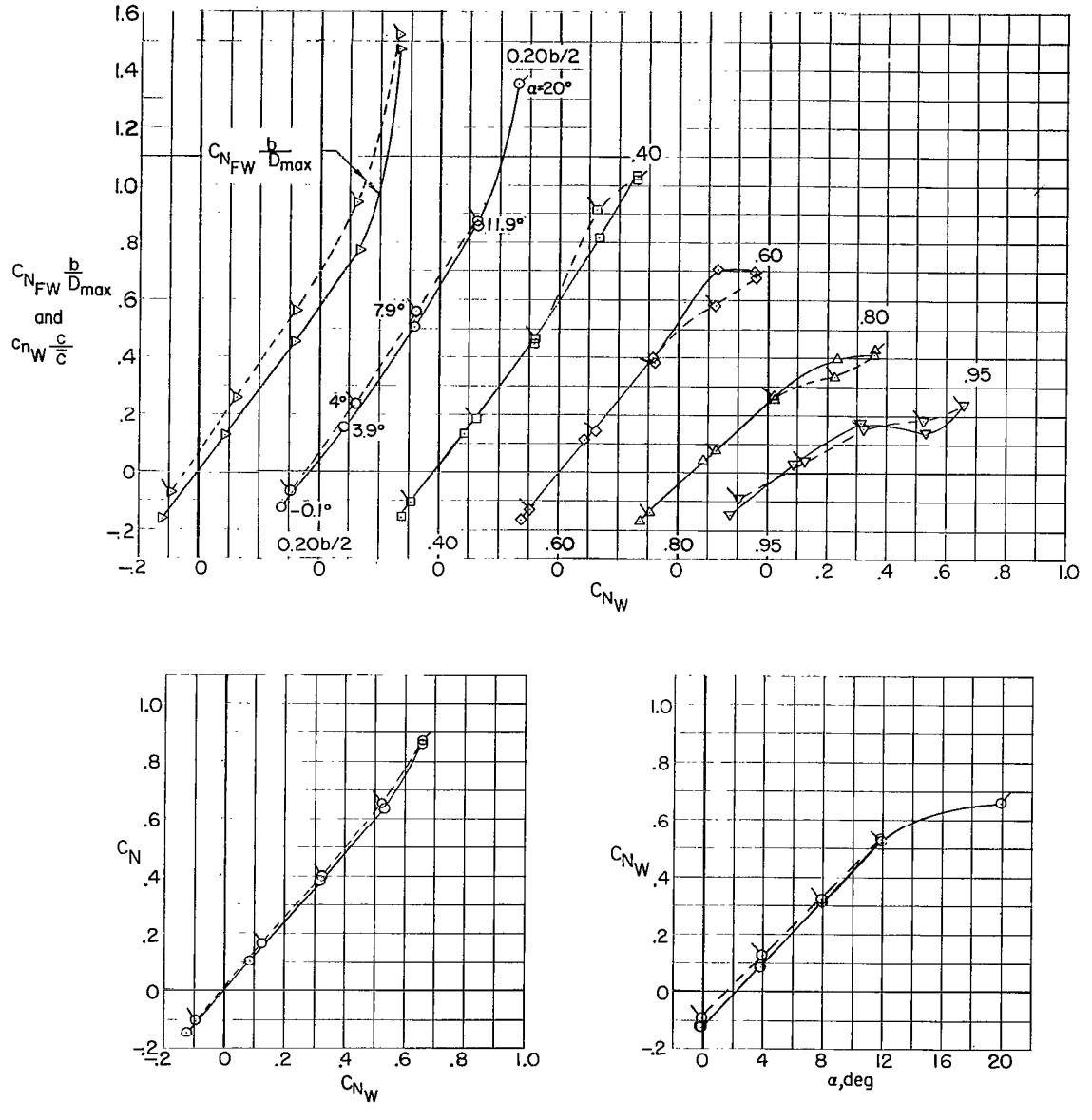

(b) $M \approx 0.80$.

Figure 7.- Continued.

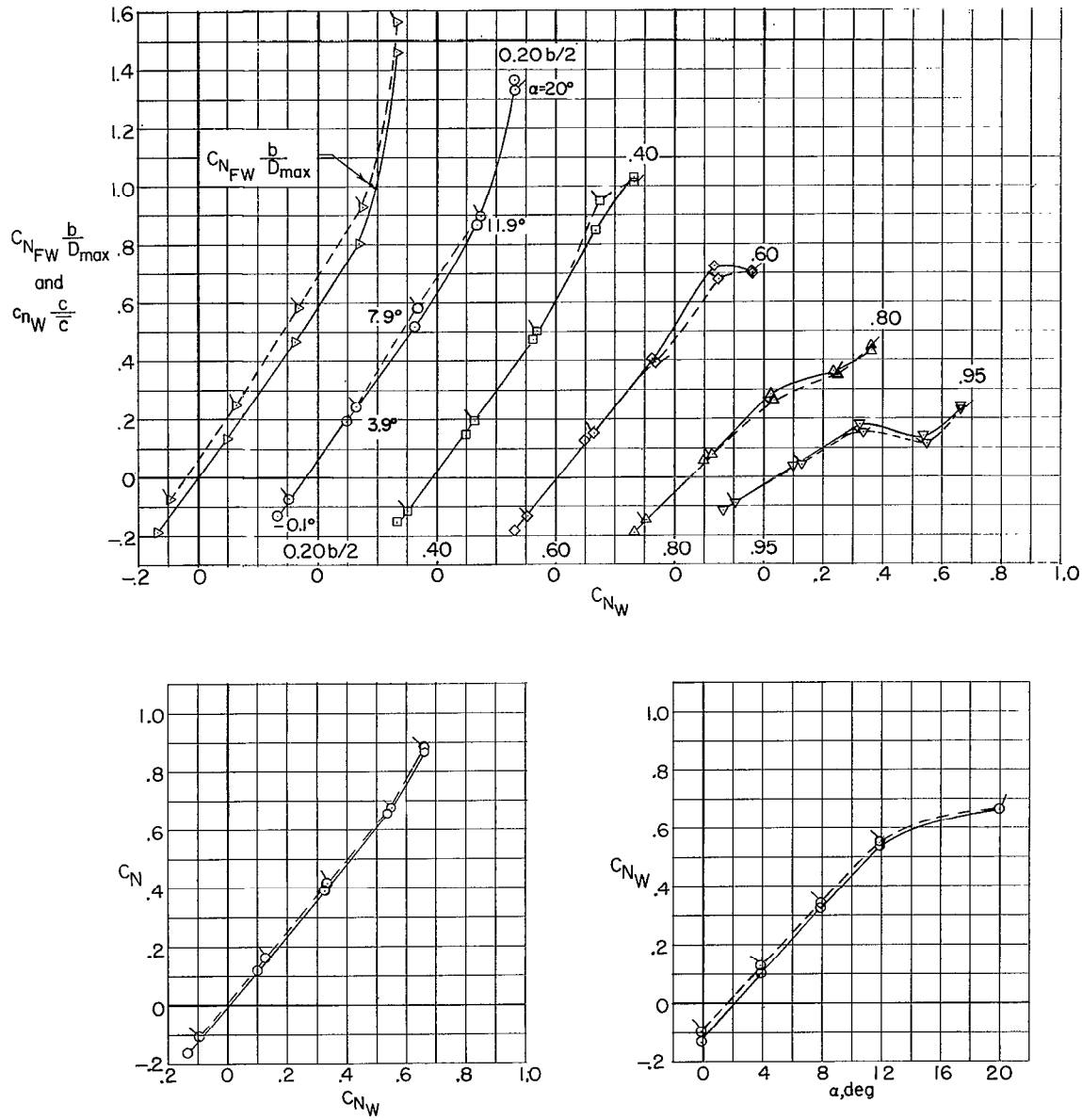

(c) M = 0.85.

Figure 7.- Continued.

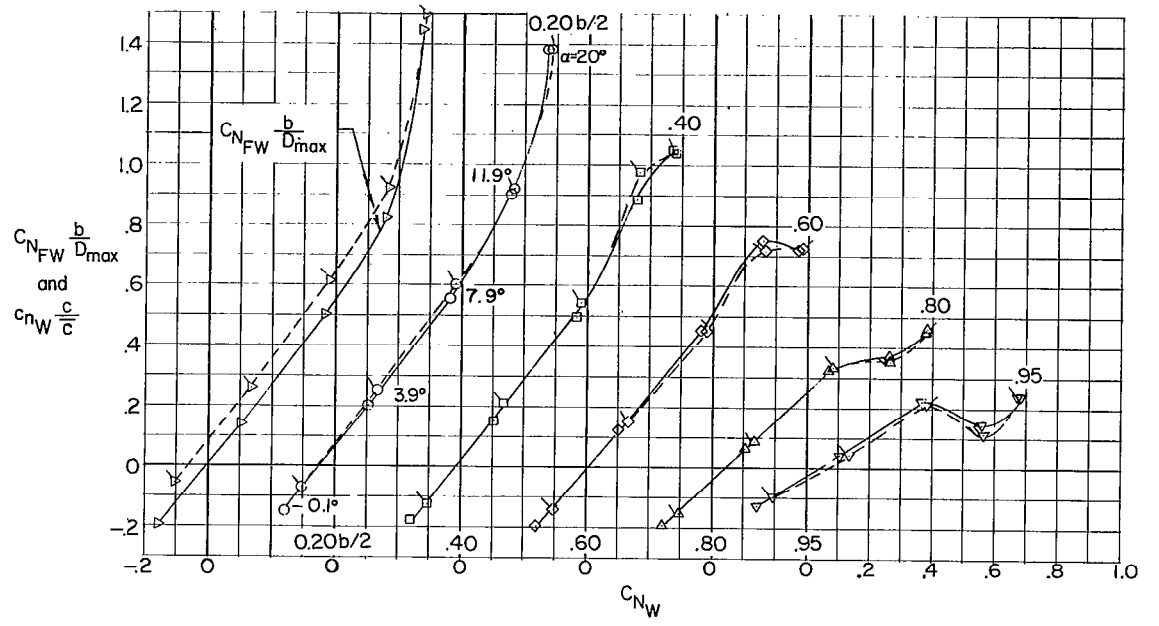

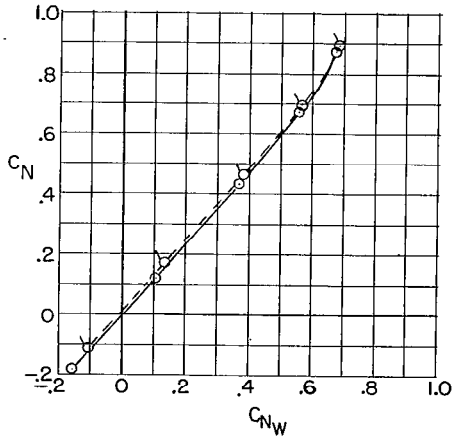

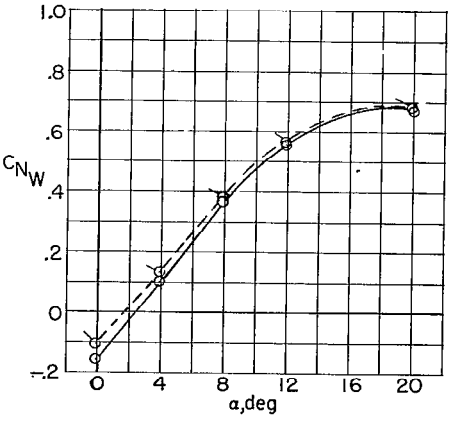

(d) M = 0.90.

Figure 7.- Continued.

[redacted]

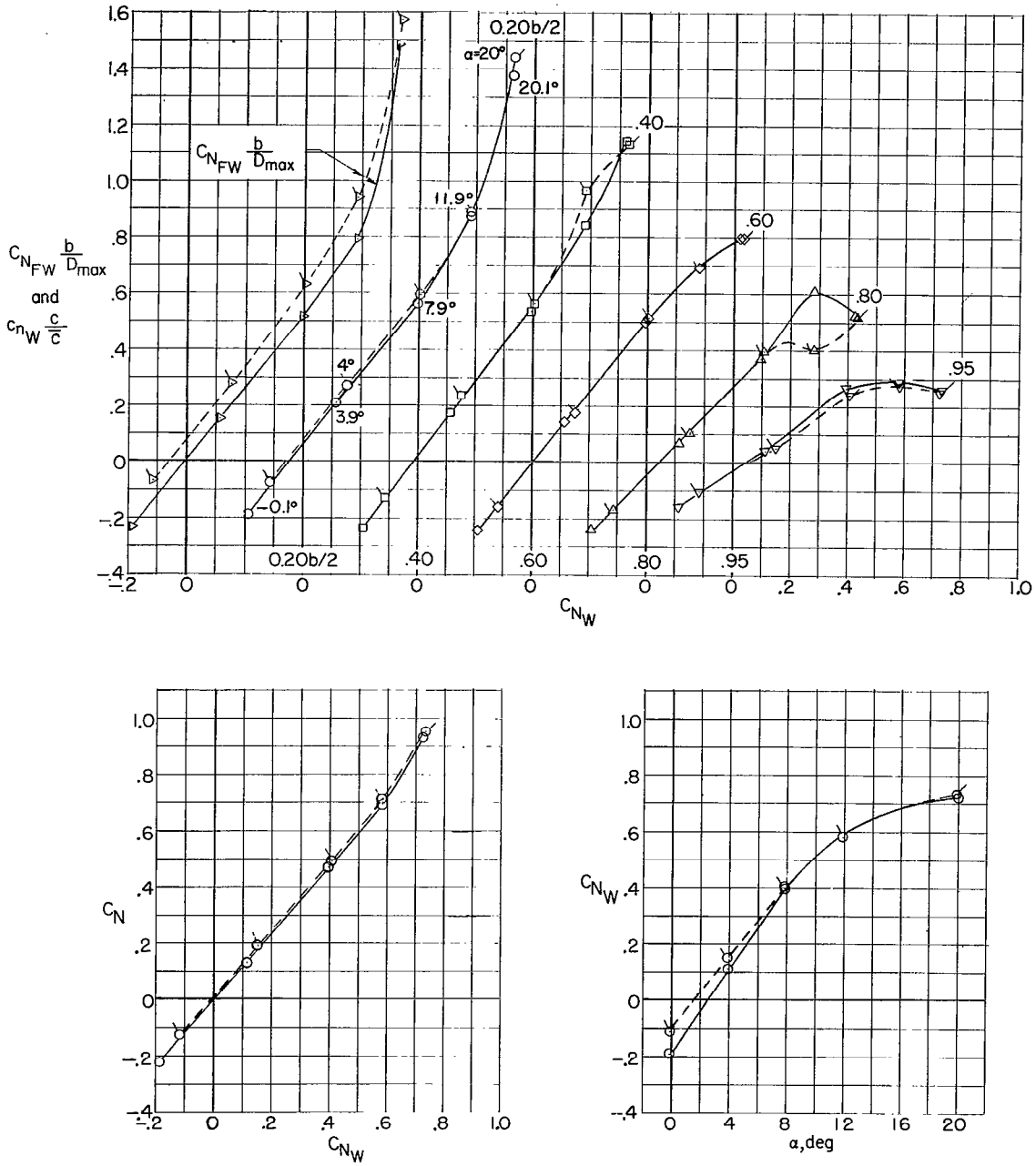

(e) M = 0.95.

Figure 7.- Continued.

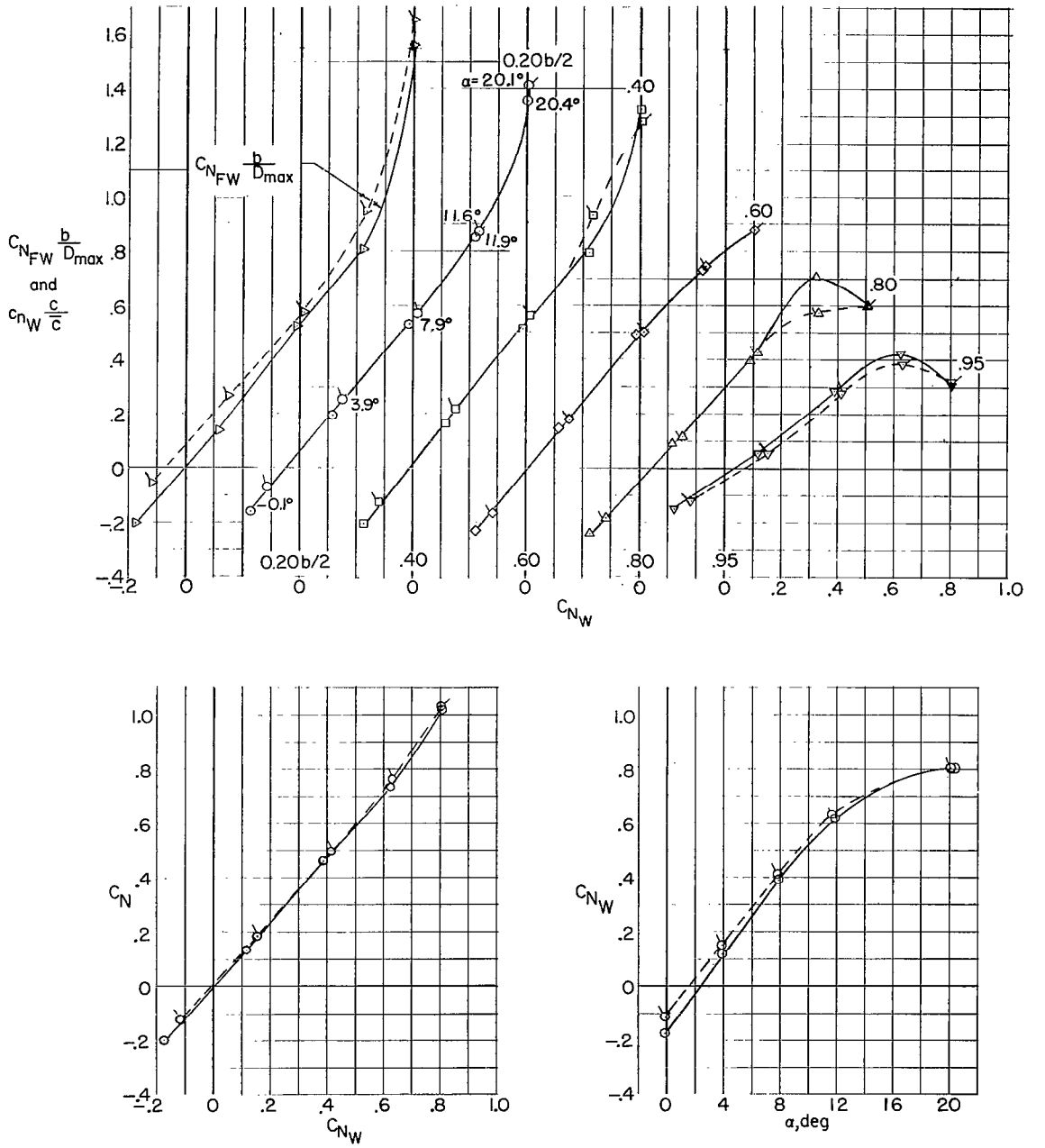

(f) M = 0.98.

Figure 7.- Continued.

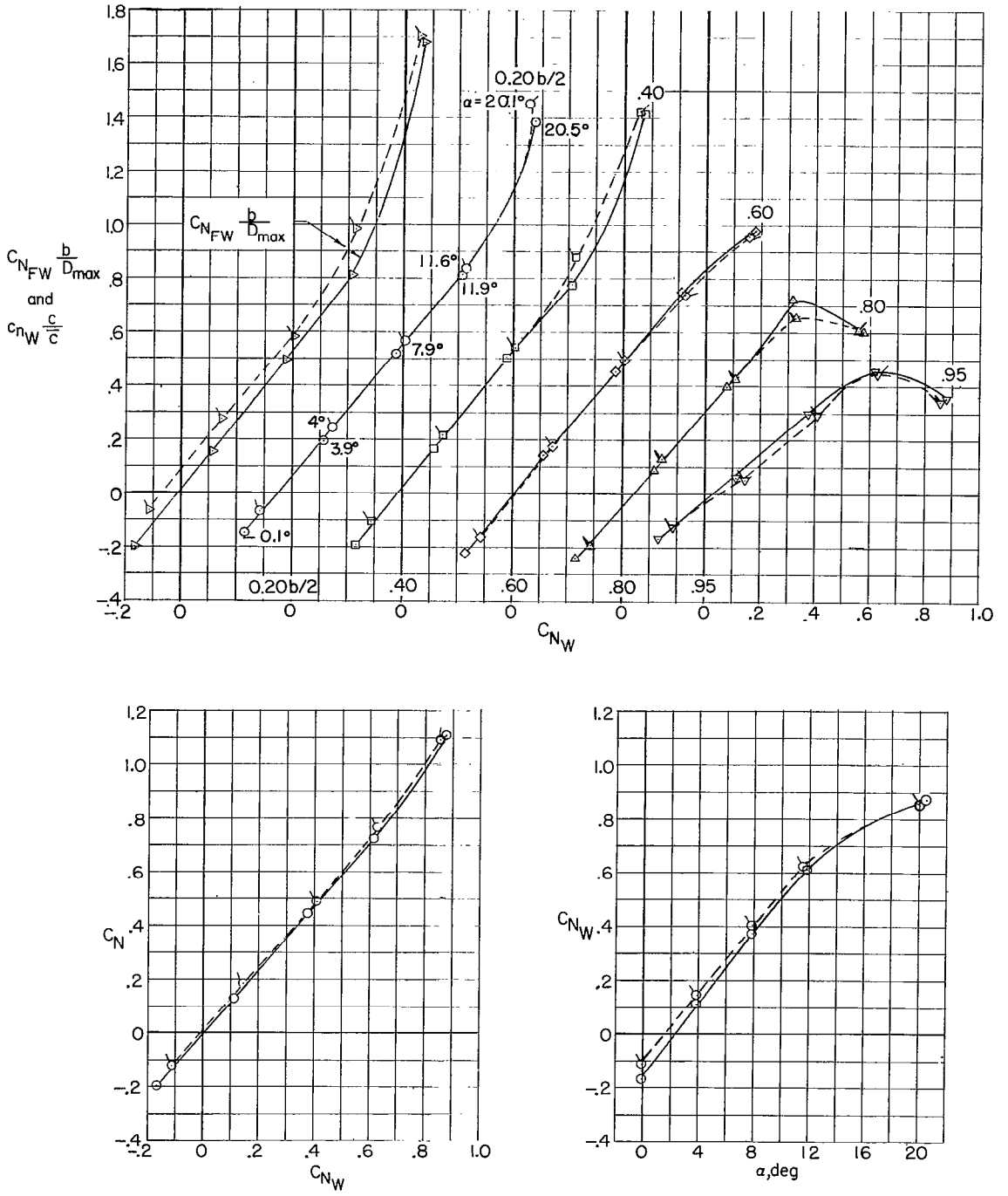

(g) M ≈ 1.00.

Figure 7.- Continued.

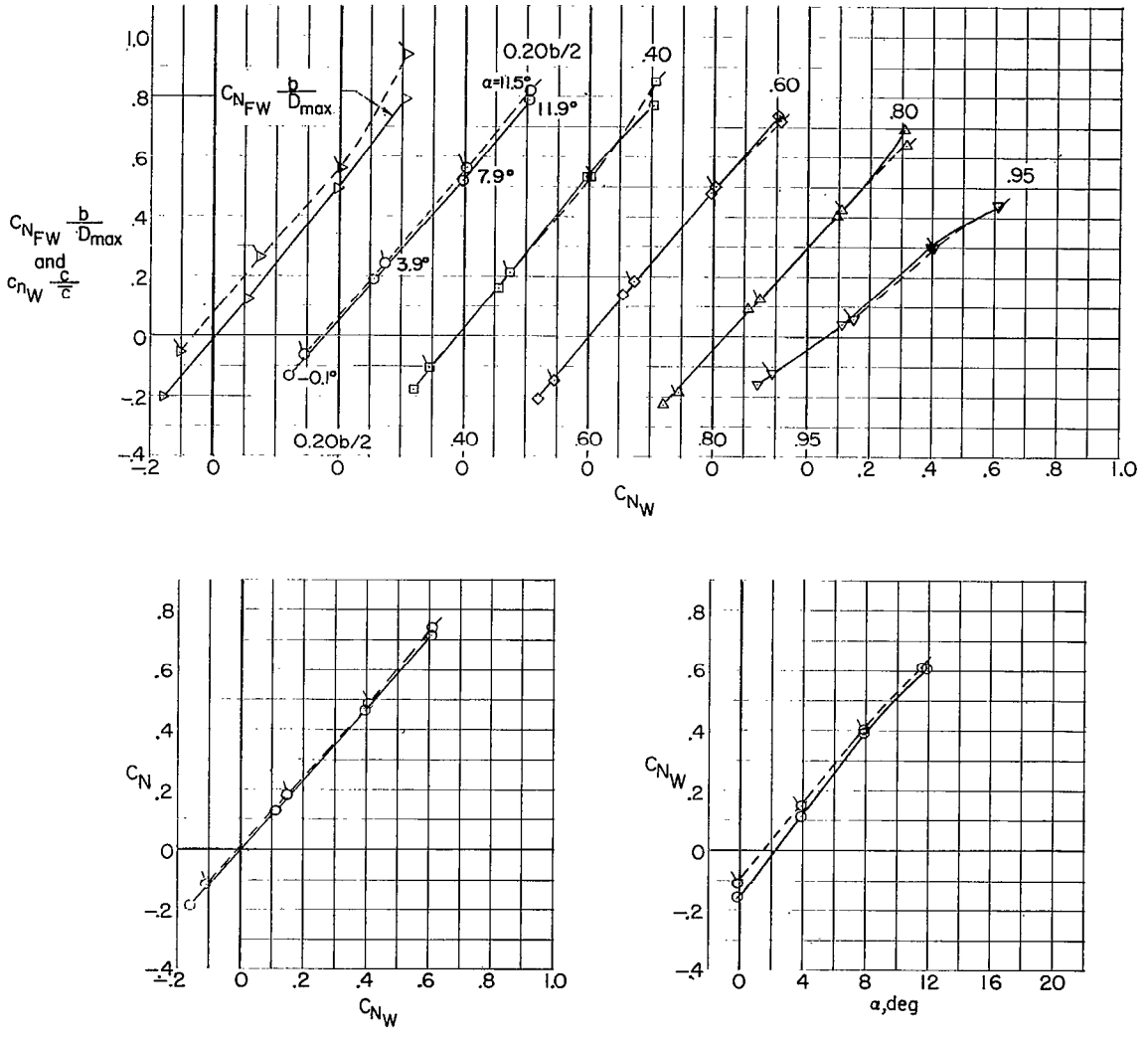

(h) M = 1.03.

Figure 7.- Continued.

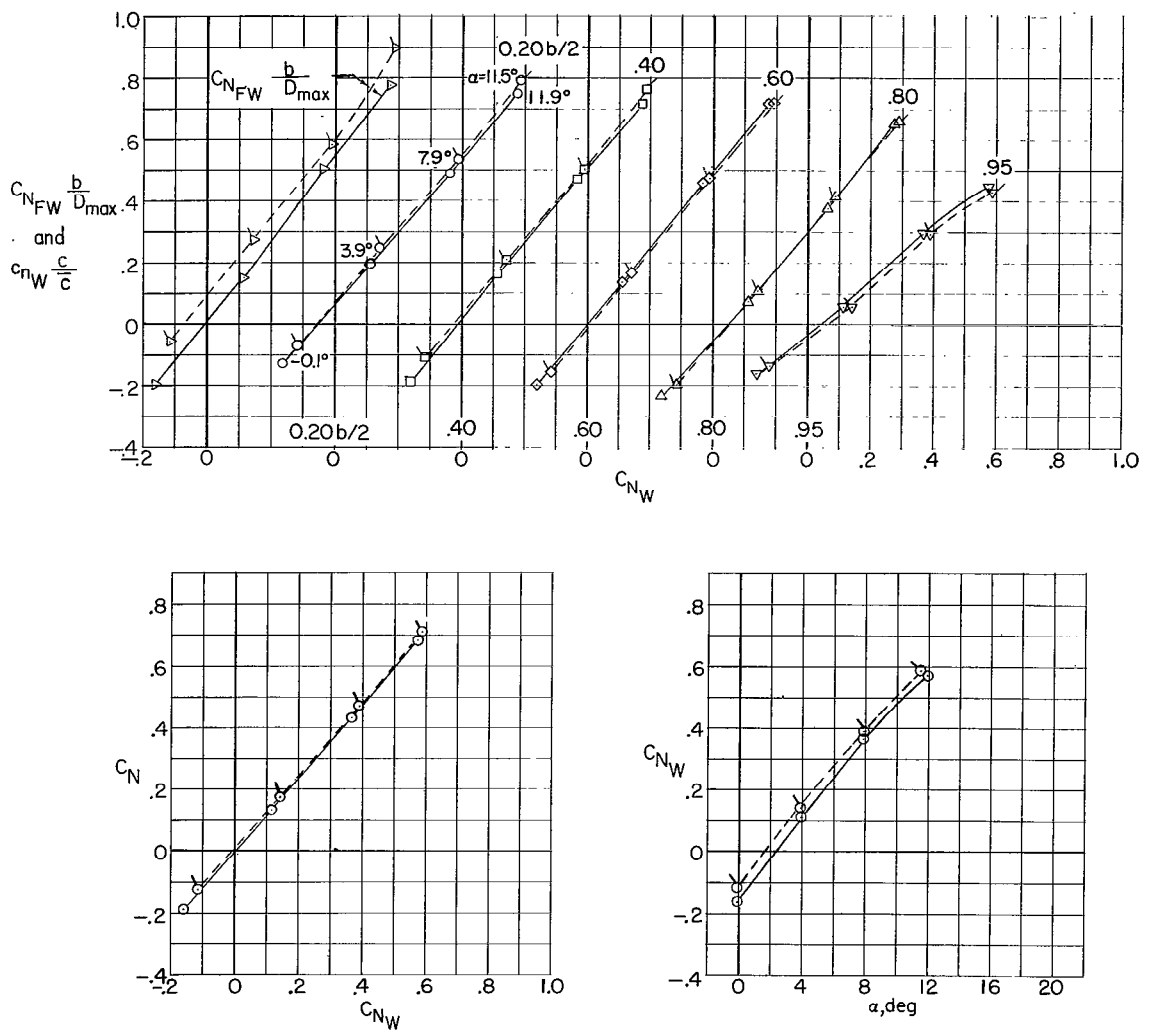

(i) M = 1.08.

Figure 7.- Continued.

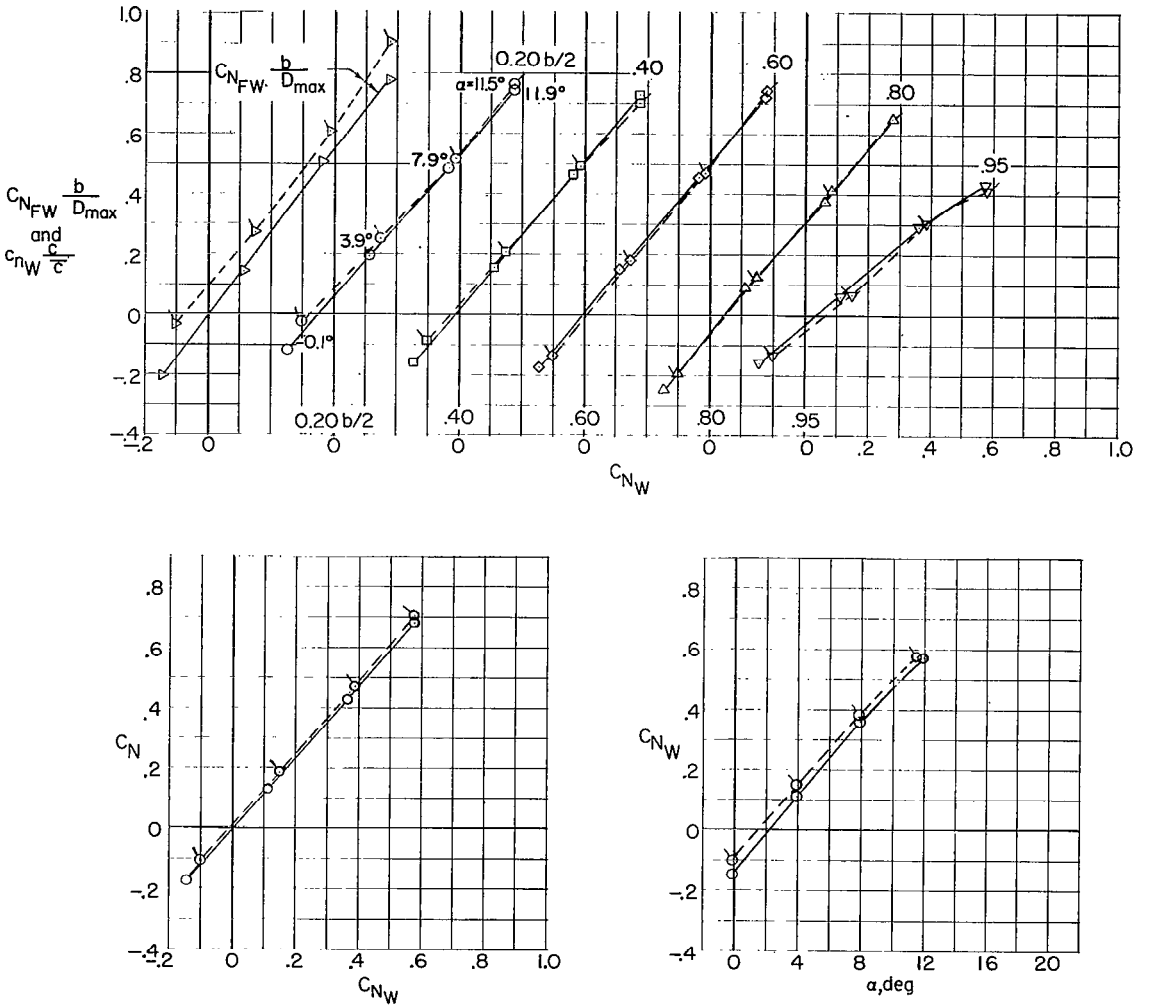

(j) $M \approx 1.10$.

Figure 7.- Continued.

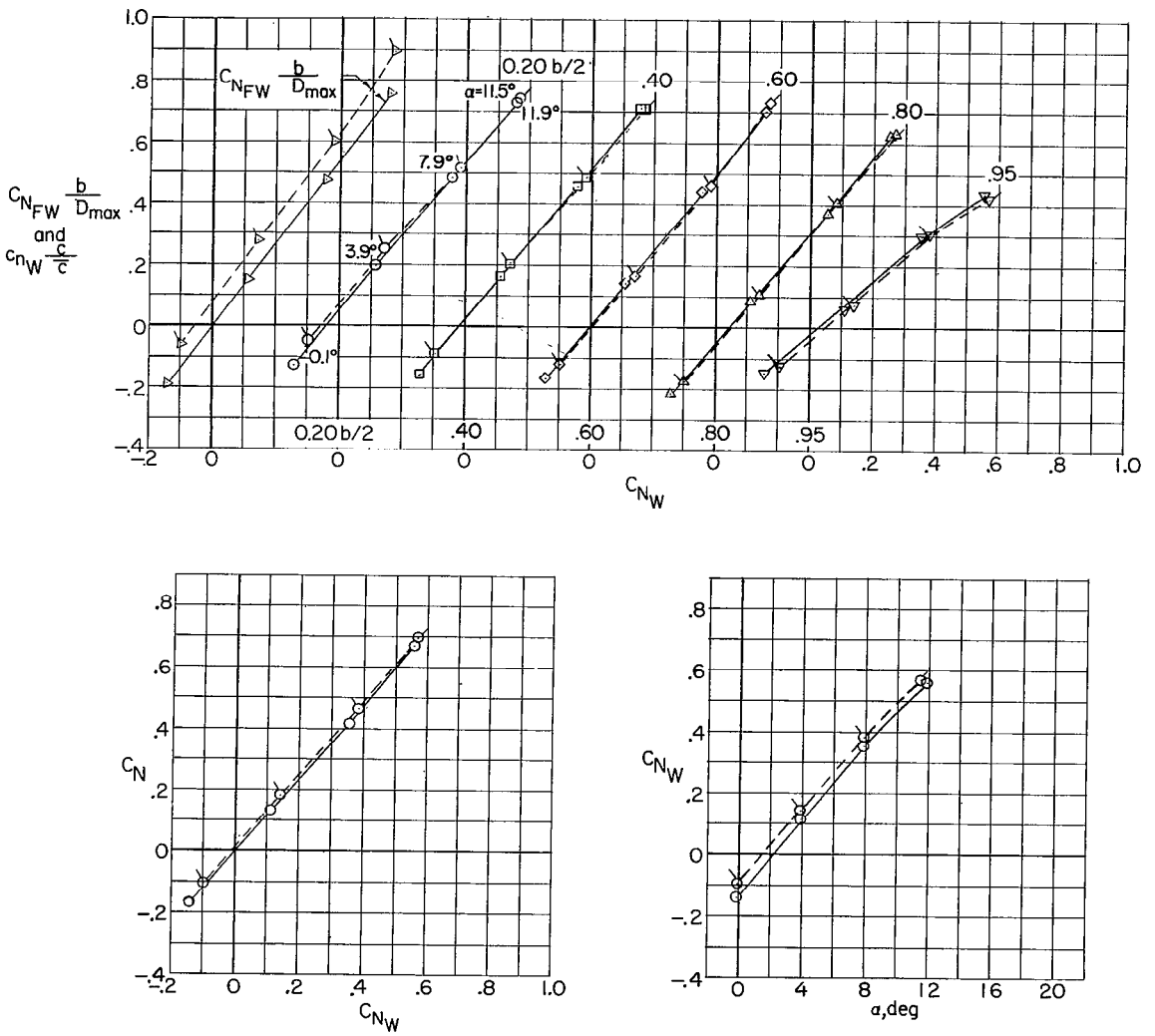

(k) M = 1.13.

Figure 7.- Concluded.

[redacted]

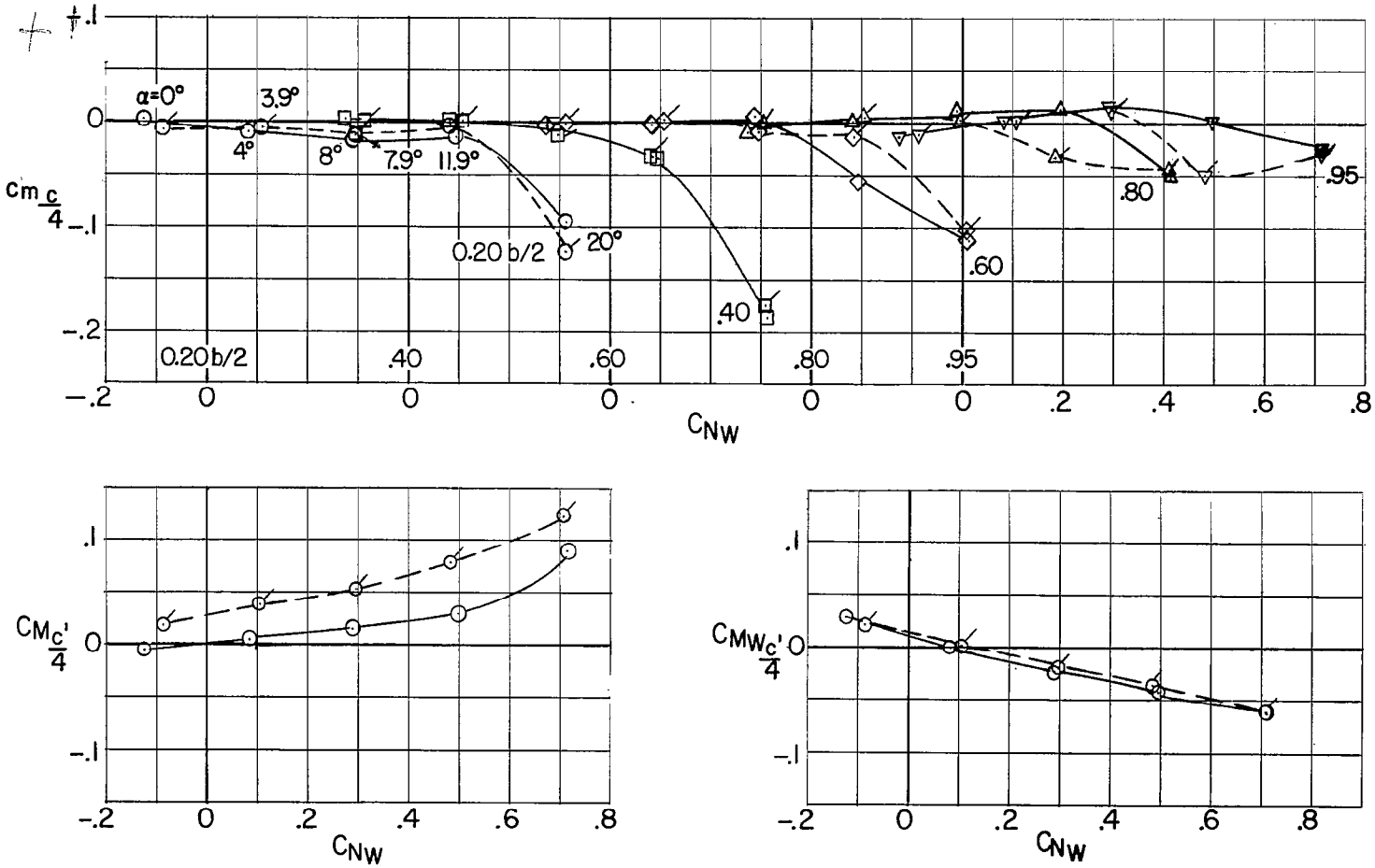

(a) M = 0.60.

Figure 8.- Wing and wing-body pitching-moment coefficient characteristics. (Flagged symbols represent 0° incidence; unflagged symbols represent 4° incidence.)

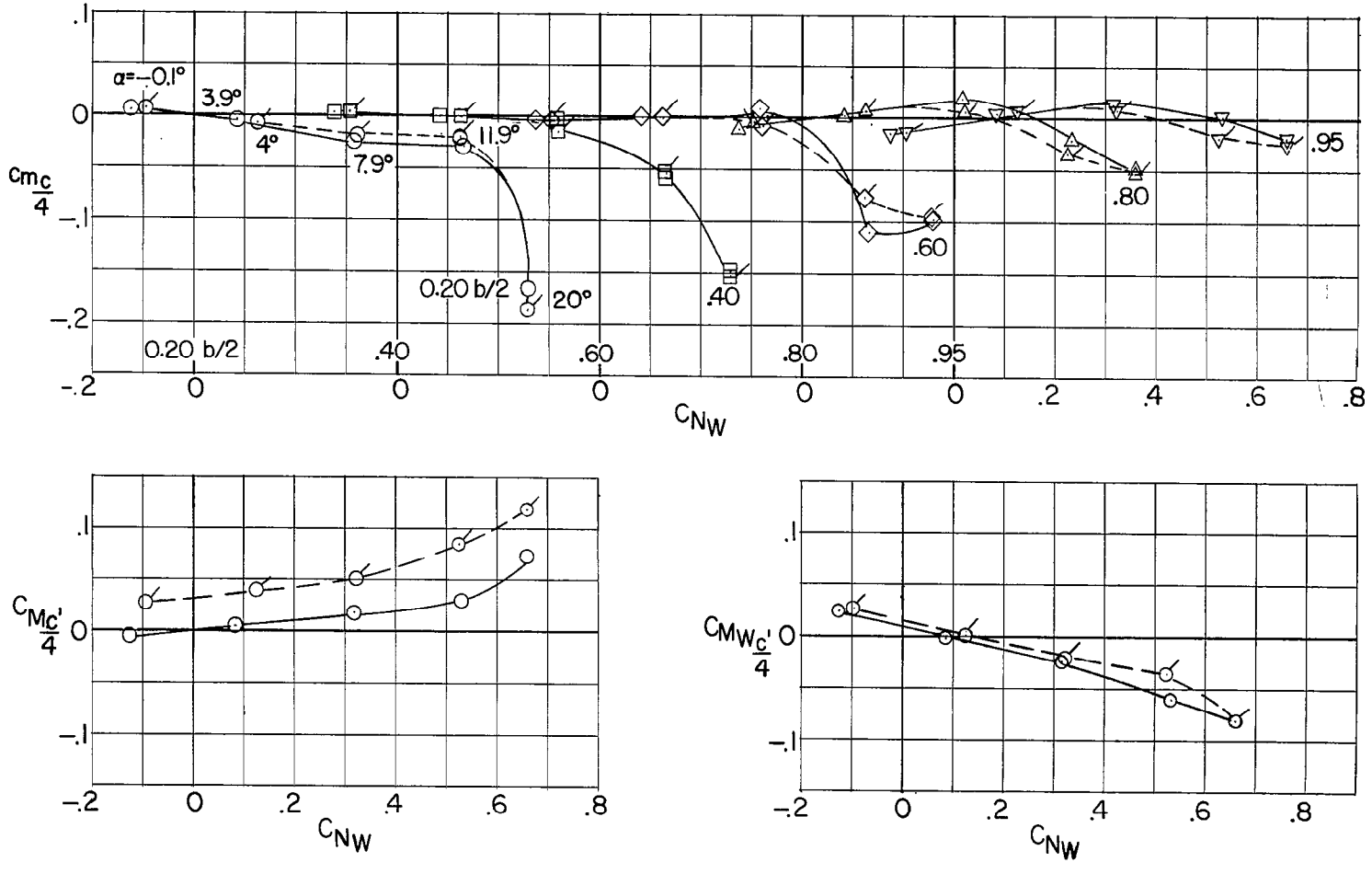

(b) M ≈ 0.80.

Figure 8.- Continued.

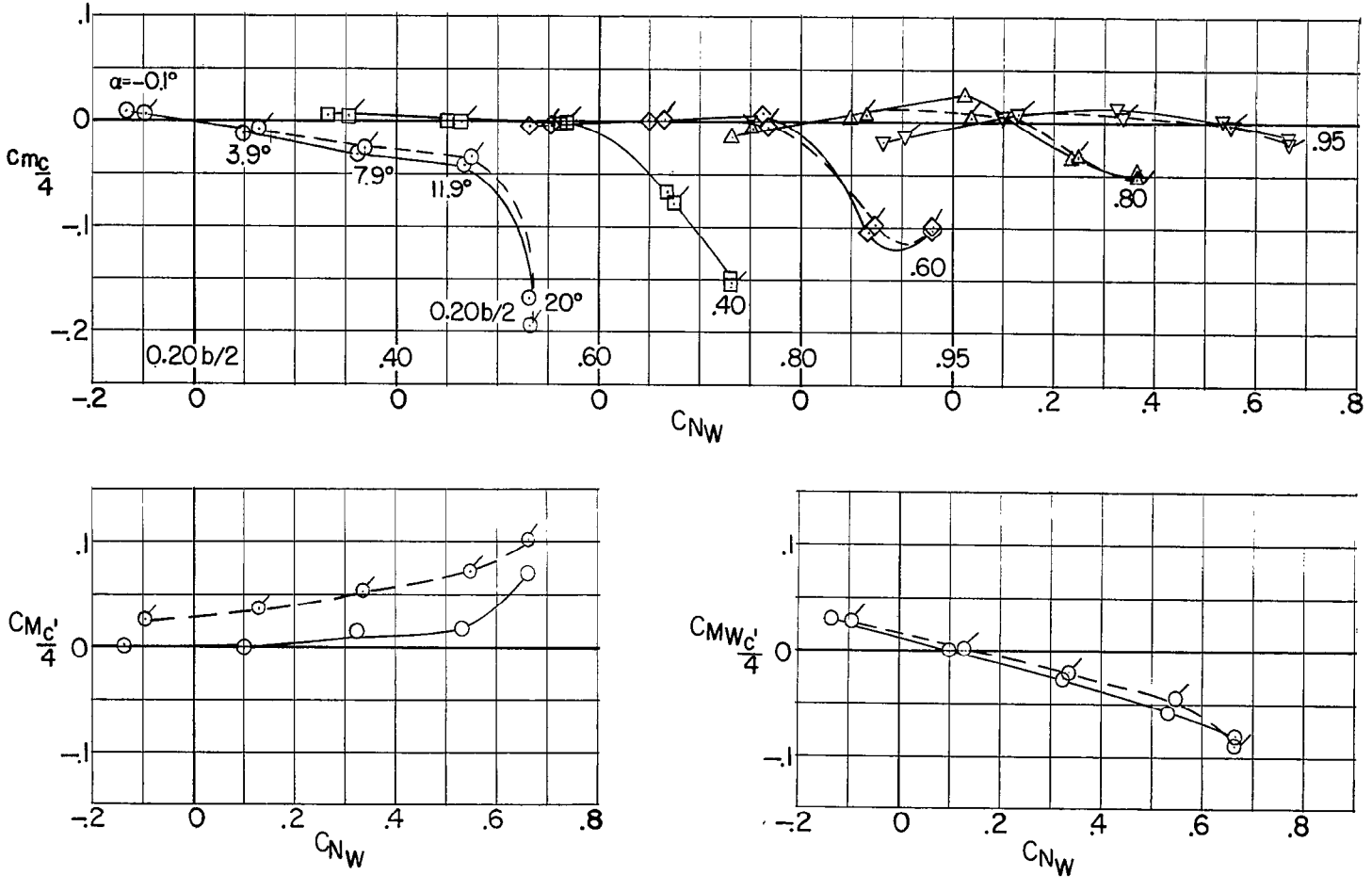

(c) M = 0.85.

Figure 8.- Continued.

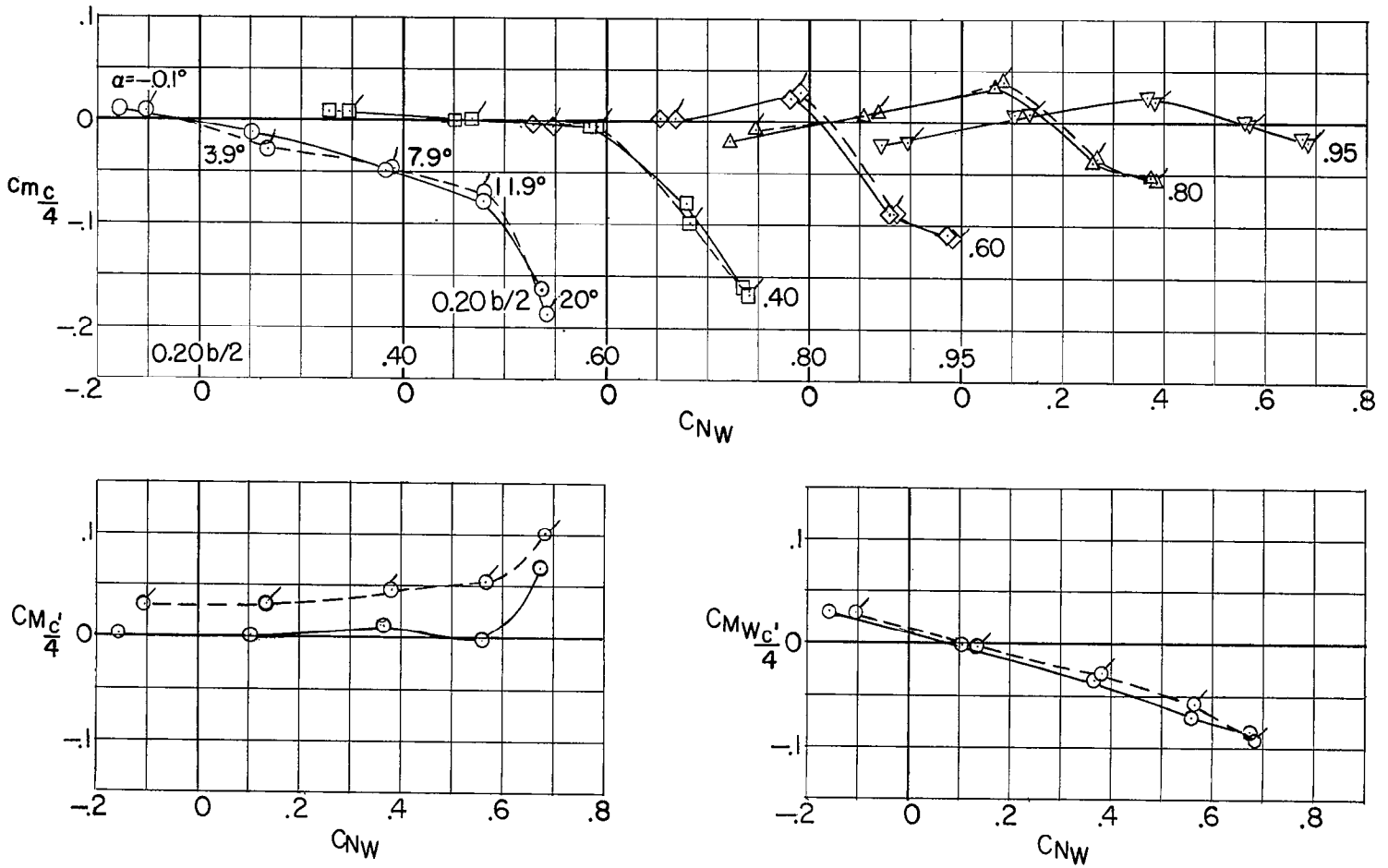

(d) M = 0.90.

Figure 8.- Continued.

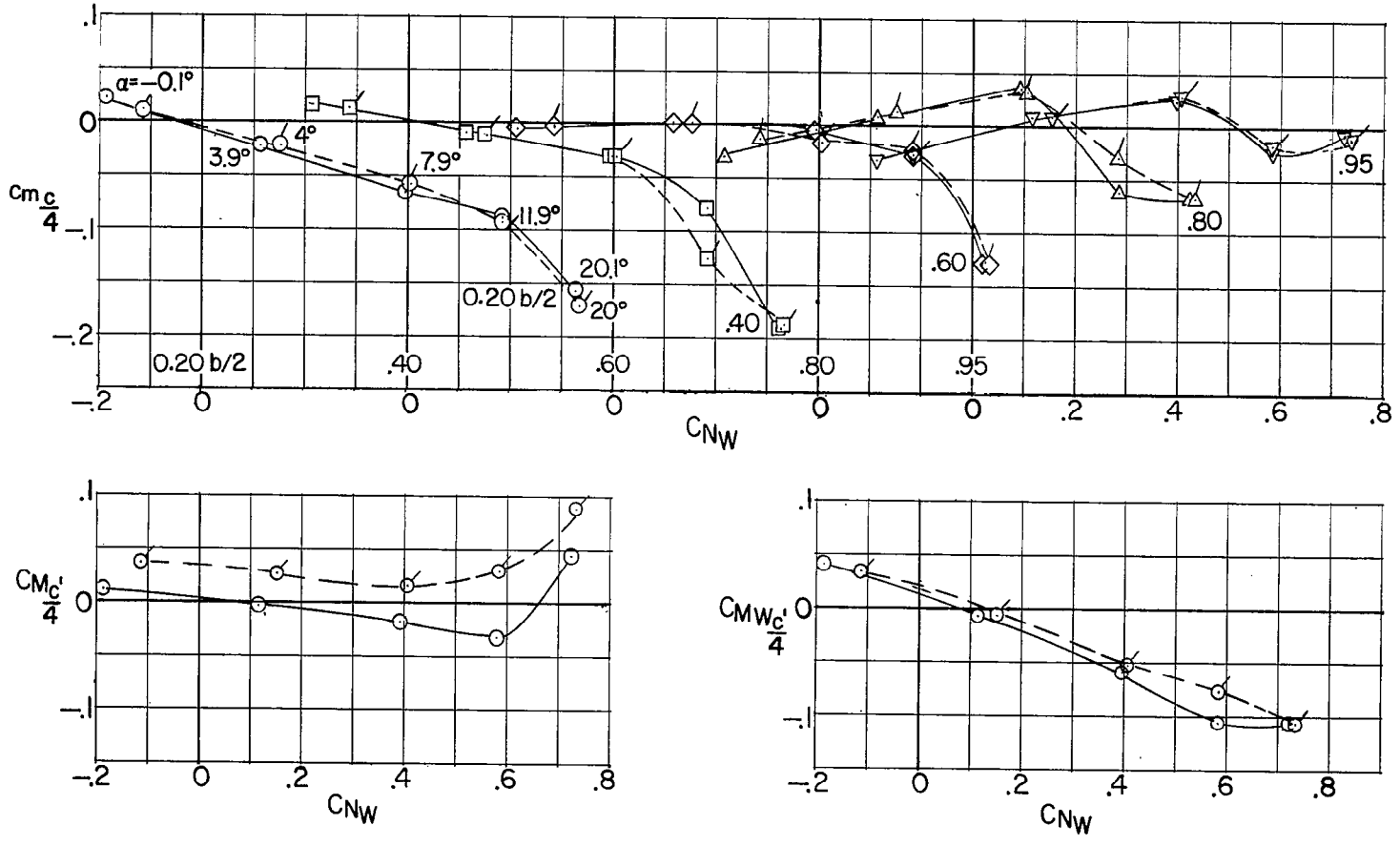

(e) M = 0.95.

Figure 8.- Continued.

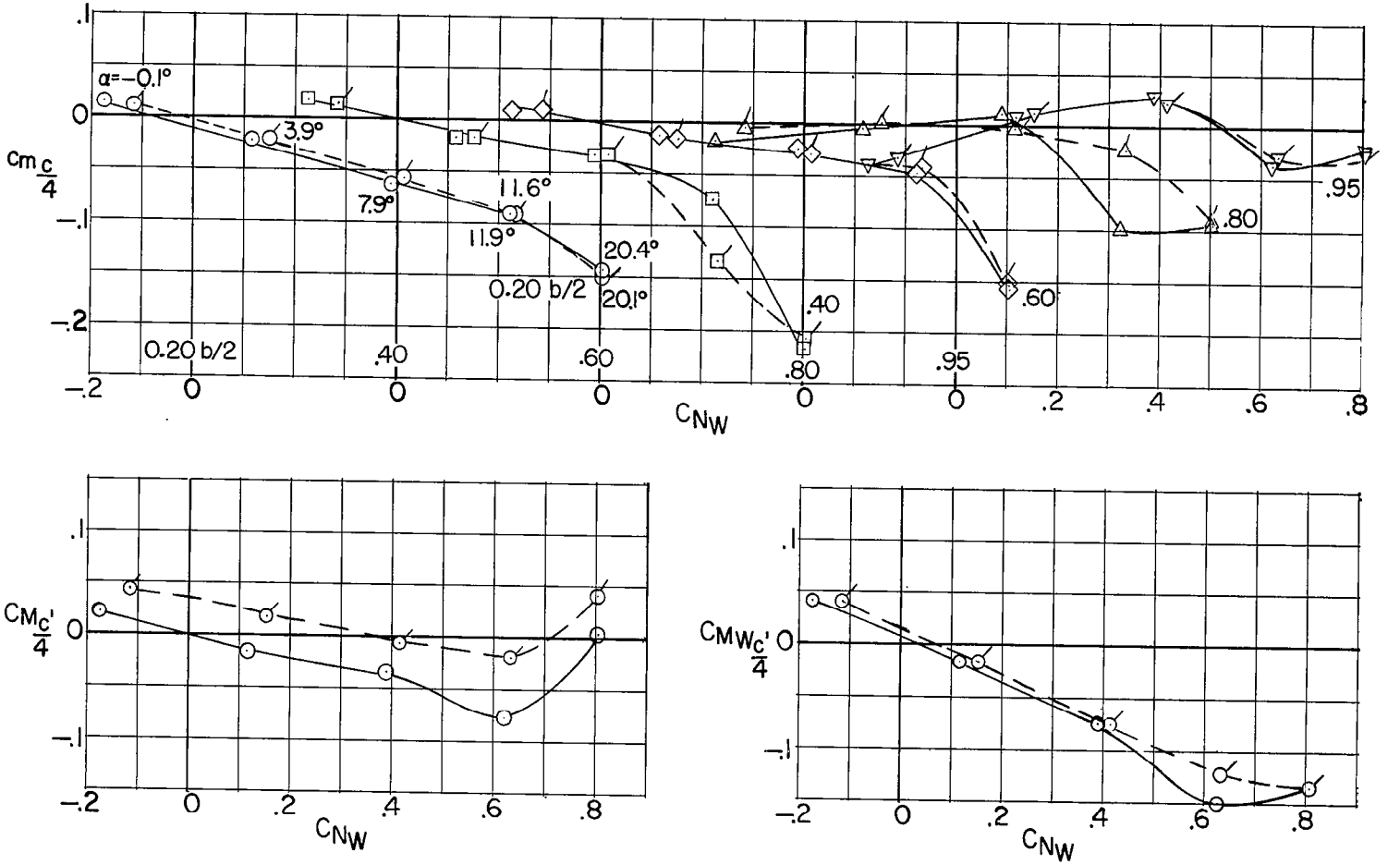

(f) M = 0.98.

Figure 8.- Continued.

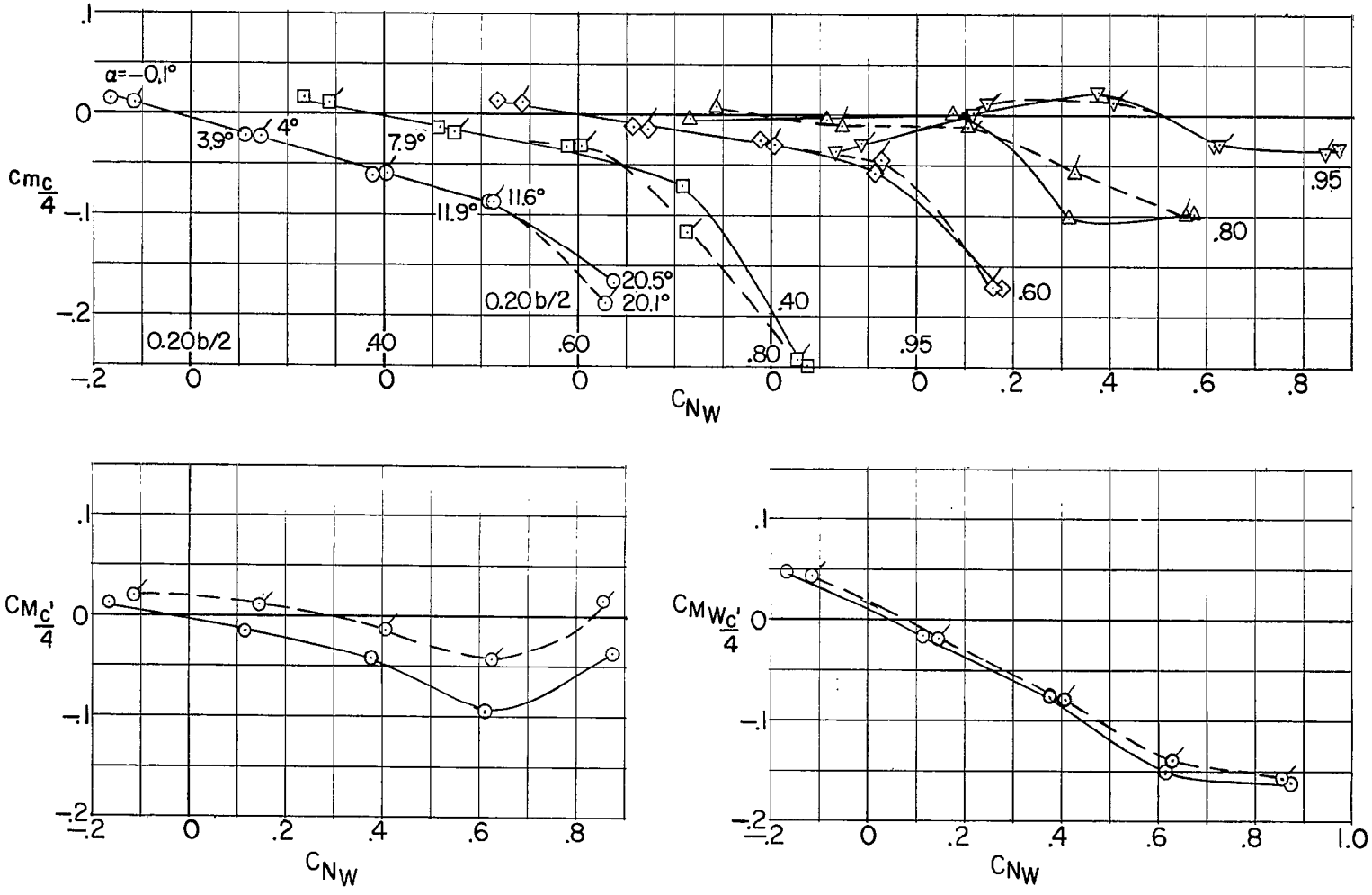

(g) M ≈ 1.00.

Figure 8.- Continued.

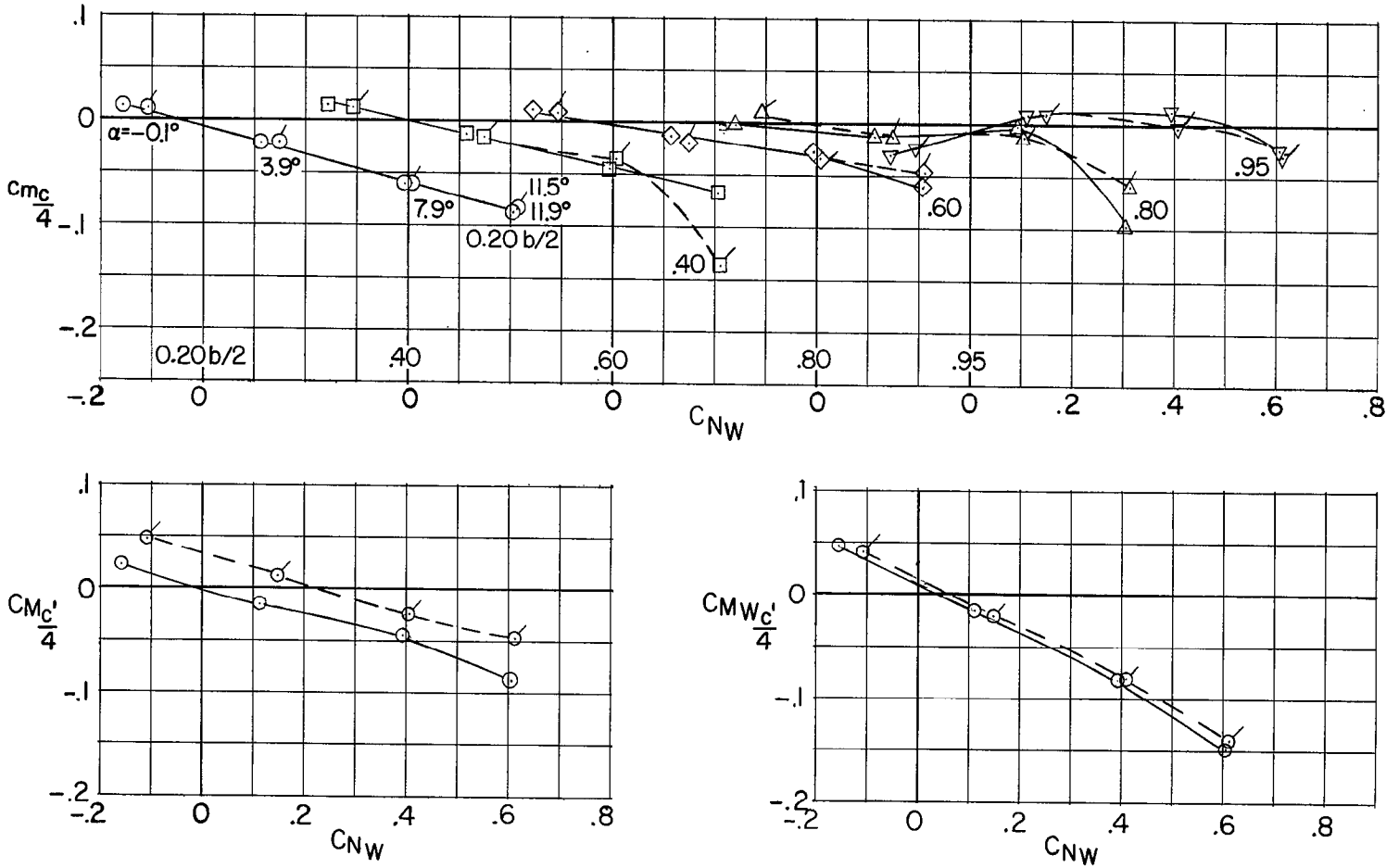

(h) M = 1.03.

Figure 8.- Continued.

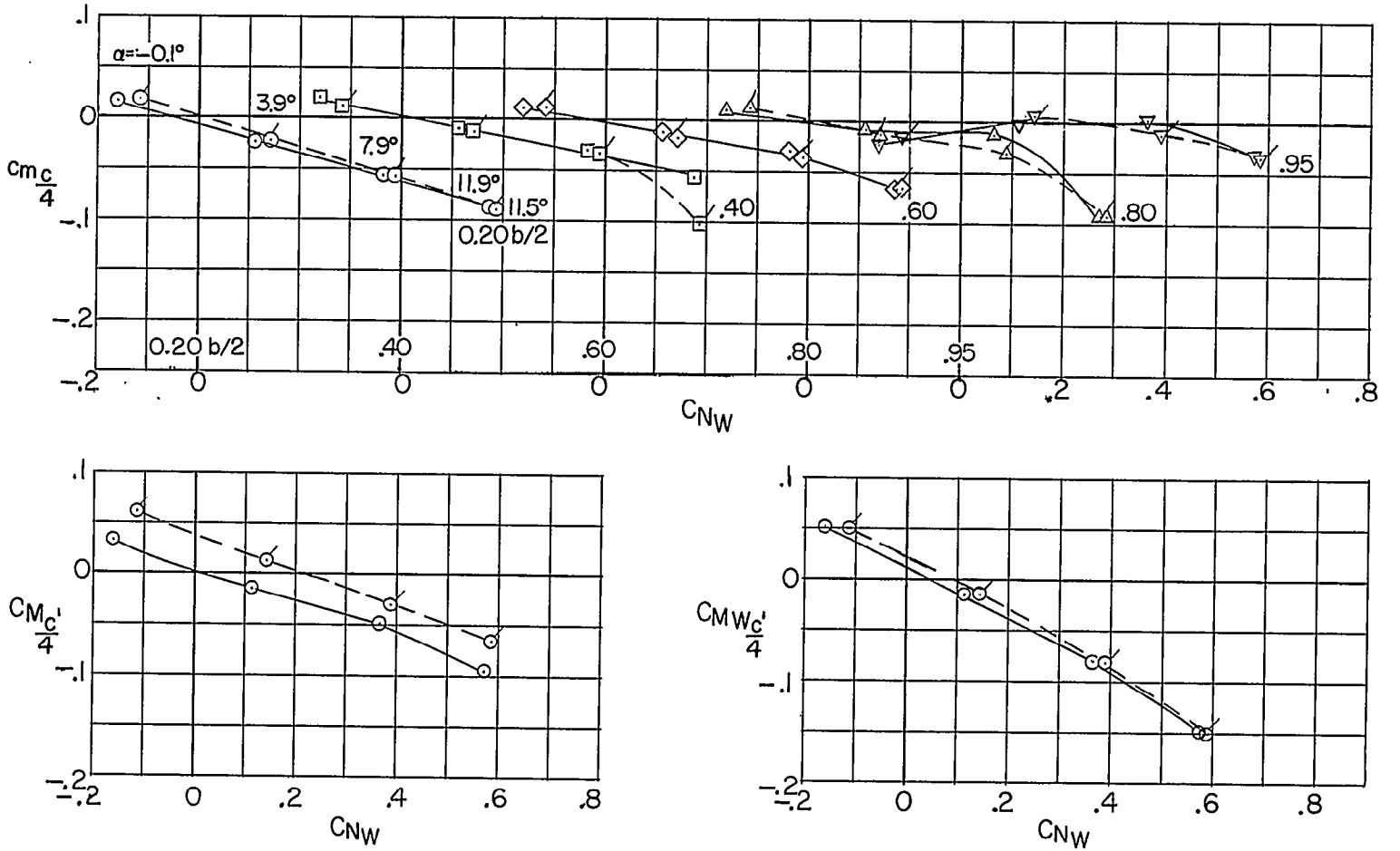

(i) M = 1.08.

Figure 8.- Continued.

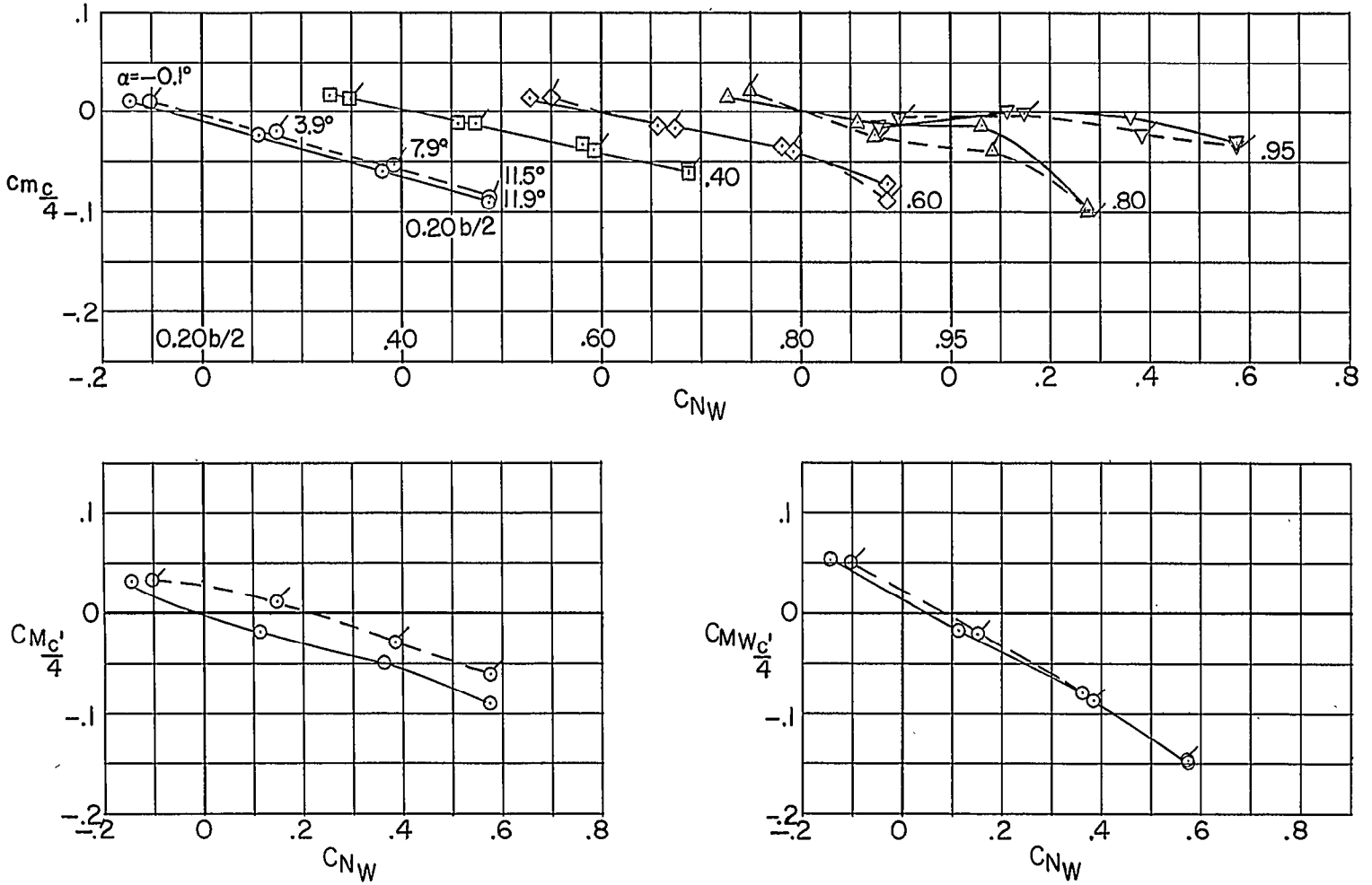

(j) M ≈ 1.10.

Figure 8.- Continued.

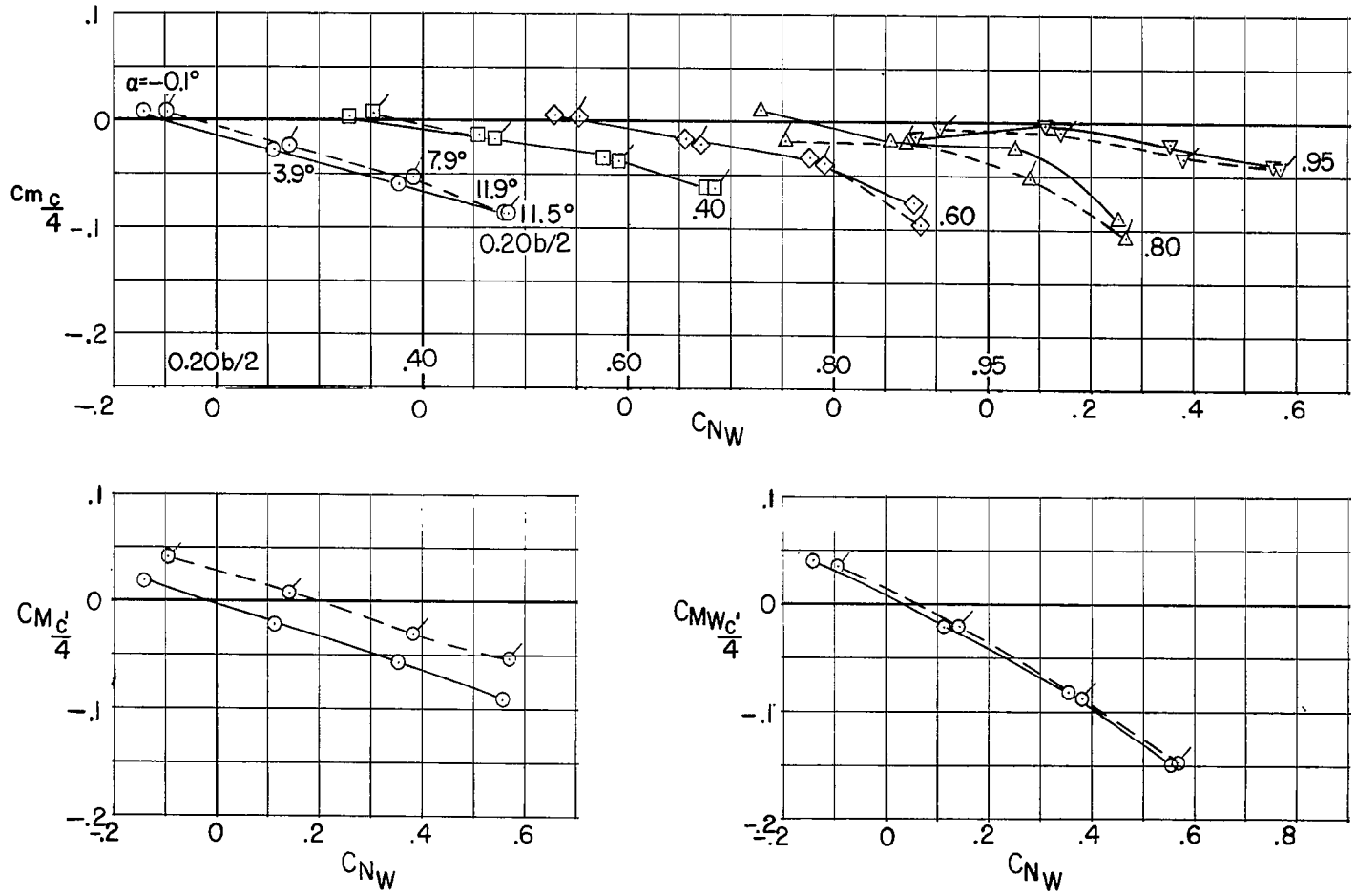

(k) M = 1.13.

Figure 8.- Concluded.

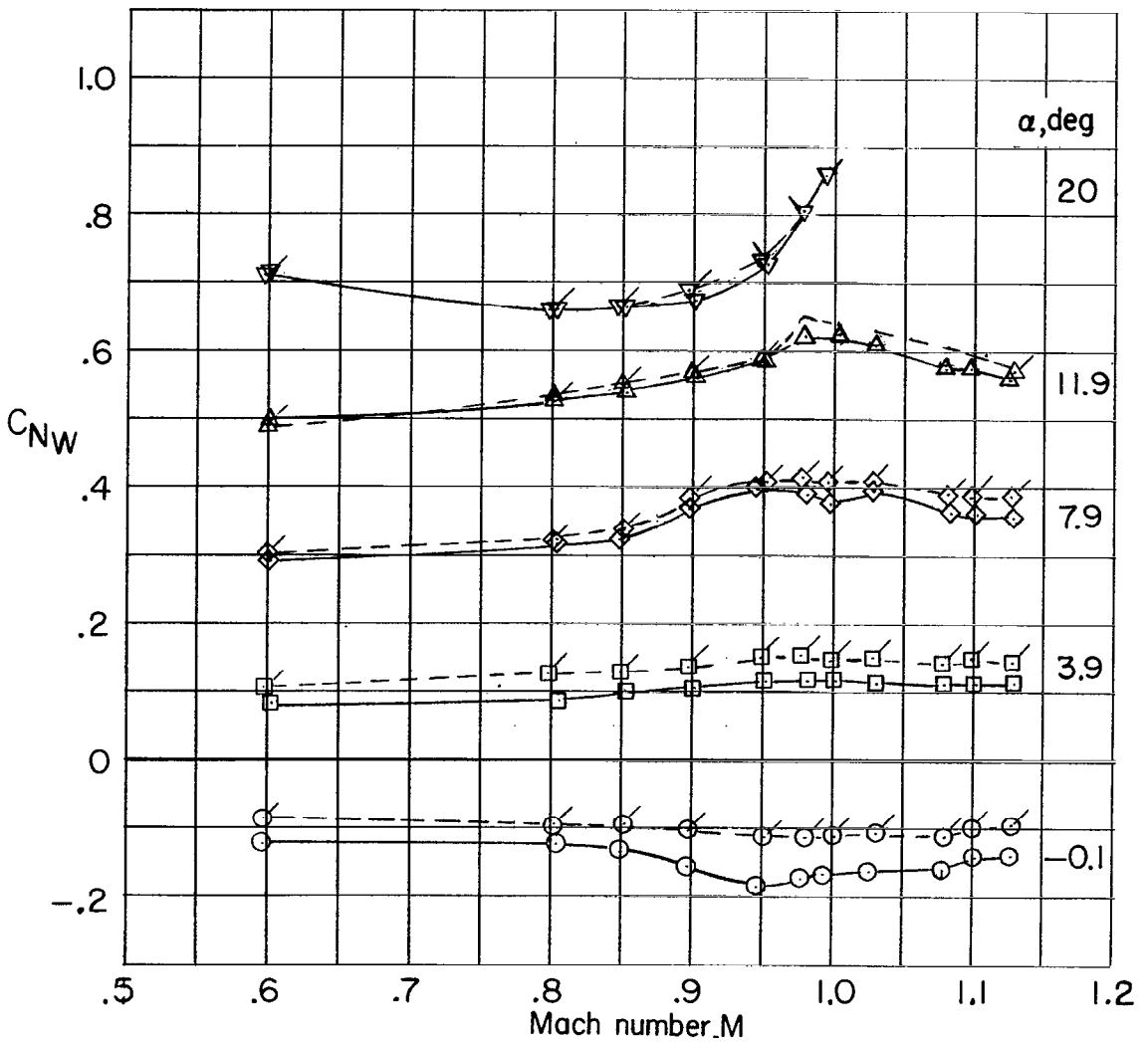

Figure 9.- Variation of wing normal-force coefficient with Mach number.

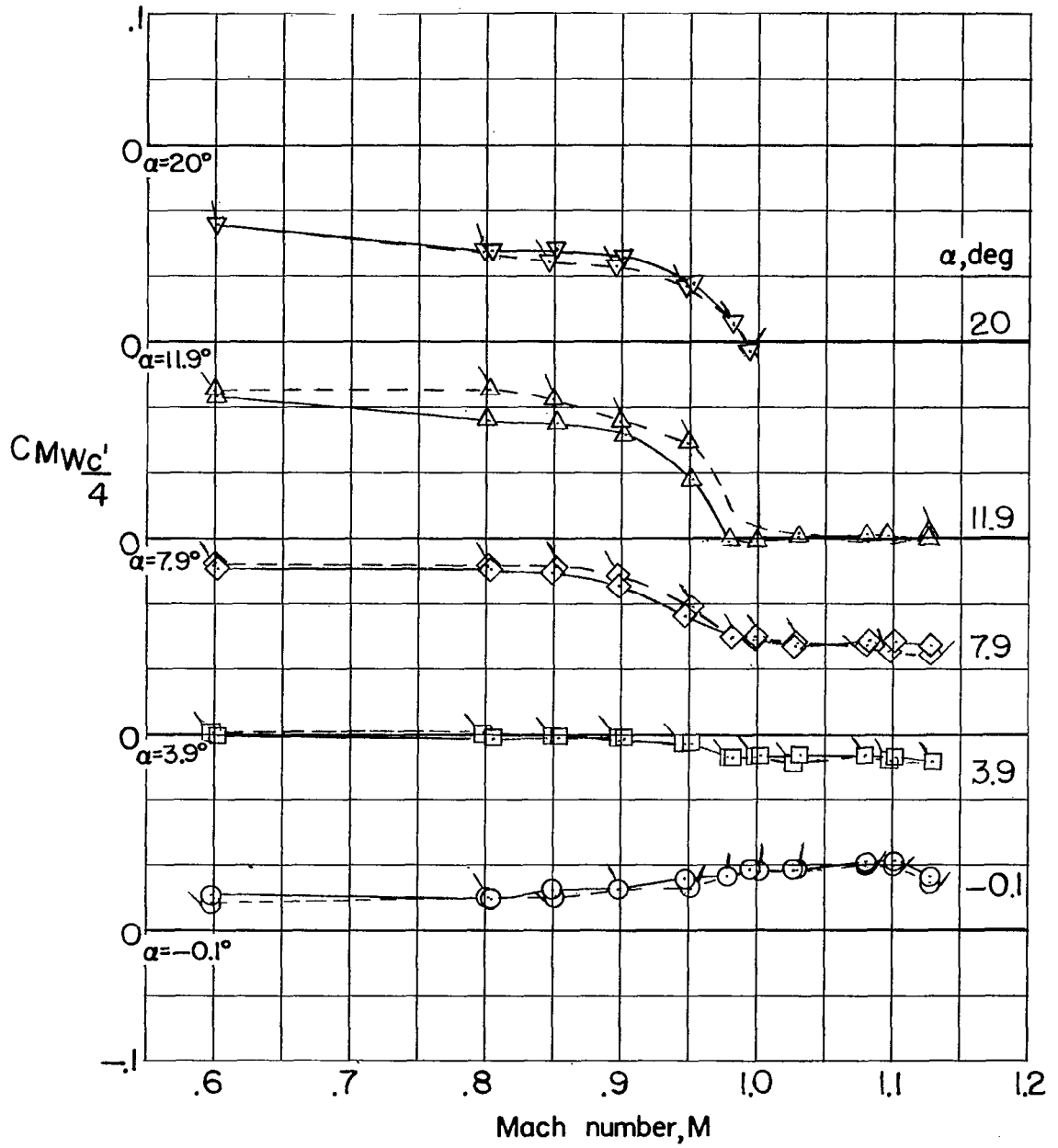

Figure 10.- Variation of wing pitching-moment coefficient with Mach number. (Flagged symbols represent 0° incidence; unflagged symbols represent 4° incidence.)

[redacted]

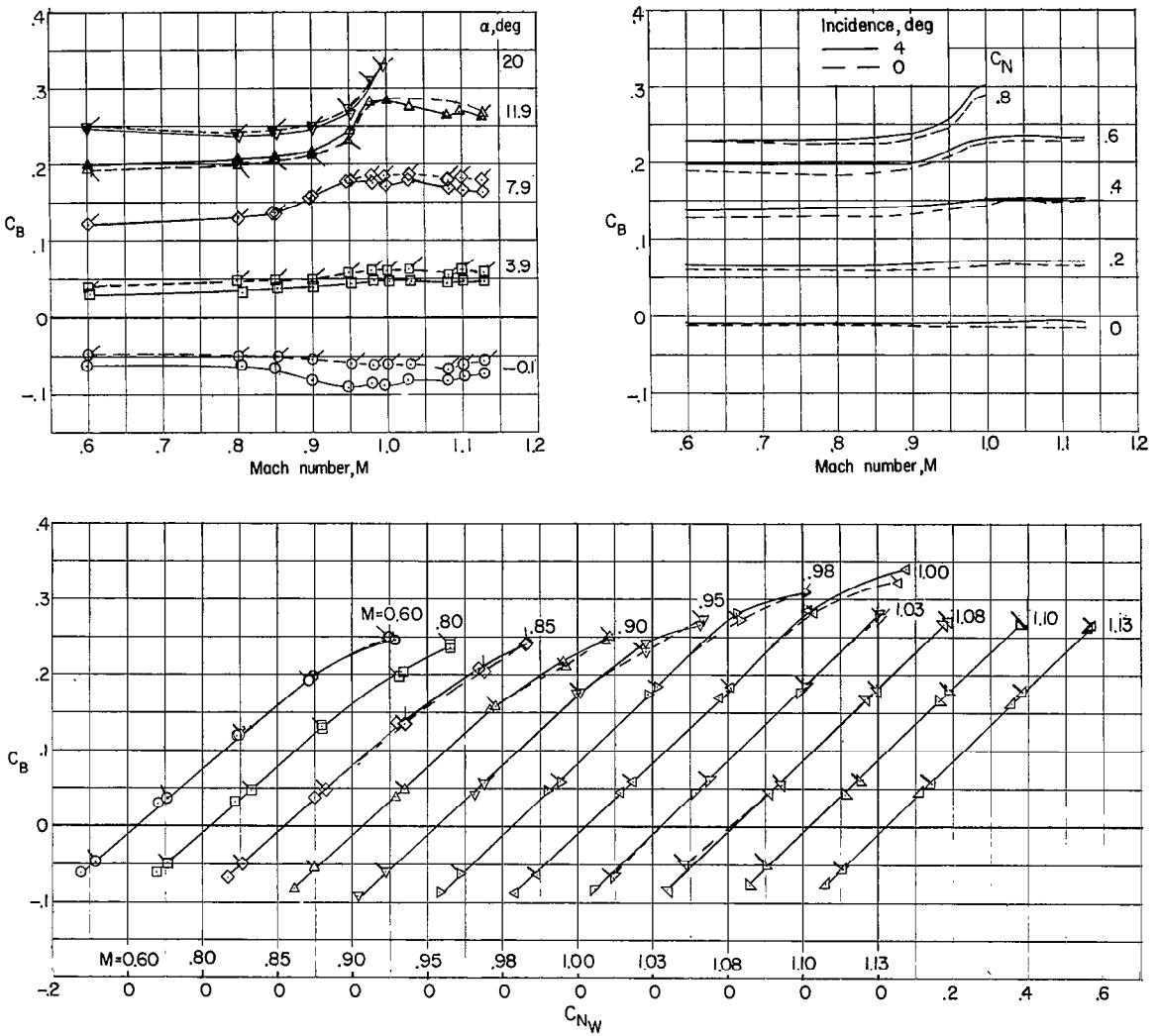

Figure 11.- Root bending-moment characteristics. (Flagged symbols represent 0° incidence; unflagged symbols represent 4° incidence.)

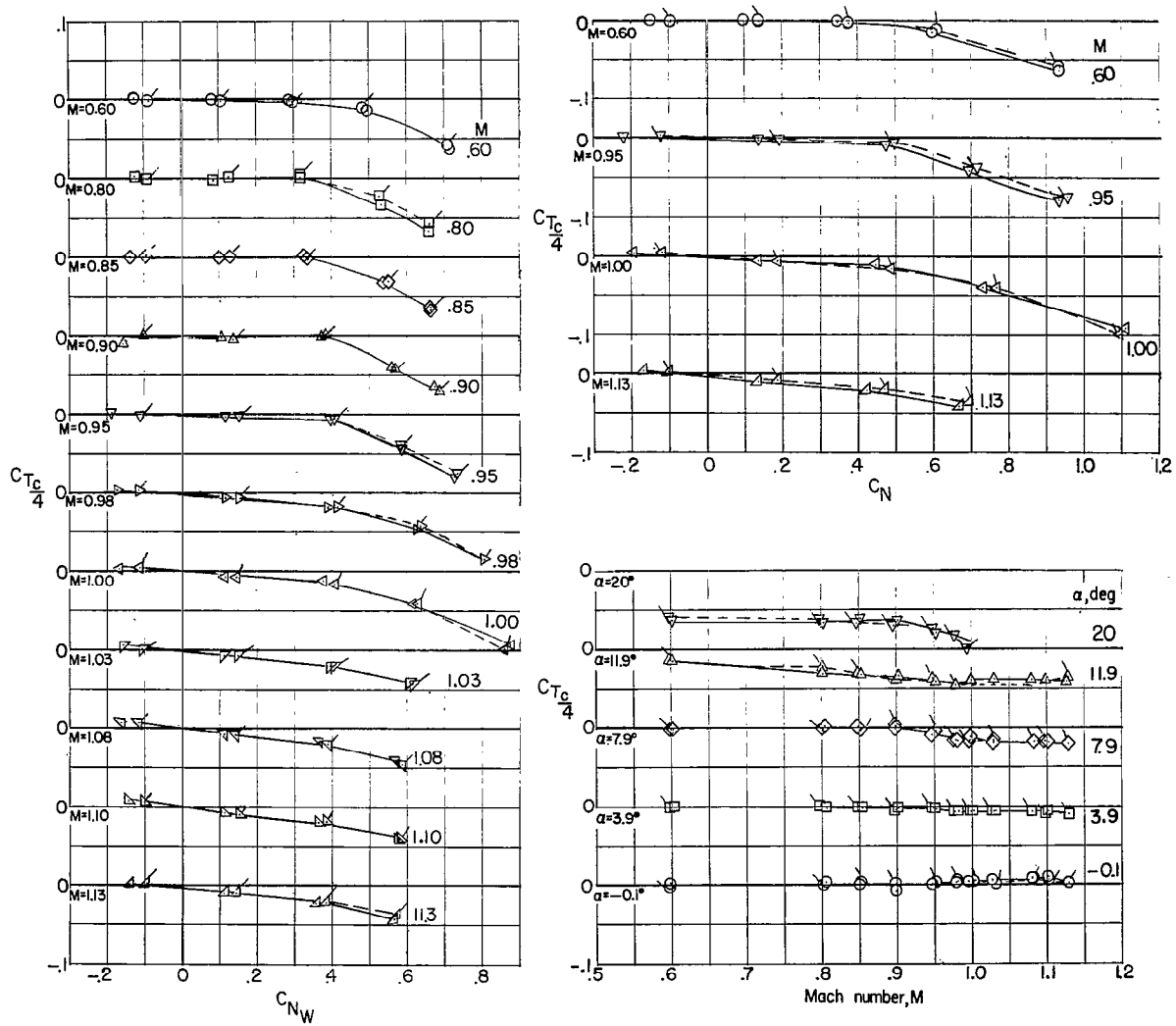

Figure 12.- Twisting-moment characteristics. (Flagged symbols represent 0° incidence; unflagged symbols represent 4° incidence.)